INTERNAL SURFACE MODIFICATION OF ZEOLITE MFI PARTICLES AND MEMBRANES FOR GAS SEPARATION

A Dissertation
Presented to
The Academic Faculty

by

Mohamad H. Kassaee

In Partial Fulfillment
Of the Requirements for the Degree
Doctor of Philosophy in Chemical Engineering
In the School of Chemical & Biomolecular Engineering

Georgia Institute of Technology
August 2012

INTERNAL SURFACE MODIFICATION OF ZEOLITE MFI PARTICLES AND MEMBRANES FOR GAS SEPARATION

Approved by:

Dr. Sankar Nair, Advisor
School of Chemical & Biomolecular Engineering
Georgia Institute of Technology

Dr. David S. Sholl, Co-Advisor
School of Chemical & Biomolecular Engineering
Georgia Institute of Technology

Dr. Christopher W. Jones
School of Chemical & Biomolecular Engineering
Georgia Institute of Technology

Dr. Haskell W. Beckham
School of Materials Science and Engineering
Georgia Institute of Technology

Dr. Ronald R. Chance
School of Chemical & Biomolecular Engineering
Georgia Institute of Technology

Date Approved: June 28, 2012

ACKNOWLEDGEMENTS

My journey of completing a doctorate degree has not been solely a great technical learning experience, but most and foremost it has been a great life training experience. I thank God for giving me great mentors, colleagues, friends and family who have guided, taught, encouraged and trusted me during my PhD studies. Without them, this journey would have been unattainable. I would like to first express my most sincere gratitude to my wife, Ameneh Cheshmehkani. Her support and understanding has helped me greatly during my graduate studies and I am very thankful to her. I also like to thank my great parents, Dr. Mohammad Z. Kassaee, and Ameneh Mahrou. They have been a source of continuous encouragement. I also like to acknowledge my brother Ali, and my sisters Lili and Maryam, and also my brother in laws, Dr. Saeed Nick and Mohammad Haji-Mirzaei.

I would like to express my sincere gratitude to my advisor, Prof. Sankar Nair, for providing me with an opportunity to work with him and for his unwavering support, guidance and commitment to help me develop my scientific skills. His trust and help are most appreciated throughout my PhD years.

I would also like to express my sincere appreciation to my co-advisor, Prof. David Sholl, for taking me as his student and for extending his great support, guidance and trust. His support has been a tremendous motivator throughout my graduate studies. His great way of thinking about scientific matters and his attitude and approach in problem solving has helped me in developing my problem solving skills and has thought me great life

lessons. I would like to thank him and his great family for their hospitality and also making me feel part of their family.

I thank my committee members Prof. Haskell Beckham, Prof. Christopher Jones, and Prof. Ronald Chance for serving on my committee and providing valuable suggestions during this work. I would like to thank John R. Copeland from Prof. Carsten Sievers group for his invaluable collaboration in performing *in situ* FTIR measurements in CO_2 adsorption study on modified zeolites. I also thank Prof. Sievers for his valuable suggestions throughout the FTIR study.

I would like to thank Dr. Preeti Kamakoti from ExxonMobil for her useful suggestions and for the financial support for my PhD work. I would also like to thank Paul Schoenecker from the Walton group, and Prof. Krista Walton, for giving me access to the adsorption instrument (IGA) in their group. Adsorption isotherms of CO_2, CH_4 and N_2 on modified crystals in Chapter 2 of this thesis have been measured using this instrument. I thank Dr. Johannes Leisen (Hanno) from Georgia Tech NMR center for training me to gain expertise in solid state NMR and for great scientific discussions.

I feel very lucky for having been a part of the two greatest research groups in our school. I like to thank all of Prof. Nair's and Prof. Sholl's group members whom I have had the pleasure of working with. In particular, I like to thank Dr. Tae-Hyun Bae, Dr. Suchitra Konduri, Dr. Yeny Hudiono, Amir Ahmadi, Wun-gwi Kim, Dr. Zhengzhi Zhou, Andrew Brown, Dr. Seda Keskin, Dr. Iyad Hijazi, Dr. Sang-Eun Jee, Sung Gu Kang, Ambarish Kulkarni, Emmanuel Haldoupis, Timothy van Heest, Jaeyub Chung and Dr. Ji Zang.

TABLE OF CONTENTS

LIST OF TABLES

LIST OF FIGURES

SUMMARY

Zeolites are a well-known class of crystalline oxide materials with tunable compositions and nanoporous structures, and have been used extensively in catalysis, adsorption, and ion exchange.[11,12] The zeolite MFI is one of the well-studied zeolites because it has a pore size and structure suitable for separation or chemical conversion of many industrially important molecules. Modification of zeolite structures with organic groups offers a potential new way to change their properties of zeolites, beyond the manipulation of the zeolite framework structure and composition.

The main goals of this thesis research are to study the organic-modification of the MFI pore structure, and to assess the effects of such modification on the adsorption and transport properties of zeolite MFI sorbents and membranes. In this work, the internal pore structure of MFI zeolite particles and membranes has been modified by direct covalent condensation or chemical complexation of different organic molecules with the silanol defect sites existing in the MFI structure. The organic molecules used for pore modification are 1-butanol, 1-hexanol, 3-amino-1-propanol, 1-propaneamine, 1,3-diaminopropane, 2-[(2-aminoethyl)amino]ethanol, and benzenemethanol. TGA/DSC and $^{13}C/^{29}Si$ NMR characterizations indicated that the functional groups were chemically bound to the zeolite framework, and that the loading was commensurate with the concentration of internal silanol defects. Gas adsorption isotherms of CO_2, CH_4, and N_2 on the modified zeolite materials show a range of properties different from that of the bare MFI zeolite. The MFI/3-amino-1-propanol, MFI/2-[(2-aminoethyl)amino]ethanol, and MFI/benzenemethanol materials showed the largest differences from bare MFI.

These properties were qualitatively explained by the known affinity of amino- and hydroxyl groups for CO_2, and of the phenyl group for CH_4. The combined influence of adsorption and diffusion changes due to modification can be studied by measuring permeation of different gases on modified MFI membranes.

To study these effects, I synthesized MFI membranes with *[h0h]* out-of-plane orientation on α-alumina supports. The membranes were modified by the same procedures as used for MFI particles and with 1-butanol, 3-amino-1-propanol, 2-[(2-aminoethyl)amino]ethanol, and benzenemethanol. The existence of functional groups in the pores of the zeolite was confirmed by PA-FTIR measurements. Permeation measurements of H_2, N_2, CO_2, CH_4, and SF_6, were performed at room temperature before and after modification. Permeation of *n*-butane, and *i*-butane were measured before and after modification with 1-butanol. For all of the studied gases, gas permeances decreased by 1-2 orders of magnitude compared to bare MFI membranes for modified membranes. This is a strong indication that the organic species in the MFI framework are interacting with or blocking the gas molecule transport through the MFI pores. The CO_2/CH_4 permeation selectivity was close to the Knudsen selectivity (0.6) for the membranes before modification. CO_2/CH_4 selectivity increased for MFI/benzenemethanol modified membrane (1.0), whereas it decreased for the MFI/2-[(2-aminoethyl)amino]ethanol modified membrane (0.5). MFI/benzenemethanol crystals were shown to have a highest sorption capacity for CH_4, whereas, MFI/2-[(2-aminoethyl)amino]ethanol crystals were shown to have a highest sorption capacity for CO_2 over all other studied molecules Higher sorption of CH_4 in MFI/benzenemethanol and higher sorption of CO_2 in MFI/2-

[(2-aminoethyl)amino]ethanol and their strong binding to the modified membrane are likely the reasons for observing higher and lower CO_2/CH_4 permeation selectivity respectively, compared to bare MFI membrane.

A further detailed fundamental study of the CO_2 adsorption mechanism in modified zeolites is necessary to gain a better understating of the adsorption and permeation behavior of such materials. Towards this end, an *in situ* FTIR study was performed in collaboration with John R. Copeland (in the group of Prof. Carsten Sievers at Georgia Tech). For the organic molecules with only one functional group (1-butanol, benzenemethanol, and 1-propaneamine), physical adsorption was found - as intuitively expected - to be the only observed mode of attachment of CO_2 to the modified zeolite material. Even in the case of MFI modified with 1,3-diaminopropane, only physical adsorption is seen. This is explained by the isolated nature of the amine groups in the material, due to which only a single amine group can interact with a CO_2 molecule. On the other hand, chemisorbed CO_2 species are clearly observed on bare MFI, and on MFI modified with 3-amino-1-propanol or 2-[(2-aminoethyl)amino]ethanol. Specifically, these are carbonate-like species that arise from the chemisorption of CO_2 to the silanol group in bare MFI and the alcohol groups of the modifying molecule. The possibility of significant contributions from external surface silanol groups in adsorbing CO_2 chemisorbed species was ruled out by a comparative examination of the FTIR spectra of 10 μm and 900 nm MFI particles modified with 2-[(2-aminoethyl)amino]ethanol.

During the course of the zeolite modification work, it was observed that MFI particles at room temperature showed an orthorhombic structure in some cases, and in other cases a monoclinic structure. This observation, although pertaining to the zeolite MFI, is not related to zeolite modification. To explain this interesting observation, it was hypothesized that the well-known orthorhombic-monoclinic phase transition of MFI was related to the particle size. This hypothesis of a correlation between particle size and phase transition temperature was evaluated by temperature-dependent X-ray diffraction studies. Such a correlation was indeed found, in that particles below a certain size (~ 8 μm) showed a much lower phase transition temperature than those above this size. However, other factors such as the synthesis method (which affects the intracrystalline grain size as well as the defect density) are suspected to also affect the phase transition temperature.

CHAPTER 1 - INTRODUCTION AND BACKGROUND

1.1. Motivation

As energy utilization and efficiency issues become more important worldwide, a new generation of technologies are necessary to replace energy-intensive thermally driven separation processes (distillation, crystallization) which account for a substantial fraction of global energy usage [13]. Conventional technologies in gas separations such as cryogenic distillation of air, condensation to remove condensable organic vapors from gas mixtures, and amine absorption to remove acid gases such as carbon dioxide from natural gas require a gas-to-liquid phase change in the gas mixture that is to be separated. The phase change adds a significant energy cost to the separation. On the other hand, using membranes or solid sorbents in gas separation does not require a phase change and offers a great reduction in operational energy cost, and is very promising in many respects as compared to conventional technologies[14]. Among different types of membranes and solid sorbents, inorganic zeolite materials offer great mechanical, thermal, and chemical stability over a large range of pressures and temperatures.

Zeolites are crystalline materials with fine-tunable compositions and nanoporous structures that have been used in catalysis, adsorption, and ion exchange[11,12]. A zeolite made up of "T-atoms" (usually silicon or aluminum) which are tetrahedrally bonded to each other with oxygen bridges. Zeolite materials incorporate highly periodic pores,

channels and cavities that can be occupied by metal ions, organic molecules, or water molecules[15]. Zeolite materials are naturally found as minerals; however, many of the technologically useful zeolites have been synthesized. There are approximately 200 different natural and synthetic zeolite frameworks with different pore/channel structures which their structures results in their different properties[16].

Zeolite membranes have been shown to have high selectivity in a number of important separations[4,17]. MFI zeolite membranes have been considered for separation of close-boiling hydrocarbons, such as xylene isomers with reported selectivity of 60-300 for *p*-xylene/*o*-xyelene[18,19]. Y-type zeolite membranes were demonstrated as potential candidates for CO_2/N_2 separation[20]. Faujasite membranes (FAU) have been considered for separation of variety of saturated/unsaturated hydrocarbon vapor mixtures with close boiling points such as benzene/cyclohaxane, and propylene/propane[19]. The separation of light hydrocarbon (C_3H_6 and C_3H_8) and N_2 mixtures was investigated using FAU membranes[21]. A ternary mixture having a composition of a typical polypropylene vent stream (12.5% C_3H_6, 12.5% C_3H_8, 75% N_2) was considered. Only C_3H_6 can be recovered from such a mixture. This result is very important because C_3H_6 is the valuable monomer and if recovered with suitable purity, it can be recycled back to the polymerization reactor[21].

In addition to high selectivity, zeolite membranes have advantages over other types of membranes for their high thermal stability, and being stable under thermal

cycling. Zeolite membranes are also stable over harsh physical and chemical environments in which other membranes cannot withstand.

1.2. Zeolite MFI

Among different zeolites, a large effort in the literature has been drawn to the synthesis of MFI (also referred to as silicalite-1 or ZSM-5) sorbents and membranes. This is due to having pore sizes that are suitable for separation of several industrially important organic molecules and the relatively large amount of information available for MFI synthesis [22]. For example, MFI zeolite membranes are ideally suited for the separation of xylene isomers since the pore size of the MFI framework (ca. 5.5-6 Å) should allow preferential permeation of *p*-xylene (kinetic diameter ca. 5.8 Å) while excluding the bulkier *o*- and *m*-xylene (kinetic diameters ca. 6.8 Å). The separation of xylene isomers is important in the petrochemical industry since they are widely used as industrial solvents and precursors. Currently, this separation is most often carried out by a crystallization process, although a zeolite adsorption-based process is also available. Figure 1.1 shows MFI crystal structure and pore sizes in different crystal orientations.

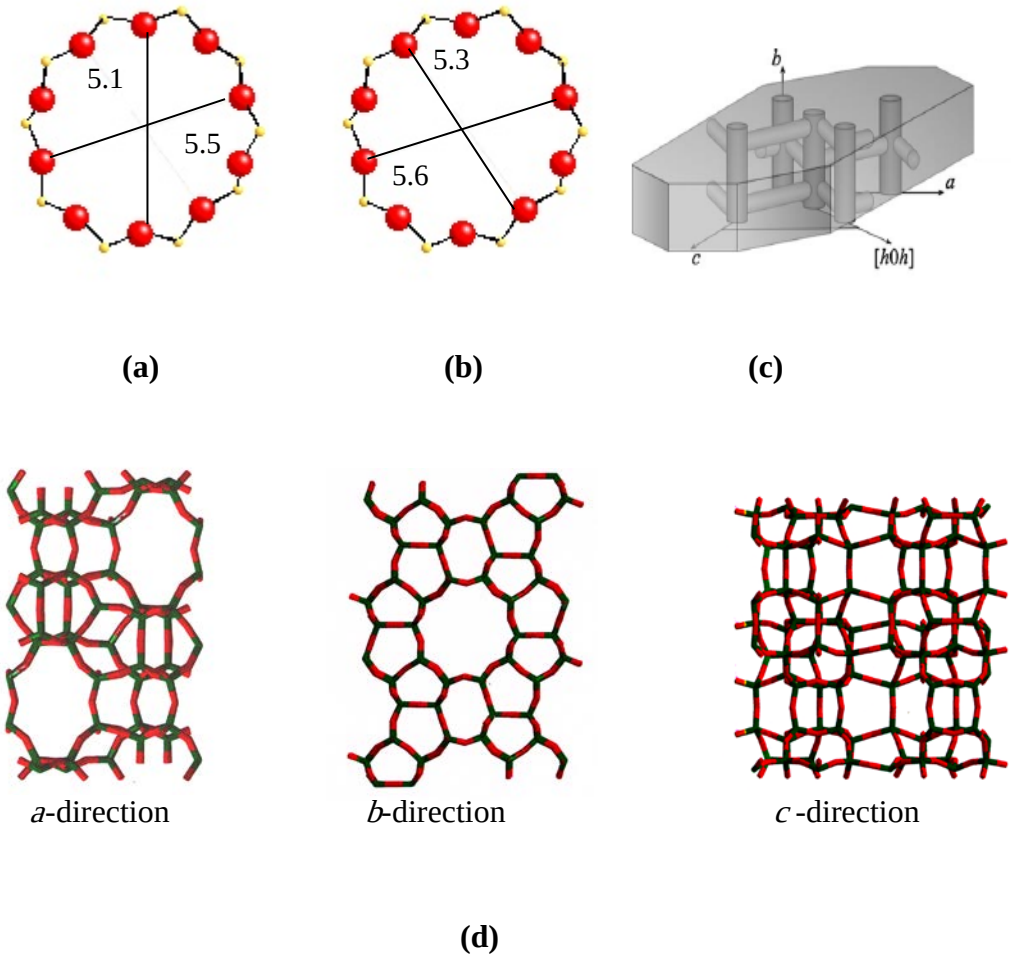

Figure 1.1: Schematic of MFI crystal structure (a) pore size in *"a"* direction *[100]* (b) pore size in *"b"* direction *[010]* (c) MFI crystal structure with interconnecting channels (d) Molecular model of MFI pore structure in *"a"*, *"b"*, and *"c"* direction. Dimensions in (a) and (b) are in Ångstrom.(Reproduced with permission from Cejka *et al* [3])

MFI type zeolites are highly siliceous with Si/Al ratios from about 10 to infinity. MFI zeolites are reported to be hydrophobic and organophilic, and for that reason useful for removing organics from water streams and stable for separations and catalysis in the

presence of water[23]. In this thesis, MFI refers to the pure silica form of the MFI zeolite with no aluminum content.

1.3. Zeolite Adsorbents and Membranes

1.3.1. Zeolite Adsorbents

Adsorption is the process whereby molecules of a gas or liquid species adhere to a solid surface. If a certain species A has a greater affinity for the solid surface than another species B in the mixture, the preferentially adsorbed species can in principle be separated from the other molecules in the gas or liquid mixture. If the solid adsorbent is to be reused the adsorbed species must be desorbed from the solid. In gas phase adsorption the adsorbed material is most often removed by changing the temperature and/or the pressure of the system along with a carrier or sweeper gas. For liquid systems a chemical desorbent must be found that preferentially displaces the desired product species from the solid. The desorbent must be easily separated from the product in another separation step.

Zeolites have been used in industry as adsorbents for different applications. Table 1.1 lists the common zeolite adsorbent applications and focuses on removal of small polar or polarizable molecules by more aluminous zeolites, and bulk separations based on molecular sieving processes[1,24].

Table 1.1: Commercial Adsorbent Applications for Molecular Sieve Zeolites[1]

A. Purification	B. Bulk Separation
I. Drying:	Normal/iso-paraffin separation
natural gas (including LNG)	
cracking gas (ethylene plants)	
insulated windows	Xylene separation
refrigerant	
II. CO_2 Removal	Olefin separation
natural gas, flue gas ($CO_2 + N_2$)	
cryogenic air separation plants	Separation of organic solvents
III. Sulfur compound removal	
IV. Sweetening of natural gas and liquefied petroleum gas	O_2 from air
	Separation of CO_2, SO_2, NH_3
V. Pollution abatement: removal of Hg, NO_x, SO_x	
VI. Removal of organic and iodide compounds from acetic acid feed streams	Sugar separation
	Separation of amino acids, *n*-nitrosoamines

Present day adsorbent applications for zeolites fall into two categories, purification applications, and bulk separation. Purification applications in general depend on surface selectivity for polar or polarizable molecules such as water, CO_2 or sulfur compounds. Bulk separations are based on molecular sieving principles. Pressure swing adsorption in air separation, originally envisaged by Milton[25] as a molecular sieving separation based on the slight difference in size of the oxygen and nitrogen molecule, is rather based on the strong specific interaction of the nitrogen molecular quadrupole with the zeolite cation[24]. Many of the purification applications also involve molecular sieving in that the zeolite adsorbent is chosen to have a pore size that excludes potentially co-adsorbed molecules. For example the use of zeolite type 3A molecular sieve in cracked

gas drying is to prevent the co-adsorption of ethylene and heavier unsaturated hydrocarbons. Refrigerant drying and purification (of halogenated hydrocarbons) is the first broadly applicable commercial use of molecular sieves.

1.3.2. MFI Membranes

Zeolite MFI membranes can serve as a continuous and less energy intensive alternative for separations processes. The progress made in the preparation and characterization of zeolite MFI membranes during the last few years has stimulated several works exploiting the shape-selectivity of zeolite MFI membranes in molecular separation[26,27]. Zeolite membranes in principle might separate continuous mixtures on the basis of differences in the molecular size and shape, but also on the basis of different adsorption properties.[28] The separation ability of a microporous membrane can be described by the interplay of the mixture adsorption equilibrium and the mixture diffusion. Zeolite films have also been targeted for other potential applications including chemical sensors, ion exchange electrodes, insulation layers in microprocessors and light harvesting devices[12,26,29].

There are two main methods available in the literature for synthesizing MFI zeolite membranes: *in situ* and secondary (seeded) growth. The *in situ* method is the first method used in which a porous support is put in contact with the synthesis solution or gel under hydrothermal conditions[30]. The major challenge in this approach is having very little control over the orientation of the membrane. This translates into finding suitable conditions so that MFI crystals nucleate and grow preferentially on the support surface

with minimal non-selective pores. This needs to be done while avoiding competitive nucleation and growth of the crystals in the solution phase.

Because of the simplicity of *in situ* method, it is quite common and has attracted researchers in the field. The drawback of this method is the long induction period, the low number of nucleation site on the support surface and the variation of membrane quality caused by the homogeneous nucleation[31,32]. *In situ* growth of MFI films on various solid supports has been investigated by Jansen *et al*.[33]. and Koegler et.al.[34], with a focus on the morphology of the zeolite layer and without consideration of permeation properties. The most interesting results were obtained for film growth on smooth silicon surfaces. Using compositions without Al or Na, they observed that early during the synthesis the surface became covered with a 0.5 μm thick layer of silica gel within which crystallites emerged at a later time, apparently detached from the solid surface. These crystallites grew to a size of 1 μm and at the end of crystallization covered over 98% of the surface, forming a layer which remained bonded to the support even after calcination at 400 °C. To explain these observations, the authors proposed that zeolite nucleation occurs at the gel-solution interface forming loose crystallites which grow by drawing nutrients from the gel and later from the clear solution. As the crystallites grow in size, they contact and bond with the surface via condensation of silanol groups on the zeolite with those on the silicon (silanols on silicon were formed by oxidation in the strongly alkaline solution)[31].

Different studies regarding growth of MFI membranes on porous and nonporous shows a large number of factors and degrees of freedom at work. The surface of the support is obviously an important factor. The chemical constitution of support can influence crystal growth by releasing selected compounds into the solution, by adsorbing amorphous precursor particles or smaller nuclei, and by providing sites e.g., OH^- groups, for crystal adhesion. With porous substrates, pore size is the major property although the chemical constitution of the material remains important for the same reasons as for nonporous substrates. As in conventional zeolite particle synthesis, the composition of the synthesis solution is of decisive importance. Composition not only controls the type of zeolite crystallized, but the quality of the zeolite layer as well. Some compositions yield a continuous layer of intergrown and interlocking crystals, other compositions yield layers that are macroscopically continuous but contain mesoporous transmembrane pathways, and still other compositions give isolated crystal patches with much of the surface remaining bare.

Acting in conjunction with the synthesis composition, synthesis temperature is another important variable in making zeolite membranes. The nucleation rate of crystals is higher at higher temperatures. In the synthesis of MFI membranes, high temperatures between 150°C and 200°C have generally been preferred[35,36]. They generally offer better zeolite coverage on the support compared to lower temperature synthesis.

Schoeman *et al.*[37] synthesized submicron pure silica MFI (silicalite-1) films on silicon wafers at 100°C. They reported that the synthesis conditions that yield the MFI

film at higher temperatures may not be suitable for the synthesis of thinner layers at low temperatures such as 100°C, where crystallization takes place much slower. With lower crystal growth rates, and therefore the possibility of synthesizing thinner zeolite films or membranes, their synthesis at low temperatures is yet an area not sufficiently studied and discovered.

The secondary growth method is considered the current 'state-of-the-art' technique for making zeolite films. In this approach, the support is seeded with crystals before hydrothermal synthesis. Therefore, the nucleation step is effectively decoupled from the film growth. By decoupling the nucleation step (at high supersaturation) from film growth (at low supersaturation), the seeds can grow in low concentration solutions under suppression of secondary nucleation[38]. For making an MFI membrane, the support (e. g. α-alumina) is coated with small MFI crystal seed particles of 100-300 nm. The seed layer is formed by drying an aqueous suspension of MFI seed crystals over the support. Then, the coated support is put in contact with the precursor solution for the hydrothermal synthesis[22,39]. Figure 1.2 shows the steps in secondary growth method. The secondary growth method would enable direct growth of the already present seeds. This makes it easier to control the film orientation by largely avoiding secondary crystal nucleation in the hydrothermal synthesis.

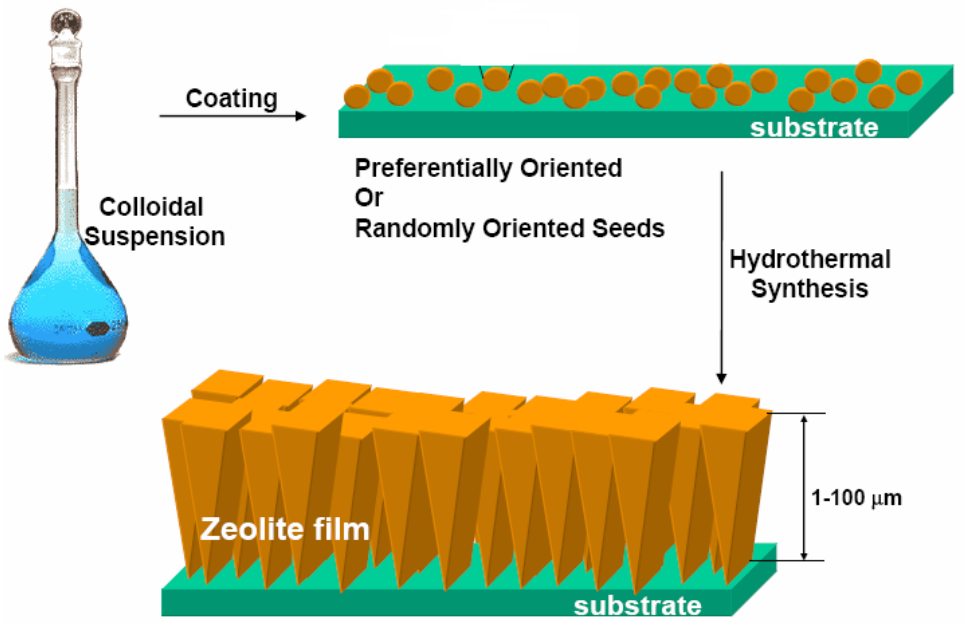

Figure 1.2. Schematic of secondary (seeded) growth technique for synthesizing zeolite membranes.(Reproduced with permission from Nair *et al.*[4])

There has been considerable progress on the secondary growth method starting from when it was first reported by Tsapatsis and co-workers[40]. This method was introduced to address the challenge of producing thin, defect-free membranes with controlled microstructure, and it has been used to synthesize not only MFI but zeolite L and zeolite A membranes as well.

Tsapatsis and co-workers[41] reported synthesis conditions where the MFI crystal growth proceeded in a preferentially oriented out of plane direction, despite the presence of a randomly oriented seed layer. This growth mechanism is explained by the 'evolutionary' Van der Drifts columnar growth, where the crystal grains with the highest

vertical velocity are most likely to dominate the structure[22]. A Van der Drifts growth mechanism shows that the grains which grow fastest perpendicular to the surface, will bury the slower growing grains, and over time the membrane will adopt a preferred orientation.

The first reported synthesis of *c*-oriented MFI zeolite membranes required 24 hours synthesis at 175 °C [40]. In these membranes the *c*-axis of the membrane crystallites is aligned normal to the support surface and the *b* - and *a* - axes are parallel to the surface. Since there are no direct pores along the *c* axis, the membrane permeance is very low and transport along the *c*-axis only occurs by a complicated series of hops between the straight and sinusoidal channels.

Lovallo *et al.* [40,41] also reported the synthesis of [*h0h*] oriented membranes where the *c*-axis is at $\alpha \sim 34°$ angle normal to the surface at 140°C and lower temperatures, with an extended growth times. Figure 1.3 shows the SEM images and XRD spectra of MFI membranes with different orientations[5].

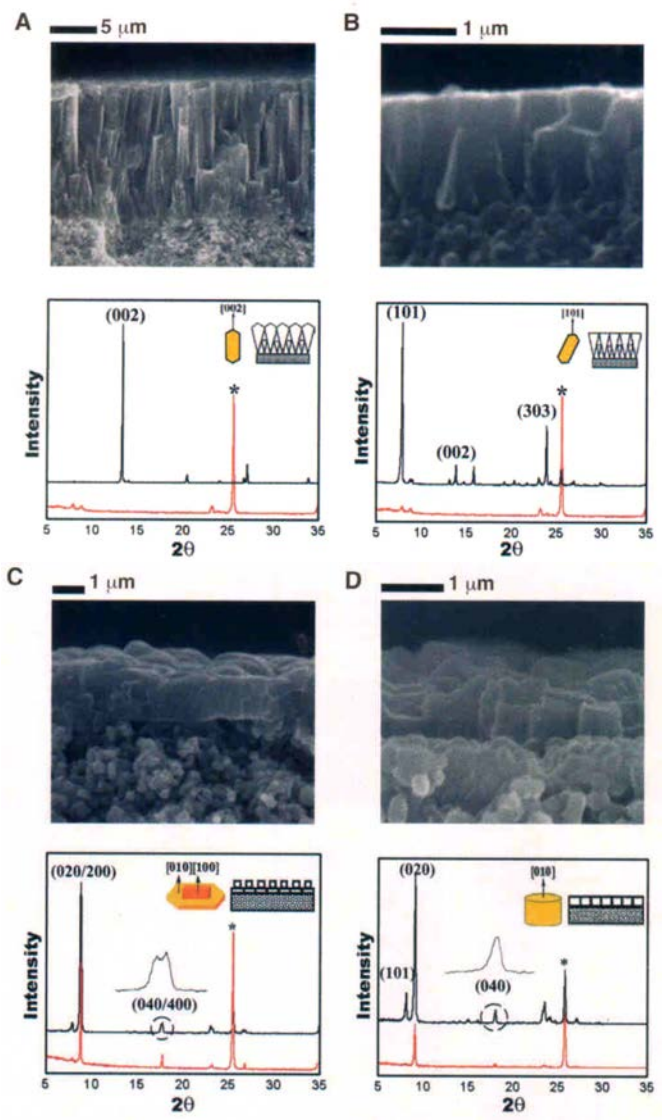

Figure 1.3. SEM cross section of membranes and corresponding XRD traces of the seed layer (bottom trace) and of the membranes (top trace) made by secondary growth of seed layers. For randomly oriented seeds, either (A) c-oriented or (B) [h0h]-oriented film were grown. For b-oriented seeds, if TPA is used (C) a/b oriented film, and if trimer TPA is used (D) b-oriented film was grown. The asterisks (*) indicates α-alumina support peaks. (Reproduced with permission from Lai *et al.*[5])

Making thin, defect free *b*-oriented MFI membranes is the thrust of research in synthesizing MFI membranes. In this membrane, the straight channels of the pores are perpendicular to the support and allow for the most efficient separation with the highest permeances. Lai *et al.*[5] synthesized *b*-oriented MFI zeolite membranes by changing the structure directing agent (SDA) in the hydrothermal growth solution from tetraproplyammonium (TPA) to a trimer-TPA. This was achieved by preparing a *b*-oriented seed layer by covalently bonding the *b*- axis of the seeds to the functionalized support. The *a*–oriented MFI membrane has been synthesized by Choi *et al.*[42], by using the trimer-TPA to synthesize the seeds used for deposition and conducting hydrothermal growth with TPA as the SDA.

There are different ways of preparing oriented seed layer, such as slow dip coating[43], deposition after cationic polymeric adsorption[44], covalent bonding on functionalized surfaces[45] and controlled evaporation[46]. It is well known that during calcination (template removal process), the mismatch in thermal behavior between the MFI layer and α-alumina (Al_2O_3)support can cause mechanical stresses, which result in post-synthesis defect formation [47]. Some post treatments are available to seal the defects, such as dip coating in surfactant-templated silica solution, and silica caulking. Another recent modification to the secondary growth method as applied to MFI membranes was to perform the hydrothermal growth on the seeded support without the use of a template. In this template free synthesis, calcination is ultimately avoided[48].

The relationship between synthesis conditions and membrane properties has been the subject of significant study. Different growth conditions can result in significantly different morphologies as shown in Figure 1.3. This also has the effect of altering the defect formation, degree of crystal intergrowth and stability. Ultimately, such differences can change the transport properties and separation behavior of the membrane.

1.4. Zeolite MFI Modification

The organic modification of porous materials has been attracting much attention because it can widen the range of their applications. By manipulating the zeolite surface properties, the interaction with various organic/inorganic guest species could be controlled. Zeolite organic-modification could be done by covalently binding organic groups within the micropore structure. The modified zeolites would then be converted to organic-inorganic hybrids with potential for a diverse range of new applications, made possible by variations in structure and functionality of the incorporated organic moieties[49]. The organic functional groups confined within the micropores of the zeolites could also be utilized as shape-selective catalysts for number of industrial important reactions[50]. These catalysts can be used in the synthesis of fine chemicals, pharmaceutical precursors and organic compounds.

Zeolite modification is in its initial stages comparing to mesoporous material modification (pore diameters ~ 2-50 nm).There have been significant studies and progress on organic modification of ordered mesoporous materials, ever since the first of

such materials were reported in the 1990s[51]. Modification of mesoporous materials is often done by three methods: (i) direct synthesis via the sol-gel process, (ii) post-synthesis modification via silane grafting, and (iii) post-synthesis reaction with organic molecules.

In the direct synthesis, modification is done by co-condensing organotrialkoxysilanes R-Si(OR')$_3$ or organochlorosilanes R-SiCl$_3$ with the tetraalkoxysilanes (Si-(OR)$_4$) that are the primary silica source for mesoporous material synthesis. This method has been shown to lead to modification in very limited cases[52,53]. Jones *et al.* succeeded in modifying *BEA-type zeolite by various terminal organic groups.[52-54] They employed organosilanes such as phenethyltrimethoxysilane and 3-mercaptopropyltrimethoxysilane as a part of silicon source and synthesized *BEA-type zeolite materials named OFMSs (organic-functionalized molecular sieves). Synthesis of OFMSs with other zeolitic structures such as FAU and MFI was attempted as well[55]. Through this hybridization, a new function can be added to a microporous zeolite material. A *BEA-type OFMS having sulfonic groups inside the pore has been synthesized and it was employed as a shape-selective acid catalyst.[52,54] The synthesized OFMS material catalyzed the acetalization of small reactant molecules, but was not active for bulky reactant molecules whose size is larger than the zeolite pore opening.

A direct synthesis method in zeolite modification is reported for making a novel organic-inorganic hybrid zeolite material: “ZOL” (zeolite with organic group as lattice)[2].

ZOL materials are synthesized from an organosilane in which a methylene group (instead of an oxygen atom) bridges two silicon atoms in the zeolite framework. ZOLs of various structures with the LTA, MFI, and BEA topologies have been reported under synthesis conditions similar to those for conventional zeolites[2].

In ZOL materials a divalent methylene group (not a monovalent pendant organic group) is introduced into zeolite, substituting for a framework oxygen atom. In this approach, ideally the inserted organic moiety will not form a structural defect or spoil the microporosity. The Si-C bond (~1.9 Å) is usually longer than the Si-O bond (~1.6 Å), therefore, the insertion of the methylene moiety into the zeolite framework looks difficult. However, the Si-C-Si angle (~109°) is smaller than the Si-O-Si angles in the zeolite framework; for example, those in MFI-type zeolite range from 140 to 170°.[56] This smaller bond angle would compensate for the distance of two silicon atoms to enable the insertion of methylene species into zeolite framework. Table 1.2 summarizes typical synthesis conditions for ZOL materials reported in literature. In general, ZOL materials are crystallized in synthesis conditions similar to those of conventional zeolites. ITQ-21- and MOR-type ZOL materials can also be synthesized.[2]

Table 1.2: Typical Synthesis Conditions for ZOL Materials[2]

Material	Gel Composition (molar ratio)[a]	T (K)	Time (days)	Topology
ZOL-1	0.5 BTESM: 0.47 TPAOH: 21 H2O	443	5	MFI
ZOL-1(F)	0.1 BTESM: 0.8 TEOS: 0.54 TPAF: 7.63 H_2O	413	14	MFI
ZOL-2	0.5 BTESM: 0.25 TEMABr: 0.13 Na_2O: 20 H_2O	413	20	MFI
ZOL-5	0.5 BTESM: 0.018 Al_2O_3: 0.042 Na_2O: 58 H_2O	463	7	MFI
ZOL-A	0.5 BTESM: 0.52 Al_2O_3: 1.64 Na_2O: 66.5 H_2O	373	14	LTA
ZOL-B(F)	0.1 BTESM: 0.8 TEOS: 0.54 TEAF: 7.63 H_2O	413	14	*BEA

[a] TPA,tetrapropylammonium; TEMA, triethylmethylammonium; TEA, tetraethylammonium

A probable crystallization scheme for ZOL materials is illustrated in Figure 1.4. First, Si-CH_2-Si linkage in the silicon source is cleaved in the hydrothermal conditions in alkaline media. Thus formed inorganic silicon species are mainly used for zeolite nucleation. When seed crystals are employed, this step can be skipped. Therefore, the crystallization can start before a large amount of Si-CH_2-Si linkage is broken, resulting in the formation of a ZOL material with higher organic contents. In the fluoride medium, fluoride anions attack silicon species only to form stable five-coordinate silicon species without cleaving Si-CH_2-Si linkage. Therefore, an inorganic silicon source such as TEOS must be added for the crystallization of ZOL materials.

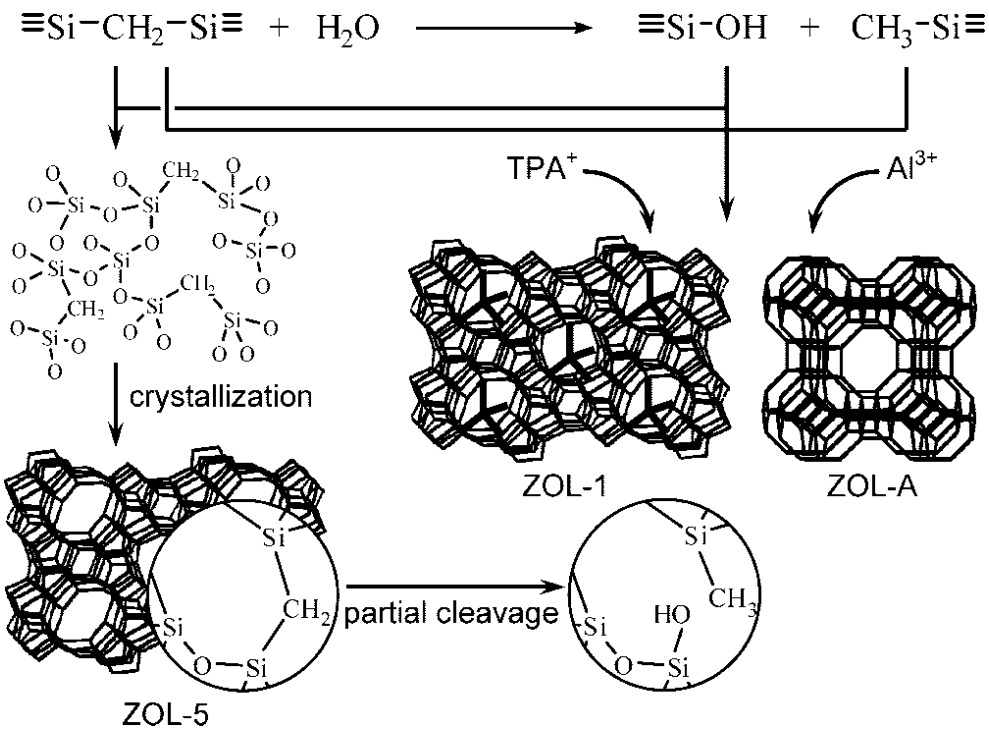

Figure 1.4: Probable crystallization scheme for ZOL materials (Reproduced with permission from Yamamoto *et al.*[2])

The post-synthesis grafting of the organic groups via silane coupling agents (NH-$(SiR)_2$, Cl-SiR_3, or RO-SiR'_3) is usually not effective in medium-pore and small-pore zeolites due to their small pore size. Owing to the smaller pore diameters of zeolites relative to mesoporous oxides, the size of the molecules that can be impregnated into the pores is limited. Su *et al.*, however, reported tetraethylenepentamine (TEPA) loadings as high as 60 wt% on commercial large pore Y-type zeolites.[57] The linear nature of the TEPA molecule likely allowed it to be transported into the pores of the zeolite.

Alternatively, direct reaction of organic molecules such as alcohols, amines and aromatics with zeolites has recently been used as a modification technique. Zeolites such as MFI are known to contain silanol defects in their structure. The number and location of

these defects depends upon the synthesis technique. Considerable evidence has emerged confirming the existence of internal silanol groups in MFI. This evidence has been based on observations of aluminum-independent cation exchange[58], ^{29}Si MAS NMR studies[59,60], and FTIR results[60]. Woolery et. al. presented FTIR. and ^{29}Si MAS NMR evidence that establishes the presence of internal silanols in highly siliceous MFI. The concentration of internal silanols is shown to increase as aluminum content decreases[61]. Datka et. al. studied hydroxyl groups and acid sites in Na-ZSM-5 zeolites with IR spectroscopy[62]. The zeolite with low Na ions (high Na deficiency) has higher acidity compared with the zeolite with high Na ions. Fore higher Na deficiency, more protons are required to neutralize the negative charge of AlO_4^- tetrahedral, and thus the structure has higher acidity due to silanol groups.

The defect sites, or silanol groups, can change depending on the zeolite synthesis method. High-silica zeolites which are made in basic medium with OH^- ions as mineralizing agents have a substantial number of framework defects[63], whereas zeolites are very poor in defect sites when the mineralizing species are F^- ions[59,64]. The recognition that fluoride ions can be used as mineralizing agents in zeolite synthesis was first reported in a patent by Flanigen and Patton,[65] and several groups have used this method in the past to make zeolites with a low defect site concentration.

There is debate[49,60,66,67] regarding the precise nature and concentration of the internal silanol defects, e.g., whether they mainly arise from silanol nests or from uncondensed silanols resulting from local disorder in the lattice. It is also not agreed upon

whether or not they can be annealed upon heating/calcination thereby reducing the silanol groups (or number of Q^3 Si atoms). Kraushaar et. al. proposed that the internal silanol (silyloxy) groups are typically clustered as a nest of four terminal groups where one T atom is missing from the highly siliceous MFI lattice[66]. FTIR studies have shown MFI silanol groups to be associated as counterions to the TPA cations (approximately four per unit cell), which are located at each channel intersection[62]. This requires one silanol group at each inter section. Dessau *et al*. argues against a cluster of four silanols, since it would be difficult, if not impossible, to accommodate four structure directing agents (SDA) in one channel intersection.[60] Based on the modification results in this thesis, having defect sites as isolated silanol groups better explain the observed loading and is more consistent with the rest of the characterization results.

Irrespective of the uncertainty prevailing in the literature regarding the precise structure of the silanol defects, it is established that they exist. Using direct condensation of organic molecules with these silanol defects, Cheng *et al*, as well as the present author, have modified the internal pores of the pure-silica MFI sorbents and membranes by aliphatic alcohols (1-butanol, 1-hexanol)[49,68], amines (1-propanamine, 1,3-propanediamine, 3-amino-1-propanol, 2-[(2-aminoethyl)amino]ethanol) and an aromatic alcohol (benzenemethanol).[68] This work is described in Chapter 2 of this thesis.

The same discussed procedures in modifying zeolite crystals can be employed to modify zeolite membranes. Zeolite modified membranes have only been reported in very limited instances yet[50,69]. Compared to limited published studies on modified zeolites,

numerous mesoporous modified membranes have been reported. For example, McCool et. al. have reported amino-functionalized silica membranes and shown enhanced CO_2 permeation[70]. These examples pertaining to mesoporous modified membranes have been used as a guide to select suitable organic groups in this thesis, and can help in the selection of promising organic groups for further studies in zeolite modification as well. More discussion about recent advanced in modifying MFI membranes are described in Chapter 3 of this thesis

1.5. Objectives and Strategy

The overall objective of this thesis is to develop a new means for altering the adsorption and transport properties of the zeolite MFI adsorbent or membrane by incorporating different functional groups into the zeolite pore structure. This objective is pursued in two interconnected parts. The first part is to functionalize the MFI particles with specific functional groups (alcohol, amine, aromatic), and characterize it with different analytical techniques to gain an understanding over the nature of organic-inorganic binding and its effect on adsorption of light gases (CO_2, CH_4 and N_2). The second part is to synthesize MFI membranes, functionalize the membrane with the desired functional group, and characterize them with gas permeation (CO_2, CH_4 and N_2) and PA-FTIR.

A broader objective in this research is to develop an alternative new means for altering the adsorption and transport properties of the zeolite MFI adsorbents or membranes by incorporating different functional groups into the zeolite pore structure. This objective is achieved and detailed in this thesis as follows: Chapter 2 presents MFI particle synthesis, modification, and characterization. Modification is performed as a post-synthesis treatment for the MFI particles. It includes seven organic molecules: 1-butanol, 1-hexanol, 3-amino-1-propanol, 1-propaneamine, 1,3-propanediamine, and 2-[(2-aminoethyl)amino]ethanol, and benzenemethanol. NMR and TGA/DSC characterization indicates that the functional groups are chemisorbed to the internal pores, and the organic molecule loading is strongly dependent on the concentration of internal silanol sites.

Adsorption isotherms of CO_2, CH_4, and N_2 are measured for the modified samples from 0-400 kPa. In the low pressure region (1-10 kPa), the organic-modified materials show gas adsorption behavior significantly different from that of the bare zeolite MFI, ranging from an enhancement in CO_2/CH_4 sorption selectivity in the amine-modified materials to an enhancement in CH_4 adsorption in the aromatic-modified material. The CO_2/N_2 sorption selectivity decreases for all the modified materials compared to bare zeolite MFI. Water adsorption isotherms were measured for all modified materials to see the effect of modification on their hydrophobicity.

In Chapter 3, MFI zeolite membrane synthesis and modification with the previously chosen seven organic groups are presented. The existence of functional groups in modified MFI membranes are shown by PA-FTIR. Single-component gas permeation measurements of H_2, N_2, CO_2, CH_4, and SF_6 are reported, and the influence of the organic groups on the permeation properties is discussed.

In Chapter 4, an *in situ* FTIR study is conducted on bare and modified MFI particles in order to understand the nature of interactions of gas molecules upon adsorption. In this chapter, I qualitatively probed and identified adsorbed species on the material upon controlled CO_2 exposure for pressure less than 10 mbar CO_2.

Chapter 5 deals with a somewhat different topic investigated during the course of this work. I report certain new observations pertaining to the MFI crystal structure, namely the dependence of the monoclinic-orthorhombic phase transition in MFI as a function of particle size as well as temperature.

Finally, in Chapter 6, concluding remarks and recommendations for future directions of this research are presented.

CHAPTER 2-ORGANIC-MODIFICATION AND ADSORPTION PROPERTIES OF MODIFIED ZEOLITE MFI CRYSTALS

2.1. Introduction

Zeolites, having nanopores less than 2 nm in diameter, have been widely used in adsorption processes and shape-selective catalysis, as well as in emerging applications such as molecular sieving membranes, sensors, and low-*k* dielectric materials[49,52,69,71-75]. By incorporating covalently bound (as opposed to physisorbed) organic groups within the micropores, these highly ordered materials can potentially be converted to organic-inorganic hybrids for a diverse range of new applications. There are three main routes[49,71,72] for functionalizing or modifying mesoporous materials and zeolites: (i) direct synthesis *via* sol-gel or hydrothermal processes involving co-condensation of organotrialkoxysilanes R-Si(OR')$_3$ or organochlorosilanes R-SiCl$_3$ with tetraalkoxysilanes (Si-(OR)$_4$) that are the primary silica source for mesoporous material formation, (ii) post-synthesis modification *via* grafting the material with silane coupling agents such as NH-(SiR)$_2$, Cl-SiR$_3$, or RO-Si-R', and (iii) post-synthesis reaction with organic molecules. The first two routes present difficulties in their application to zeolite materials. Direct co-condensation has been shown to lead to organic-modified zeolites only in rare cases, whereas the grafting of organic groups to the internal surfaces of zeolites using silane coupling agents is impeded by the small pore size of the zeolite. The third route of direct reaction of molecules such as alcohols, amines and aromatics with zeolite surfaces offers a variety of possibilities for modification.

Several reports[49,71] investigate the esterification reaction of alcohols on silica particles that converts their hydrophilic external surfaces into hydrophobic surfaces. Pure-silica zeolites such as MFI are known to usually contain a number of silanol defects within their internal pore structure. Organic-modification of these defects may lead to hybrid materials with new molecular recognition properties, but little is currently known regarding the preparation and characterization of such materials.

Cheng *et al.*[49] reported the internal surface modification of pure silica MFI particles by covalent condensation of the silanol defects with aliphatic alcohols such as 1-butanol and 1-hexanol. The observed alcohol loading was strongly correlated with the concentration of internal silanol defects in the zeolite. Two previous reports[72,73] studied the properties of high-silica MFI functionalized with methylamine (MA). Based upon FT-IR and NMR characterization, the formation of Si–N–Si linkages in the framework was proposed. The MA-functionalized MFI zeolite showed basic properties. Guo *et al.*[72] investigated the modification of high-silica MFI with various alkyl amines. The basicity of these materials, as measured by CO_2-TPD, is 1–2 orders of magnitude stronger than that of the initial high-silica zeolite. It has also been suggested that the N-containing hybrid zeolites may be useful in base-catalysis applications such as partial oxidation[74], halogen elimination[75], and especially Knoevenagel condensation[76]. Modification of internal zeolite pores with aromatics is also attractive, since they can be further modified to yield a variety of chemically active sites[77,78].

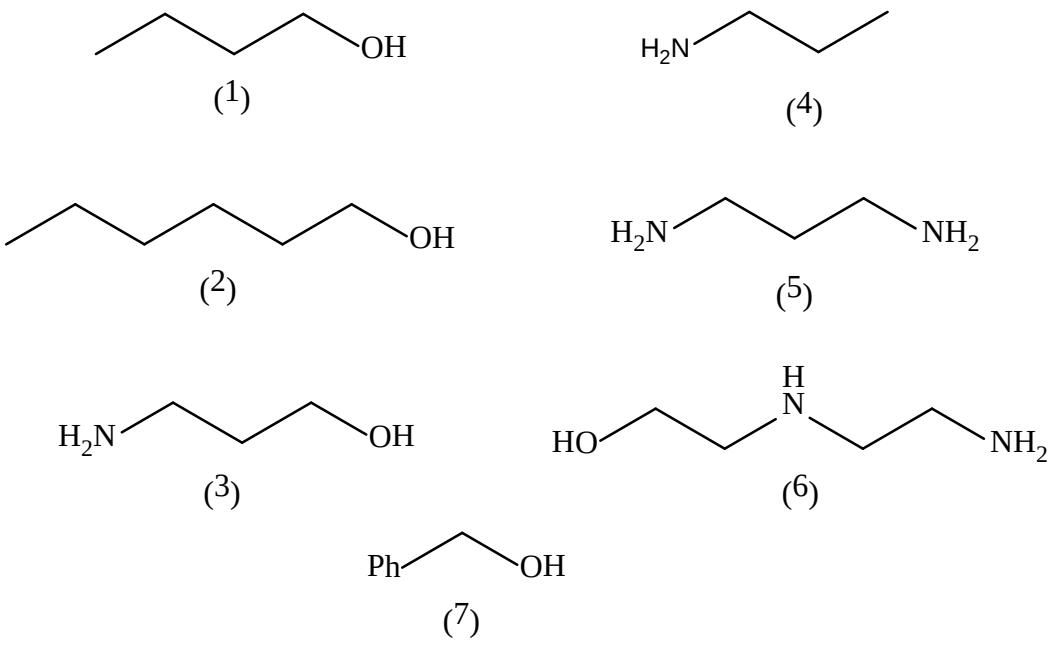

Figure 2.1: Organic molecules used in modifying pure silica MFI: (1) 1-butanol, (2) 1-hexanol, (3) 3-amino-1-propanol, (4) 1-propaneamine, (5) 1,3-diaminopropane, (6) 2-[(2-aminoethyl)amino]ethanol, (7) benzenemethanol.

The objective of the present work is to ascertain whether significant differences can be found in the interactions of gas molecules with organic-modified MFI in relation to bare MFI. I modify the internal pore structure of MFI with systematically chosen organic molecules in order to understand the nature of the host-guest bonding and thermal stability of different functional groups; and then examine the gas adsorption characteristics of these modified materials. Specifically, MFI is modified with four types of organic molecules: aliphatic alcohols (1-butanol, 1-hexanol), aromatic alcohols (benzenemethanol), amino-alcohols (3-amino-1-propanol, 2-[(2-aminoethyl)amino]ethanol), and amines (1-propanamine, and 1,3-propanediamine). Figure 2.1 shows the organic molecules used in this thesis for modification.

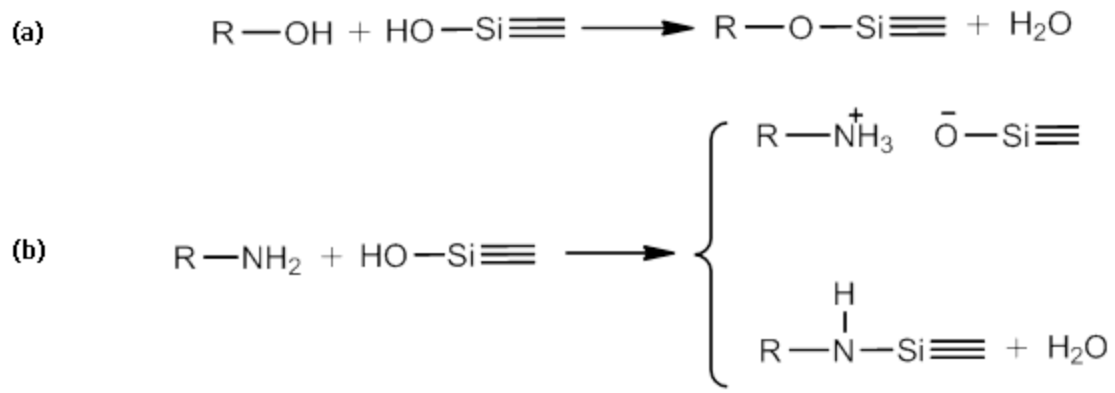

Figure 2.2: Possible reactions of an MFI silanol defect with organic molecules containing –OH **(a)**, and –NH_2 groups **(b)**.

Figure 2.2 shows the hypothesized schemes for the reactions of organic molecules containing –OH and –NH_2 groups with a silanol defect in the zeolite MFI structure. Molecules containing –OH groups condense with the silanol defect to form a covalent R-O-Si linkage. Molecules containing –NH_2 may form two possible products: a hydrogen-bonded complex or a covalent Si-N-R bond[72,73]. Although the exact nature of the reaction product is still controversial, it is clear that a strongly-bound (chemisorbed) species is formed. For molecules containing both –NH_2 and –OH groups, a mixture of the above reaction products is expected. These functional groups provide the potential for a variety of polar and hydrophobic interactions with gas molecules. The structure of these hybrid zeolite-organic materials is studied in detail by a number of characterization techniques. I present water adsorption isotherms for modified materials, which show no substantial change in their hydrophobicity. I then present the CO_2, CH_4 and N_2 gas adsorption isotherms of these materials, which show a clearly different behavior from that of the bare zeolite MFI framework. These results are explained in terms of changes in the

interactions between the adsorbate and the zeolite framework, as created by the presence of the modifying organic groups.

2.2. Experimental Methods

2.2.1 Pure Silica MFI Crystal Synthesis

In order to minimize external surface contributions, I synthesized 10 μm crystals of pure-silica MFI *via* the procedure of Agger *et al.*[79] For 10 μm particles, the external surface area is less than 1% of the total surface area and would contribute a negligible organic loading (< 0.001 mmol/g SiO_2) upon modification.[80,81] A 20.5 g quantity of tetraethylorthosilicate (TEOS) is added dropwise to the solution of 177 g DI water, 0.4 g sodium hydroxide (NaOH) and 2.71 g tetrapropylammonium bromide (TPABr) while stirring. The molar ratio is 1 TEOS/ 0.1 TPABr / 0.1 NaOH / 98 H_2O. The solution is vigorously stirred for 48 hrs at room temperature and then it is aged for 7 days at 50 °C. The resulting solution is transferred to reaction bombs for hydrothermal synthesis at 130 °C for 48 hours. The particles are washed with DI water three times, dried, and calcined at 550 °C for 8 hours.

2.2.2 Organic-Modification Procedures

Organic modification reactions were done under neat conditions. In a 100 ml round-bottom flask, 1 g calcined MFI particles was degassed at 250 °C for 8 hours and then approximately 20 g of the desired organic material was added. The flask was connected to the dried distillation head and then purged with nitrogen for several minutes.

The flask was then immersed in silicone oil bath at 110 °C for 48 hours while stirring. The 1-butanol, 1-hexanol, benzenemethanol, 3-amino-1-propanol, 1,3-propanediamine, and 2-[(2-aminoethyl)amino]ethanol modifications were carried out at 110 °C, while 1-propaneamine was carried out at 25 °C. For 1-butanol and 1-hexanol, the resulting material was centrifuged and redispersed in hexane by sonication three times. For the other modifications, the solid was separated from liquid phase by centrifugation. The particles were then dried with a Rotovap, and then degassed at room temperature for 8 hours. This is followed by 24 hours of vacuum at 150 °C before performing other characterizations.

2.2.3 Characterization Methods

Scanning electron microscope (SEM) images of the MFI zeolite crystals were taken on a LEO 1530 operating at 10 kV. Powder X-ray diffraction (XRD) patterns were obtained on a Philips X'pert Pro diffractometer equipped with X'celerator using Cu Kα radiation. Samples were analyzed over a range of 5-55° 2θ with a step size of 0.02°. TGA and DSC were used to determine the organic content of the modified material by measuring the mass loss in the temperature range of 200-800°C. The measurements were performed on a Netzsch STA409. Samples were heated under a nitrogen-diluted air stream (30, 30 ml/min) from 30 to 900 °C at a rate of 10 °C/min. The chemical environment of the organic molecules in the zeolite structure was investigated with ^{13}C cross-polarization magic-angle spinning (CP-MAS) NMR, ^{29}Si MAS NMR, and ^{29}Si CP-MAS NMR. ^{13}C CP-MAS spectra were recorded at 38.45 MHz on a Bruker DSX300 with a spinning rate of 5 kHz and the chemical shifts were referenced to adamantine. ^{29}Si MAS and ^{29}Si CP-MAS NMR measurements were performed on a Bruker DSX300

spectrometer operating at 59.64 MHz with a spinning rate of 5 kHz. Spectra were acquired using a 7 mm probe with ZrO_2 rotors and a 10 s recycle delay. For ^{29}Si NMR, chemical shifts were referenced to 3-(trimethylsilyl)-1-propanesulfonic acid sodium salt. Adsorption isotherms of CO_2 and CH_4 were measured for the bare and modified samples up to a pressure of 400 kPa. The measurements were carried out on an Intelligent Gravimetric Analyzer (IGA) made by Hiden-Isochema Inc. To obtain reliable estimates of error bars, multiple samples were modified and measured. Water Adsorption isotherms were obtained by gravimetric analysis with IGASorp instrument made by Hiden-Isochemica Inc.

2.3. Results and Discussion

2.3.1 Structure of the Organic-Modified MFI Materials

Figure 2.3 shows the powder XRD pattern (PXRD) of synthesized 10 μm MFI particles along with an SEM image. The powder XRD pattern shows that the synthesized particles are highly crystalline and have the MFI structure. The XRD patterns for the modified samples are similar in crystallinity to those of the bare zeolite, showing that the MFI structure has been preserved after modification. The SEM image in Figure 2.3 shows that the crystals are essentially uniform in size, with a negligible particle size distribution. Significant twinning of some of the MFI crystals is observed; however, no evidence that the twinning affects the internal modification of the MFI particles was found in this work.

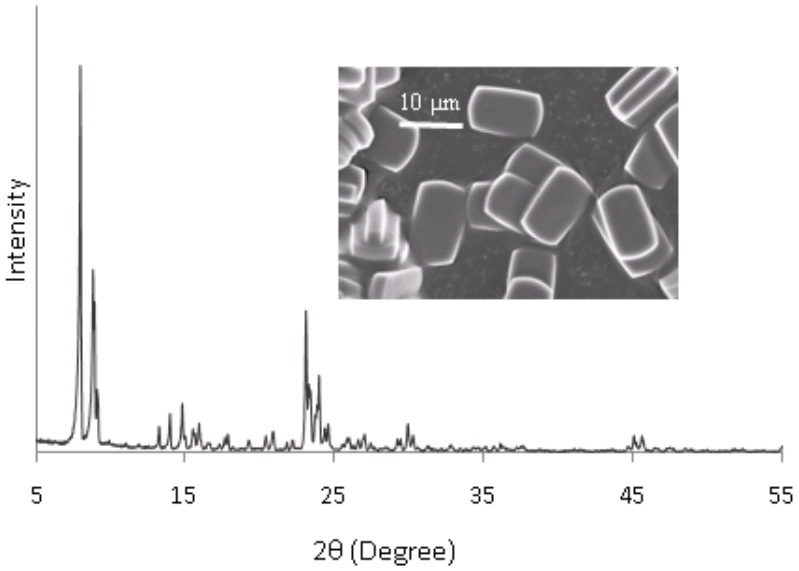

Figure 2.3: PXRD pattern and SEM image of as-synthesized 10 µm pure-silica MFI particles.

Table 2.1 shows the organic loadings obtained for different organic-modified MFI materials. The organic loadings are in the range of 0.38-1.08 mmol/SiO_2, and are comparable to the content of the tetrapropylammonium (TPA) structure-directing agent content in the as-made MFI materials before calcination (0.81 mmol/g SiO_2). The modified particles showed no mass losses before 200 °C, strongly indicating that the organic molecules are chemisorbed to specific sites in the zeolite structure rather than being weakly physisorbed. Micropore volumes were determined from N_2 physisorption (BET) measurements by the t-plot method. The micropore volumes of the modified MFI materials are smaller than that of the calcined bare MFI zeolite, as expected for a material where some of the interior pores are occupied by functional groups. Due to the small size of the 1-propanamine molecule, and its very low loading, no appreciable change in micropore volume (within error bar) could be detected in comparison to the calcined MFI

crystals. Error estimates in organic loading were explicitly determined for as-made MFI, MFI/1-butanol, and MFI/1,3-propanediamine, and were ~0.05 mmol/g SiO_2. Error estimates in micropore volume were explicitly determined for calcined MFI, MFI/1-butanol, and MFI/1,3-propanediamine, and were ~0.01 cm^3/g. The error bars are expected to be very similar for the other organic modifications. The specific surface area calculated from the t-plot is somewhat decreased after modification (typically around 20%). The reason for this is that the organic molecules are located on specific adsorption sites (~4 such sites per unit cell). As shown in this work, the interactions of the organic groups with the gas molecules are sufficient to cause substantial changes in the gas adsorption properties of the zeolite MFI material

Table 2.1: Organic loading of pure-silica MFI 10-µm particles after modification with different organic molecules as measured by TGA mass loss in the temperature range of 200-800°C, and micropore volumes of the modified materials as obtained from N_2 physisorption measurements.

Modifying organic molecule	**Organic loading (mmol/g SiO_2)**	**Micropore volume (cm^3/g)**
As-made MFI (contains TPA cations)	0.81 ± 0.05*	-
Calcined MFI (empty pores)	-	0.12 ± 0.01
1-butanol	0.64 ± 0.05*	0.10 ± 0.01
1-hexanol	0.50	0.10
1-propaneamine	0.38	0.12
1,3-propanediamine	0.74 ± 0.05*	0.10 ± 0.01
3-amino-1-propanol	0.84	0.08
Benzenemethanol	0.45	0.11
2-[(2-aminoethyl)amino]ethanol	1.08	0.08

* Error estimates are assumed to be similar for the remaining organic molecules.

Figure 2.4 shows the ^{13}C CP-MAS NMR spectra of calcined pure-silica MFI (10 μm) modified with 1-butanol, 1-hexanol, 3-amino-1-propanol, 1-propaneamine, 1,3-diaminopropane, 2-[(2-aminoethyl)amino]ethanol and benzenemethanol. The ^{13}C CP-MAS NMR chemical shifts for different modifying organic molecules are listed in Table 2.2. The spectra clearly show the existence of the functional groups in the zeolite structure. Spectrum 1 in Figure 2.4 shows chemical shifts at 65, 33, 24 and 14 ppm, corresponding to the α, β, γ, and δ carbons of the 1-butanol molecule respectively[82]. The splitting of the peak corresponding to the γ carbon (19 and 24 ppm) is due to the interactions between these carbon atoms with the two types of channels in MFI structure[82]. The chemical shift in the region of 61-66 ppm is associated with the carbon attached to the hydroxyl group. This peak can also be seen in Spectra 1, 2, 3, 6, and 7, wherein the particles are modified with the hydroxyl group.

In Spectrum 3 (MFI modified with 3-amino-1-propanol), the presence of the functional group is observed with three peaks at 62 ppm, 40 ppm and 29 ppm that correspond to the carbon attached to the hydroxyl group, carbon attached to the amine group, and the middle carbon, respectively.

Spectra 4 and 5 correspond to MFI modified with 1-propaneamine and 1,3-diaminopropane, respectively. The chemical shifts for 1-propaneamine in D_2O at 40 °C are reported to be 44.24 ppm, 26.90 ppm and 12.17 ppm for α, β, and γ, carbons[83]. The chemical shifts for 1,3-diamine propane in D_2O at 40 °C are reported to be 40.07 ppm for the two carbons attached to the amine and 36.66 ppm for the middle carbon[83]. Two major

peaks at 30 ppm and 40 ppm are seen in both Spectra 4 and 5. For 1,3-diaminopropane, the area under the 40 ppm peak is about twice the area under the 30 ppm peak, as expected. However, in Spectrum 4, no distinguishable peaks are found near 12 ppm and the spectrum is very similar to the MFI/1,3-diaminpropane spectrum.

Spectrum 6 corresponds to MFI modified with 2-[(2-aminoethyl)amino]ethanol. The chemical shifts for 2-[(2-aminoethyl)amino]ethanol in $CDCl_3$ are reported as 41.5 ppm (1), 51.6 ppm (2), 52.1 ppm (3), and 60.4 ppm(4), where carbon numbering starts from the carbon attached to the primary amine [84]. Three major peaks are seen in spectrum 6 at 61 ppm, 52 ppm and 41 ppm. Similar to the rest of the spectra, the carbon close to oxygen is assigned at 61 ppm. The peak at 41 ppm is attributed to the carbon neighboring the primary amine. This peak also appears for all materials containing primary amine (Spectra 3-5). The broad peak at 52 ppm is assigned to the two carbons neighboring the secondary amine in 2-[(2-aminoethyl)amino]ethanol.

In Spectrum 7, the peaks at 128 ppm and 141 ppm are indicative of the phenyl group within the zeolite, whereas the peak at 61 ppm is attributed to the carbon attached to the hydroxyl group in MFI modified with benzenemethanol.

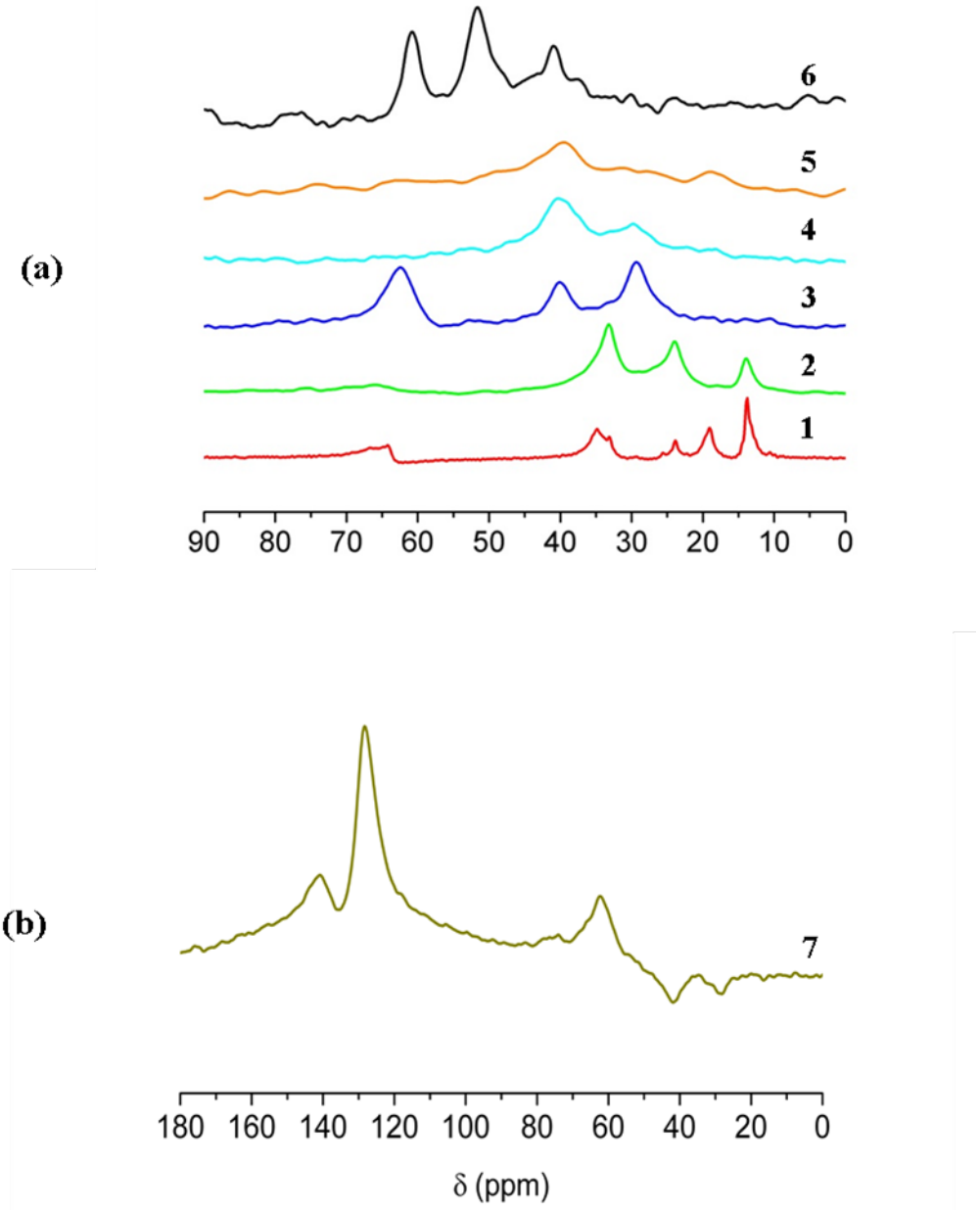

Figure 2.4: ^{13}C CP-MAS NMR spectra of calcined pure-silica MFI modified with: (a) 1-butanol (1), 1-hexanol (2), 3-amino-1-propanol (3), 1-propaneamine (4), 1,3-diaminopropane (5), 2-[(2-aminoethyl)amino]ethanol (6), and (b) benzenemethanol (7).

Table 2.2: ^{13}C CP-MAS NMR chemical shifts for the modified particles.

Modifying Organic Molecule	Chemical shifts, δ (ppm)			
1-butanol	65	33	24	14
1-hexanol	64	32	24	14
1-propaneamine	39	30		
1,3-propanediamine	40	30		
3-amino-1-propanol	62	40	29	
benzenemethanol	61	141	128	
2-[(2-aminoethyl)amino]ethanol	61	52	41	

Figure 2.5 and Figure 2.6 show the ^{29}Si MAS and ^{29}Si CP-MAS NMR spectra of MFI 10 μm particles before and after modification, respectively. The number of Si atom defects (silanol groups) can be estimated from the Q^3:Q^4 ratio in ^{29}Si MAS NMR spectra. The ideal chemical formula of pure-silica MFI is $Si_{96}O_{192}$. The ratio of the Q^3 and Q^4 peak integrated areas is $4x/(96-5x)$, wherein x denotes the number of silanol groups[85]. Silanol groups on the external surface can be neglected for the 10 μm particle size used in this study.

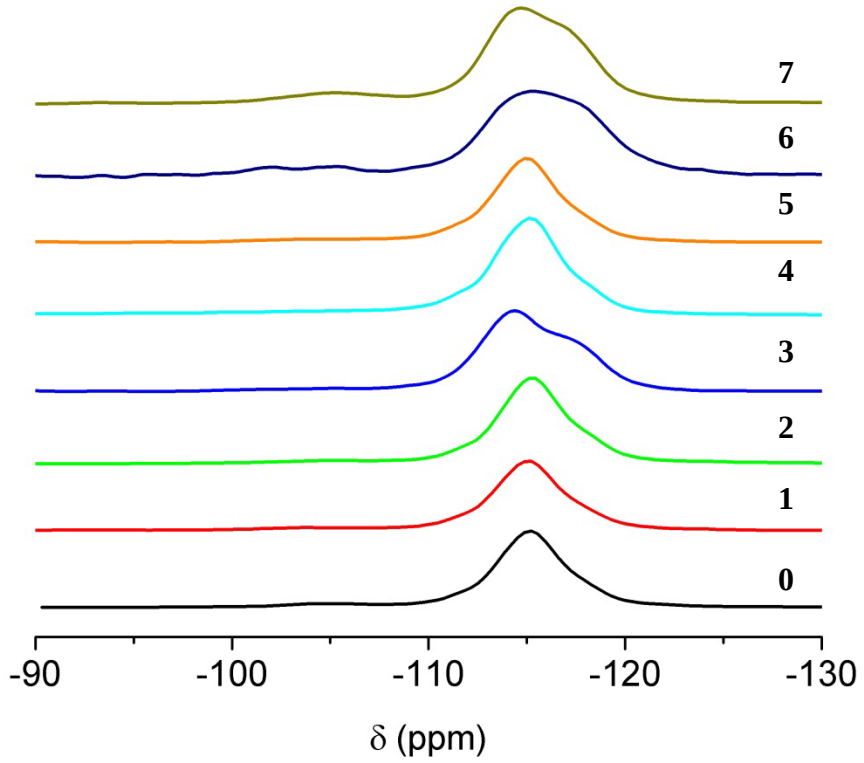

Figure 2.5: ^{29}Si MAS NMR spectra of pure-silica MFI crystals (0) modified with 1-butanol (1), 1-hexanol (2), 3-amino-1-propanol (3), 1-propaneamine (4), 1,3-diaminopropane (5), 2-[(2-aminoethyl)amino]ethanol (6), and benzenemethanol(7).

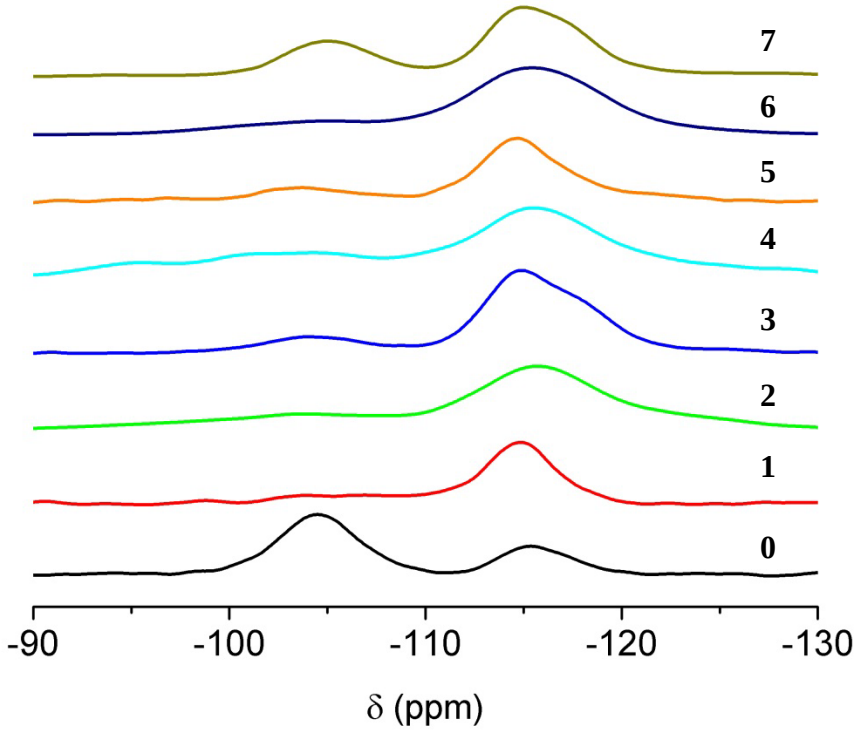

Figure 2.6: ^{29}Si CP MAS NMR spectra of pure-silica MFI crystals (0) modified with 1-butanol (1), 1-hexanol (2), 3-amino-1-propanol (3), 1-propaneamine (4), 1,3-diaminopropane (5), 2-[(2-aminoethyl)amino]ethanol (6), and benzenemethanol (7).

Table 2.3: The estimated Q^3:Q^4 ratio for calcined MFI 10 µm particles, before and after modification with different organic molecules as measured from ^{29}Si MAS and ^{29}Si CP-MAS NMR spectra.

Modifying organic molecule	Q^3/Q^4	
	^{29}Si MAS	^{29}Si CP-MAS
Calcined MFI (empty pores)	0.06	2.33
1-butanol	0.05	0.23
1-hexanol	0.05	0.19
1-propaneamine	0.04	0.37
1,3-propanediamine	0.07	0.27
3-amino-1-propanol	0.04	0.19
benzenemethanol	0.08	0.46
2-[(2-aminoethyl)amino]ethanol	0.10	0.33

Table 2.3 shows the estimated Q^3:Q^4 ratio for calcined MFI 10 µm particles, before and after modification with different organic molecules as measured from ^{29}Si MAS and ^{29}Si CP-MAS NMR spectra. The Q^3:Q^4 ratio, as measured without cross-polarization (CP), is not very sensitive to the modification of the silanol groups. However, the Q^3:Q^4 ratio of the ^{29}Si CP-MAS NMR spectrum from the bare samples is much higher (2.33), due to the enhancement of the Q^3 signal by the protons of the silanol groups. This Q^3:Q^4 ratio decreases sharply in all of the modified samples, and is in the range of 0.19-0.46. The large reduction in the CP signal from the Q^3 groups in the modified samples clearly suggests a reduction in the proton concentration near the Si defects due to substitution by the organic molecule. The reduction in Q^3 signal is also consistent with the fact that the ^{1}H-^{29}Si cross-polarization signal falls off as the sixth power of the distance between the Si nuclei and the nearest protons[67]. As in the work by

Cheng *et al.*[49] and others[68], the reduction in the Q^3 peak is attributed to condensation of the alcohol groups with the silanol groups to form Si-O-R covalent bonds rather than the formation of hydrogen-bonded complexes. TGA results support this hypothesis, since the organic molecules do not leave the MFI structure until at least 200 °C.

Among the modified materials reported here, MFI/benzenemethanol and MFI/1-propaneamine have the highest Q^3:Q^4 ratios in ^{29}Si CP-MAS NMR (0.46 and 0.37). This is consistent with the TGA data, which shows a relatively smaller loading of these two molecules. Furthermore, the MFI/3-amino-1-propanol material has the highest organic loading and the lowest Q^3:Q^4 ratio (0.19). All the above observations clearly suggest that chemical modification of the silanol groups plays a key role in all of the organic-modification examples presented in this study.

2.3.2. Water Adsorption Properties

Water adsorption measurements were performed to see the effects (if any) of modifications on hydrophobicity compared to the bare MFI. Figure 2.7 shows water adsorption isotherms at 293 K for bare and modified material, over 5-95 Relative Humidity (RH). The experiments were conducted in flowing air at 1 bar.

Bare MFI is hydrophobic based on the Figure 2.7, and I see that these modifications have not changed the hydrophobicity of the hybrids substantially. From the Figure 2.7, 1-propaneamine seems to have become more hydrophobic; however, considering very low water loadings for these materials and the limited accuracy of the instrument, one cannot conclude that its hydrophobicity has change substantially.

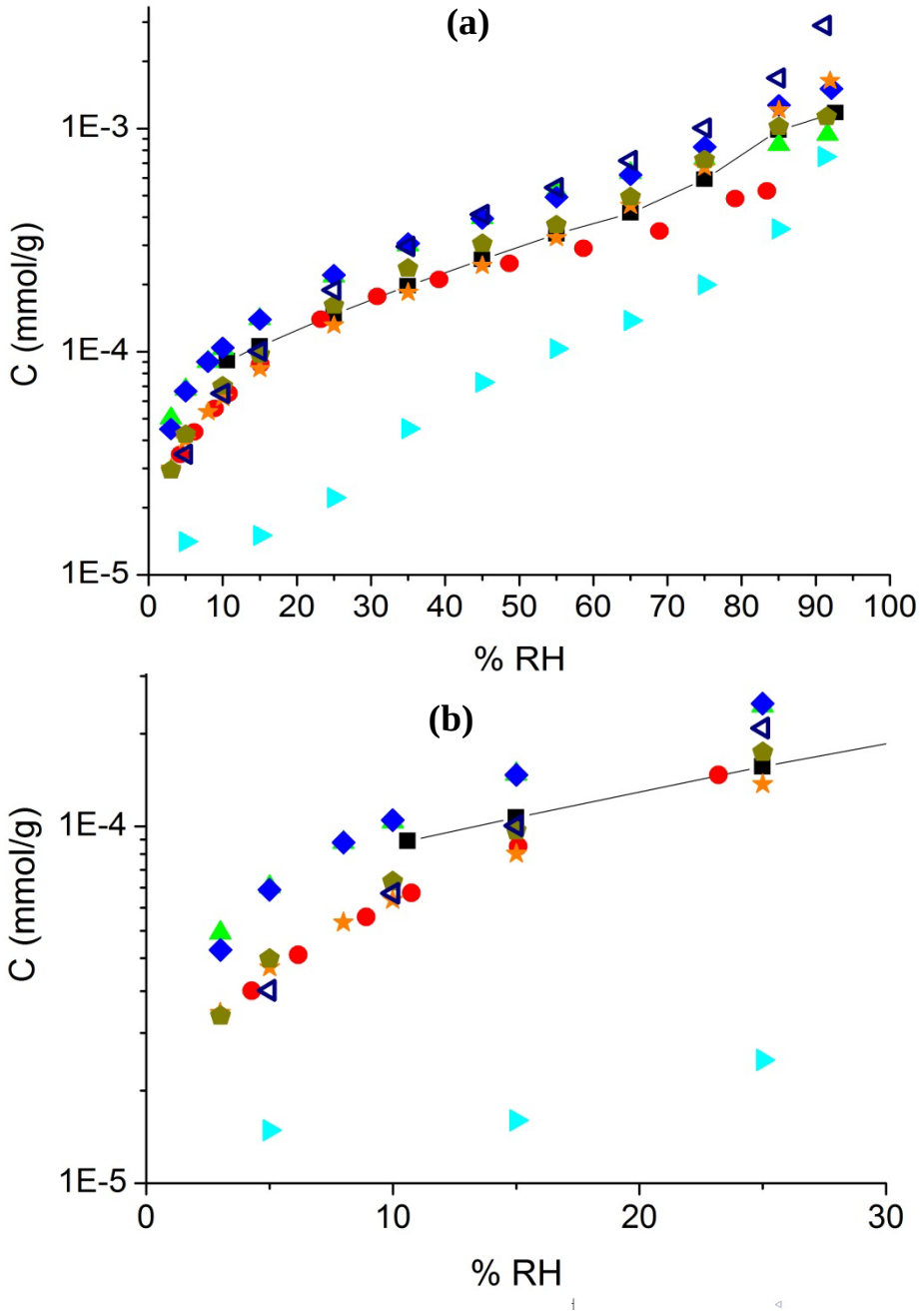

Figure 2.7: Water adsorption isotherm from 5-95 RH (a) and from 5-30 RH (b) at 1 bar, on pure silica MFI before modification (—■—), and modified with 1-butanol (●), 1-hexanol (▲), 3-amino-1-propanol (◆), 1-propaneamine (▶), 1,3-diaminopropane (★), 2-[(2-aminoethyl)amino]ethanol (◀), and benzenemethanol (⬟),.

2.3.3 Gas Adsorption Properties

Figure 2.8 shows the adsorption isotherms for CO_2, CH_4, and N_2 at 293 K before and after modification over the full range of pressure (0-400 kPa) measured. In order to allow a physicochemically meaningful comparison, the masses of the modified MFI adsorbents are normalized to the equivalent amount of bare MFI adsorbent material based upon the known loading of the functional group. Experimental error bars based on repeated measurements have been shown for bare MFI, MFI/benzenemethanol and MFI/1-propaneamine. The other materials are expected to have similar error bars. All the modified materials show overall changes in gas adsorption behavior in comparison to the bare zeolite MFI. In the high-pressure region, all the modified materials show a decrease in sorption capacity in relation to bare MFI, as expected due to the occupation of a part of the MFI pore volume by the modifying organic groups. The difference in gas sorption capacity between the six modified materials is not only a function of their organic loading and micropore volume (as seen in Table 2.1), but also of the adsorbing gas and the type of organic group present (Figure 2.8).

(a)

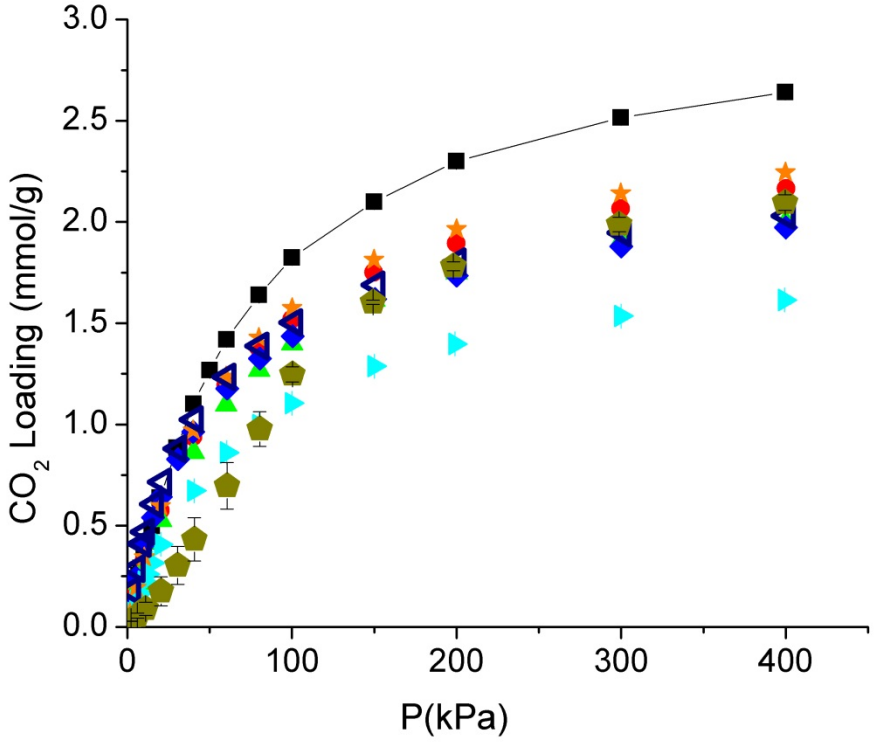
3.0
2.5
2.0
1.5
1.0
0.5
0.0
CO_2 Loading (mmol/g)
0
100
200
300
400
P(kPa)

(b)

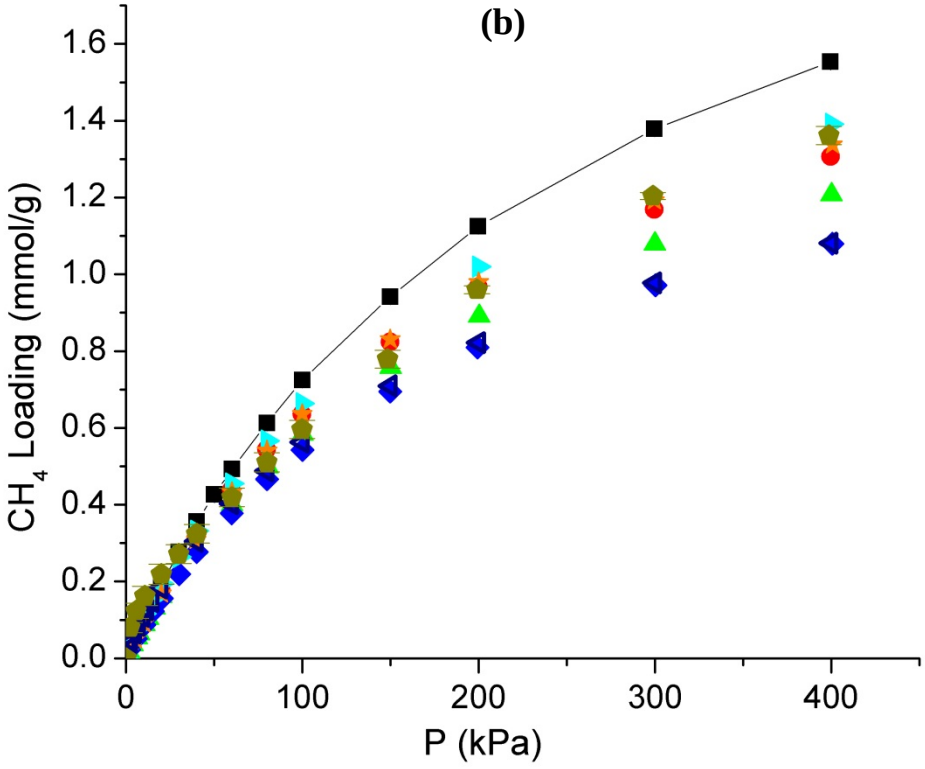
1.6
1.4
1.2
1.0
0.8
0.6
0.4
0.2
0.0
CH_4 Loading (mmol/g)
0
100
200
300
400
P (kPa)

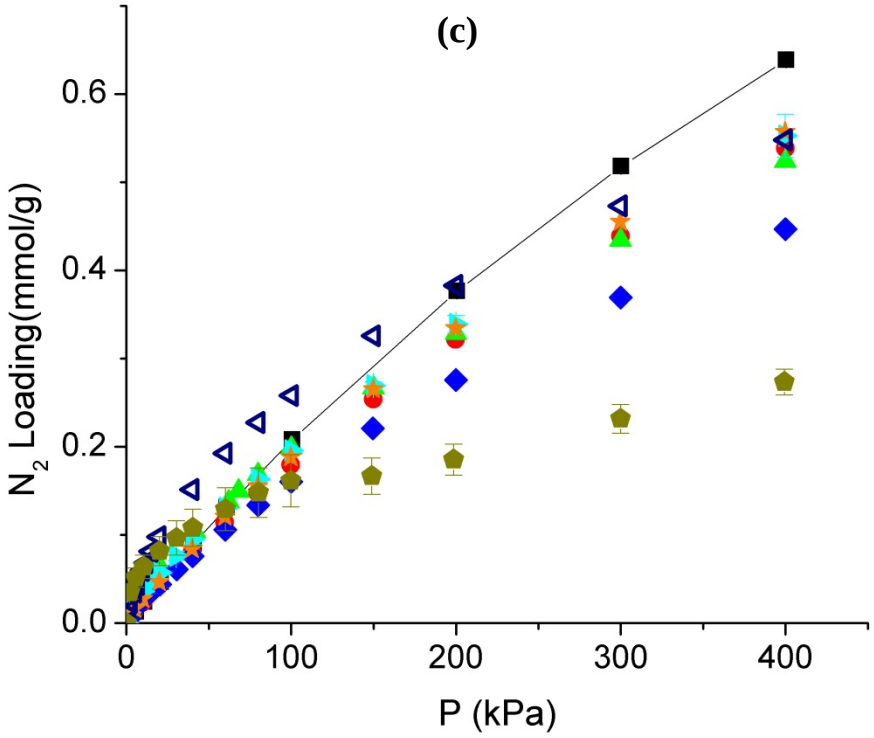

Figure 2.8: Sorption isotherms of CO_2 **(a)**, CH_4 **(b)**, and N_2 **(c)** in 0-400 kPa on pure silica MFI before modification (—■—), and modified with 1-butanol(●), 1-hexanol (▲), 3-amino-1-propanol(◆), 1-propaneamine(▶), 1,3-diaminopropane(★), 2-[(2-aminoethyl)amino]ethanol(◁), and benzenemethanol(⬟).

To examine the effects of specific adsorbate-framework interactions, it is necessary to evaluate the adsorption behavior in the low pressure region (approximately 0-10 kPa), which is free from the effects of adsorbate molecule packing and adsorbate-adsorbate interactions that become important at high pressures.

Figure 2.9a shows the adsorption isotherms of CO_2 in the low pressure region. Compared to bare MFI, MFI/2-[(2-aminoethyl)amino]ethanol and MFI/3-amino-1-propanol show distinctly higher CO_2 loading at low pressure, whereas MFI/benzenemethanol shows a distinctly lower loading compared to the bare MFI before modification. The CO_2 loadings for the other modified materials are close to that of bare MFI. Figure 2.8a shows that the affinity for CO_2 (i.e., the Henry's constant, obtained as the slope of the adsorption isotherm in the low-pressure region) is highest in MFI/2-[(2-aminoethyl)amino]ethanol and MFI/3-amino-1-propanol samples. Both 2-[(2-aminoethyl)amino]ethanol and 3-amino-1-propanol molecules can bind to the internal silanol groups either through the hydroxyl group or the amine group at its ends. I attribute the increased affinity to CO_2 in the modified material to the amine and hydroxyl groups in the structure that are free to interact with CO_2. On the other hand, the amine groups in 1-propaneamine and 1,3-diaminopropane appear to be bound to the silanol sites in such a way as to prevent significant interactions with CO_2 molecules. It should be noted that all the experiments are done in anhydrous conditions, where the interaction of CO_2 with basic groups is weaker than in the presence of water[86,87]. MFI/benzenemethanol shows the lowest affinity to CO_2, consistent with the observation that the aromatic phenyl ring is not known to have a favorable interaction with CO_2.

Figures 2.9b-2.9c show the adsorption isotherms for CH_4 and N_2 in the low pressure regime. MFI/benzenemethanol shows a considerably higher CH_4 loading than bare MFI, which is attributed to the favorable interaction of CH_4 with the phenyl rings in the functional groups in this material[88,89]. The remaining materials show a loading of CH_4 comparable to bare MFI. In Figure 2.9c, all the materials show a low adsorption affinity and loading for N_2. The error bars are shown for bare MFI, MFI/1-propaneamine, and MFI/benzenemethanol. It is observed that the modified MFI materials exhibit a slightly higher loading than the bare MFI at low pressure. However, the mechanism underlying the variations in N_2 gas adsorption capacity between the bare and different modified materials is not well-understood at this stage, and is a subject for future investigation.

(a)

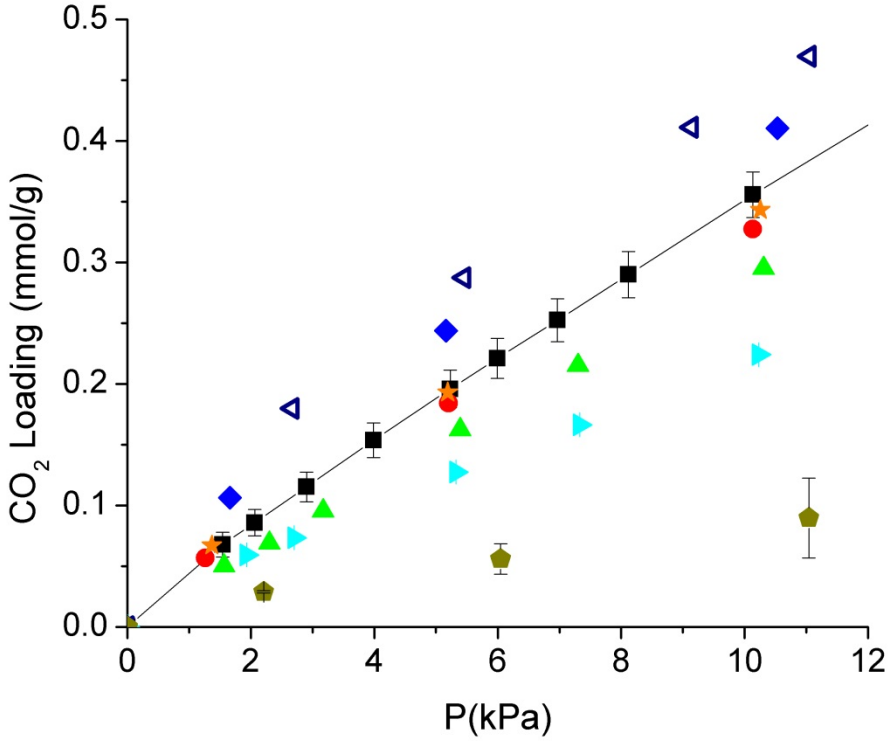
0.5
0.4
0.3
0.2
0.1
0.0
CO_2 Loading (mmol/g)
0
2
4
6
8
10
12
P(kPa)

(b)

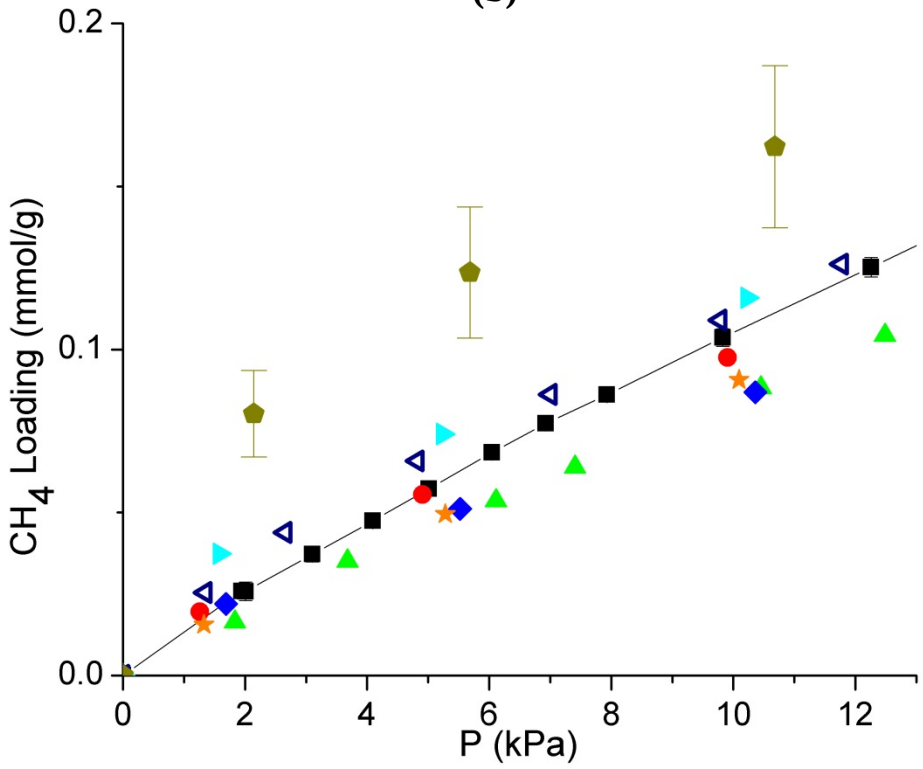
0.2
0.1
0.0
CH_4 Loading (mmol/g)
0
2
4
6
8
10
12
P (kPa)

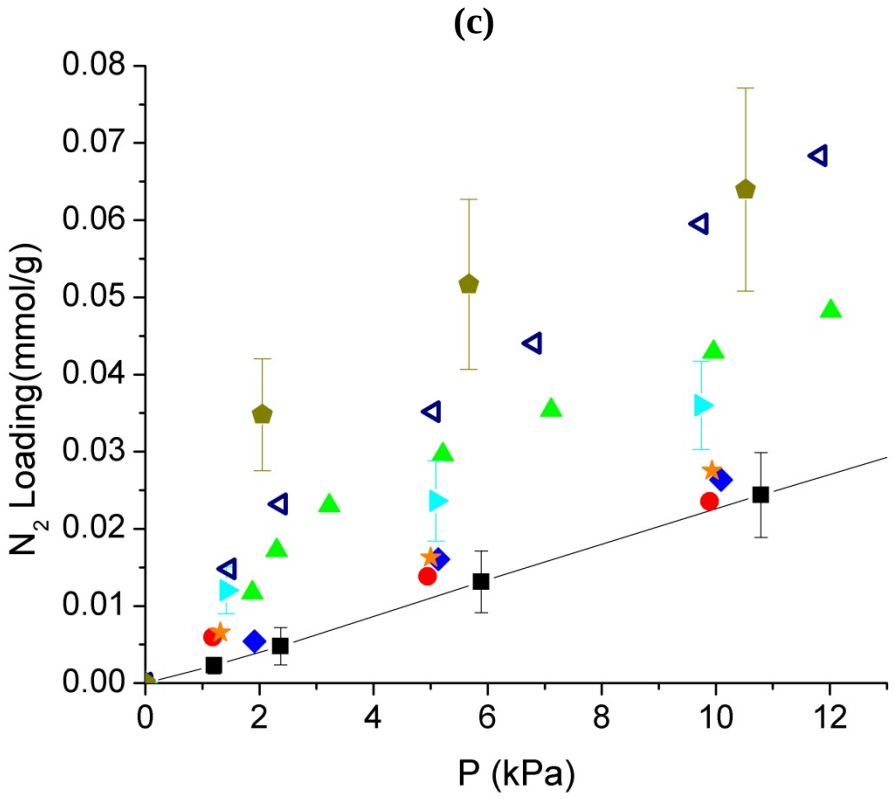

Figure 2.9: Adsorption isotherms in the low pressure region for CO_2 **(a)**, CH_4 **(b),** and N_2 **(c)** on pure silica MFI before modification (—■—), and modified with 1-butanol (●), 1-hexanol (▲), 3-amino-1-propanol(◆), 1-propaneamine (▶),1,3-diaminopropane (★), 2-[(2-aminoethyl)amino]ethanol (◁), and benzenemethanol (⬟).

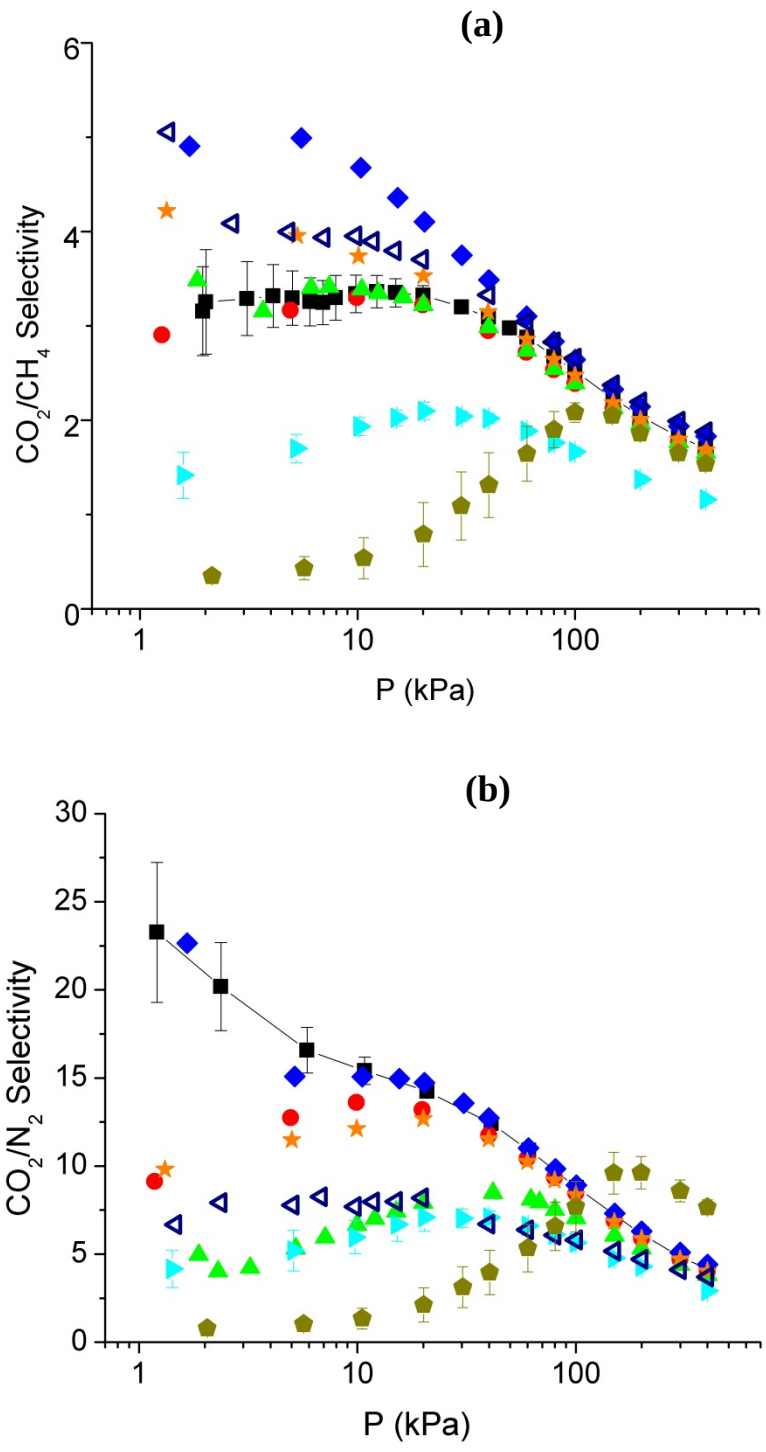

Figure 2.10: CO_2/CH_4 **(a)**, and CO_2/N_2 **(b)** single component adsorption selectivity at 293 K for pure silica MFI before modification (—■—), and after modification with 1-butanol (●), 1-hexanol (▲), 3-amino-1-propanol (◆), 1-propaneamine (▶), 1,3-diaminopropane (★) , 2-[(2-aminoethyl)amino]ethanol (◀), and benzenemethanol (⬟).

Figures 2.10a-2.10b show the CO_2/CH_4 and CO_2/N_2 ideal adsorption selectivity of all the zeolitic materials in the 0-400 kPa pressure range based on the measured single-component isotherms. Modification of MFI with 3-amino-1-propanol leads to the largest increase (67%) in the CO_2/CH_4 selectivity, while modification with benzenemethanol suppresses the selectivity to the greatest extent (83%).

On the other hand, the CO_2/N_2 adsorption selectivity of the modified materials generally shows a large decrease in comparison to the bare MFI material. In the low pressure region, MFI/3-amino-1-propanol shows the highest CO_2/N_2 selectivity among the modified materials due to favorable interactions with CO_2, and MFI/benzenemethanol shows the lowest selectivity. However, at pressures above 100 kPa, the MFI/benzenemethanol material shows higher selectivity than other modified materials as well as bare MFI. This is due to its much lower N_2 adsorption at higher pressures than the other materials. Overall, the organic-modified materials show a range of interesting adsorption selectivity behavior in comparison to the bare MFI material.

2.4. Conclusions

In this chapter, I have investigated and reported the gas adsorption properties of zeolite MFI/organic hybrid materials. I have shown that the interactions of zeolite MFI with CO_2, CH_4, and N_2 can be influenced by internal-surface modification with organic molecules, thereby providing a “handle” to tune the adsorption and transport properties of zeolitic materials above and beyond their framework structure and composition. To demonstrate this, several types of organic species have been chemisorbed on the silanol

sites in zeolite MFI, obtaining loadings in the range of 0.38-1.08 mmol/g SiO_2. TGA/DSC and $^{13}C/^{29}Si$ NMR characterizations indicated that the functional groups are chemically bound to the zeolite framework, and the loading is strongly related to the concentration of internal silanol defects. Gas adsorption isotherms of the modified zeolite materials show a range of properties different from that of the bare MFI zeolite, with the MFI/3-amino-1-propanol and MFI/benzenemethanol materials showing the largest differences from bare MFI. These properties are qualitatively explained by the known affinity of amino- and hydroxyl groups for CO_2, and of the phenyl group for CH_4, respectively. Although not presented in this thesis, my findings also lead to the expectation that the chemisorbed organic species will have significant effects on the diffusion behavior of molecules in the zeolite channels.

CHAPTER 3- ORGANIC-MODIFICATION AND CHARACTERIZATION OF ZEOLITE MFI MEMBRANES

3.1. Introduction and Background

3.1.1. Introduction

In the last two decades, the preparation and separation properties of zeolite membranes have been extensively studied[17]. Zeolite membranes, in principle, might separate gas or liquid mixtures on the basis of differences in the molecular size and shape[27], but also on the basis of different adsorption properties[28]. The separation ability of a microporous membrane can be described by the interplay of the mixture adsorption equilibrium and the mixture diffusion.

Different methods for the controlled preparation of supported zeolite membranes have been established[90]. They can be distinguished as either *in situ* methods or secondary growth (seeded) methods. In the secondary growth method, the conditions of zeolite nucleation and crystal growth may be optimized independently, by decoupling them. With this method, secondary nucleation may be reduced or suppressed during crystal growth[41]. The first step is the deposition of the crystal seeds (usually 100-300 nm) on the surface of a support. This is usually done through dip-coating the support several times in the diluted seed suspension, or by spin coating. The seeding step is followed by crystal growth in hydrothermal reaction. The advantage of the membranes made by secondary growth over *in situ* method is the possibility to have oriented membranes by orienting the

seed crystals[5] and having a better control over optimizing different parts of the synthesis procedure.

The drawback of synthesizing zeolite membranes is the ease of formation of defects or non-zeolitic pores. These pores form intercrystalline pathways larger than the zeolite pores, and therefore are not usually selective. I have synthesized pure silica MFI membranes (silicalite-1) on lab made Al_2O_3 supports. The quality of membranes was checked by N_2/SF_6 or H_2/CO_2 single component permeation selectivity.

The objective of this chapter is to investigate whether significant differences can be found in the transport of gas molecules through organic-modified MFI membranes in comparison to bare MFI membranes. Based upon the results in Chapter 2 of this work, the same organic-modification strategy of particles is used to modify the internal pore structure of MFI membranes. Photoacoustic IR (PA-FTIR) spectroscopy is used to verify the existence of functional groups in the MFI membrane. For PA-FTIR characterization, MFI membranes were functionalizaed with 1-butanol, 1-hexanol, 3-amino-1-propanol, 1-propaneamine, 1,3-diaminopropane, 2-[(2-aminoethyl)amino]ethanol, and benzenemethanol.

Single-component permeation measurements of several gases were performed on the bare and modified MFI membrane to see the overall change in properties of the membrane due to the presence of modifying organic groups. For permeation measurements, MFI membranes were modified with 1-butanol, 3-amino-1-propanol, 2-

[(2-aminoethyl)amino]ethanol, and benzenemethanol. The results were explained in terms of changes in the interactions between the adsorbate and the zeolite framework, as created by the presence of the modifying organic groups.

3.1.2. Zeolite Membrane Modification

Zeolite modified membranes have only been reported in very limited instances yet[50,69]. Modifications of the DDR and MFI types of zeolite membranes have been reported in an attempt to enhance the H_2 selectivity. The DDR type membranes were modified by counter diffusion chemical vapor deposition (CVD) of silica using tetraethylorthosilicate (TEOS) as a precursor to reduce the size of the intercrystalline pores.[91,92] The MFI-type zeolite membranes were modified by catalytic thermal cracking of preadsorbed methyldiethoxysilane (MDES) to deposit molecular silica in the intracrystalline pores and intercrystalline spaces.[93,94] The MDES molecule is nearly linear with a kinetic size of 0.4×0.91nm, which is small enough to enter the MFI zeolitic pores of 0.56 nm in size. TEOS and tetramethoxysilane (TMOS) are common precursors for the modification of MFI zeolite external surfaces and intercrystalline pores in membranes. The TMOS and TEOS molecules are nearly spherical with large sizes of 0.89 and 0.96 nm, respectively. MFI modification with TMOS and TEOS is done by the CVD method, and because these molecules are too large to enter the intracrystalline MFI zeolite pores, zeolite external surfaces and intercrystalline pores are modified. After the CVD modifications, the H_2 selectivity with respect to CO_2 increased to more than 100. The H_2 permeance decreased by approximately an order of magnitude, although it still remained high[95].

Tang *et al*.[69] modified zeolite MFI membranes by depositing molecular silica at a small number of active sites in the internal surface. This procedure increased H_2 selectivity without drastically decreasing the H_2 permeance and was done by *in situ* catalytic cracking of a silane precursor. The limited silica deposition reduced the effective size of the zeolitic channels, dramatically enhancing the H_2/CO_2 selectivity without causing a large increase in H_2 transport resistance. The modified zeolite membrane achieved H_2/CO_2 permselectivity of 141 with a H_2 permeance of 3.96×10^{-7} $\frac{mol}{Pa.m^2.s}$ at 450 °C.

Yeong *et al*.[96] synthesized propylsulfonic acid-functionalized MFI membranes and arenesulfonic acid-functionalized MFI membranes for *m*-xylene isomerization reactions. These membranes were synthesized over α-alumina supports via one-step *in situ* hydrothermal crystallization and subsequent post-synthesis modification. The total acid capacity increased with increase in organosilane concentration in the synthesis mixture. Both membranes were tested for their catalytic activity in *m*-xylene isomerization reaction in the temperature range of 355–450 °C. Due to higher acid density, arenesulfonic acid-functionalized MFI membrane gave higher catalytic activity compared to propylsulfonic acid-functionalized MFI membrane.

Unlike the limited work that has been reported for zeolite modification, many modified mesoporous particles and materials have been reported in literature[70]. These examples pertaining to mesoporous modified membranes can be used as a guide to select suitable organic groups for zeolite modification.

3.1.3. MFI Membrane Characterization

X-ray diffraction has been widely used for verifying membrane framework structure and for determining the orientation of the membrane. SEM imaging of the cross section and the top of membrane is used to assess the thickness of the membrane and check the quality of membrane for possible cracks on the top surface. Step-scan photoacoustic (SS-PAS) FT-IR spectroscopy has been utilized to investigate the distribution of guest molecules embedded in zeolite membranes[6,97,98]. Concentration profiles of guest molecules in a membrane were determined using theoretical analysis methods combined with experimental PA-FTIR data. SS-PAS offers a spatially resolved, *in situ,* nondestructive measurement of the concentration distributions of organic molecules through a membrane system. In SS-PAS, IR radiation modulated (chopped) at an acoustic frequency (5-1000 Hz range) is absorbed by a sample and converted to heat, which propagates out of the sample as an acoustic wave to create modulated pressure in the gas surrounding the sample in the cell. This signal is detected by a sensitive microphone and transformed to an IR spectrum. Figure 3.1 shows different parts of the SS-PAS experimental set up. The depth (μ_s) over which the thermal signal is generated is directly related to the modulation frequency (*f*) as shown by Equation 3.1.

$$\mu_s = (\alpha/\pi f)^{0.5} \tag{3.1}$$

In Equation 3.1, α is the thermal diffusivity (m^2/s) of the material. Zeolite materials have low thermal diffusivities ($\alpha < 10^{-6}$ m^2/s) and the membrane is characterized as “thermally thick”. This means that the thermal diffusion length (μ_s) is

much smaller than the optical absorption length (μ_β)[98]. Depth-dependent information can be obtained by varying the modulation frequency. For example, using a modulation frequency of 100 Hz, approximately probes the sampling depth of 50 μm in a continuous zeolite film. The use of a step-scan interferometer allows the chosen modulation frequency to provide the same sampling depth over the entire spectral range. Figure 3.1 shows the experimental set up for SS-PAS experiment that can be used for probing molecules permeating through the zeolite membrane.

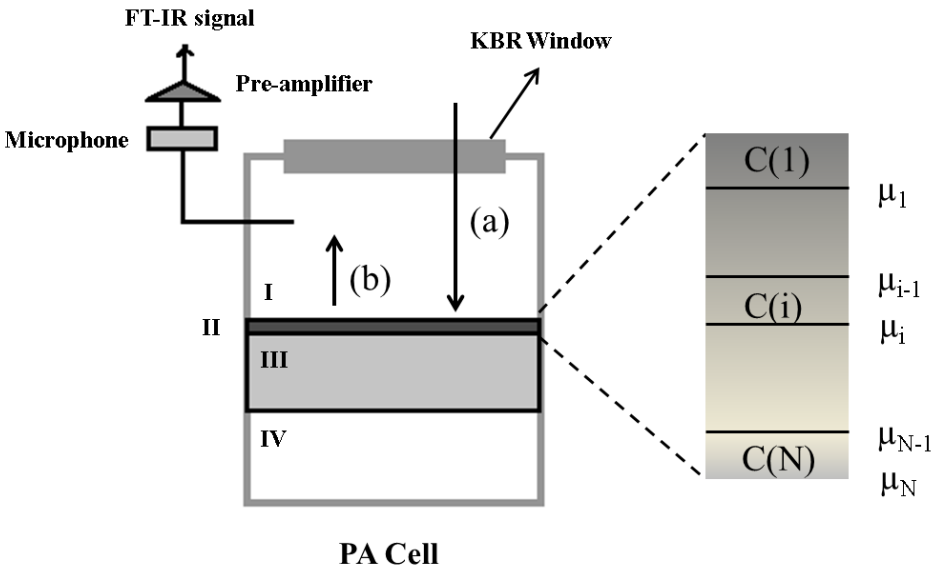

Figure 3.1: Schematic of SSPAS experiment: (a) frequency-modulated incident IR signal, (b) generated acoustic signal. Region (I) feed side: He or a guest vapor mixed with He carrier gas, (II) MFI membrane, (III) α-alumina substrate, and (IV) He as a sweep gas (Adapted with permission from Oh *et. al*[6])

Oh *et. al.*[6,98] proposed analytical expressions describing the strength of the photoacoustic signal from a membrane of continuously varying composition and its application in creating a concentration profile from SS-PAS measurements for zeolite

MFI membrane system. In this thesis, SS-PAS FTIR measurements were utilized to confirm the existence of functional groups in the modified membranes. It has not been used to determine the depth profile of functional groups. SS-PAS FTIR has been referred to as PA-FTIR in the rest of the thesis for brevity.

3.1.4. MFI Membrane Permeation Measurements

Preparations of MFI zeolite membranes (also containing non-zeolitic pores) were first reported in early 1990s. Bakker *et al*.[99] reported the temperature dependence of single-component permeation through MFI membrane for various gases. Adsorption and diffusion have contradicting effects on permeation as the temperature is changed. The amount of adsorption decreases with increasing temperature due to its exothermic nature. Diffusion, on the other hand, increases with increasing temperature because more molecules are able to overcome the diffusion activation barrier. Adsorption can often be modeled with a Langmuir isotherm in zeolites (Equation 3.2 and 3.3). In this model, θ is the fractional occupancy, q (mmol/g) is the loading amount, K is the adsorption equilibrium constant, and ΔH_{ads} (kJ/mol) is the heat of adsorption. One can fit this model to the experimental adsorption data and get q^{sat}, K_0 and ΔH_{ads}. The heat of adsorption is particularly important because it contains information about the nature of interactions between the sorbate molecules and the zeolite.

$$\theta = \frac{q}{q_{sat}} = \frac{KP}{1+KP} \tag{3.2}$$

$$K = \exp(\frac{-\Delta G}{RT}) = \exp(\frac{\Delta S}{R} + \frac{-\Delta H_{ads}}{RT}) = K_0 \exp(\frac{-\Delta H_{ads}}{RT}) \tag{3.3}$$

For single component permeation of several gases through MFI membranes, one can observe that permeation increases with increasing temperature, goes through a maximum and then decreases. Bakker *et al.*[99] proposed a surface-diffusion model in combination with activated gas diffusion to explain the temperature dependence of single-component permeance. At low temperatures, the transport of the permeating species through a MFI membrane is dominated by adsorption and can be described by adsorption followed by surface diffusion. Mass transport mechanism in the adsorbed phase can be pictured as molecules hopping between fixed sites. However, at high temperatures, the activated gas diffusion controls the permeation process.

The existence of three main types of permeation pathways through zeolite membranes have been considered as contributing simultaneously to membrane permeance in the literature[18]: (1) zeolitic pores of nominal size 5.5 Å for MFI; (2) nonzeolitic micropores of size <10 Å, possibly formed by gaps between adjacent zeolite crystals; and (3) mesopores or macropores of pore size >20 Å. Mesopores can arise from large defects such as dome defects formed in areas of low coverage of seed crystals on the support prior to secondary growth or cracks formed after calcination for template removal, as suggested by Dong *et al.*[47]. The temperature dependence of permeation through zeolitic or nonzeolitic microporous pathways is determined by the relative magnitude of the activation energy for diffusion, E_D, and the heat of adsorption, Q_{st}.[100] In the case of $Q_{st} > E_D$ (e.g., strong adsorption in the micropores), the permeation flux usually shows a maximum with temperature, whereas in the case of $E_D > Q_{st}$ (e.g., high

hindrance for diffusion), the permeation flux increases monotonically with temperature. Permeation through larger mesoporous pathways (~2 - 50 nm in diameter) follows Knudsen diffusion transport mechanism. Knudsen diffusion occurs when the mean free path of the gas molecules is larger than the pore radius of the membrane. In this case, there are more collisions with the pore walls than between the gas molecules. Knudsen diffusion decreases with temperature according to the inverse square root law[101].

The Maxwell –Stefan equations of transport have been used to model transport in zeolites[102,103]. In this method, the flux is proportional to the chemical potential gradient ($\frac{\partial \mu}{\partial z}$) as the driving force of transport. With this model, adsorption and diffusion effects can also be studied separately. The Maxwell-Stefan equations for single component transport are shown in Equation 3.4 and 3.5.[102,103]

$$J = -\rho q_{sat} \theta \frac{D_{MS}}{RT} \frac{\partial \mu}{\partial z} = -\rho q_{sat} D_{MS} \Gamma \frac{\partial \theta}{\partial z} \tag{3.4}$$

$$\Pi = \frac{J}{\Delta P} \tag{3.5}$$

In these equations, J is the flux, ρ is the density of the membrane, Γ is the thermodynamic correction factor, D_{MS} is the Maxwell-Stefan diffusion, Π is the permeance and ΔP is the pressure difference over the membrane. The thermodynamic correction factor can be obtained from the adsorption isotherms. The Fick diffusivity, also known as the transport diffusivity, (D_{Fick}) can be measured experimentally for

zeolite particles (Equation 3.6) and is related to the Maxwell-Stefan diffusivity (D_{MS}) by the Darken equation (Equation 3.7):[99,104,105]

$$J = -\rho q_{sat} D_{Fick} \frac{\partial \theta}{\partial z} \tag{3.6}$$

$$D_{Fick} = D_{MS} \Gamma \tag{3.7}$$

If the adsorption isotherm and diffusion data is available, one can predict single-component flux and permeability using the Maxwell-Stefan equations. The Maxwell-Stefan equations can be generalized to give multicomponent permeation as well. Van den Broeke *et al.*[7,106] have used the generalized Maxwell-Stefan (GMS) equations together with ideal adsorption theory to model the fluxes and the separation factor of CO_2/CH_4 mixtures through zeolite membranes. The binary gas selectivity is quite different from the predicted ideal single-component selectivity.

In Figure 3.2, Van den Broeke[7] reports that CO_2 permeances far exceed those of CH_4 in the binary permeation experiments, contrary to the ideal solution predictions based solely on single-component permeation.

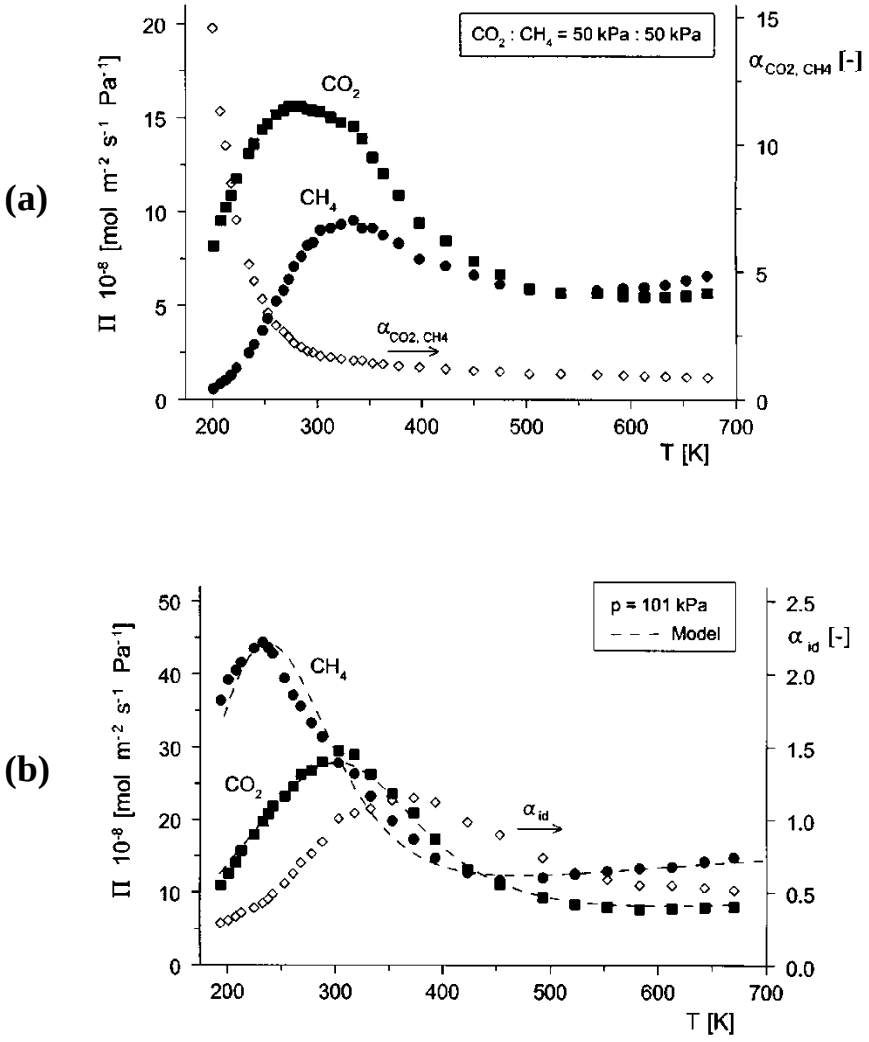

Figure 3.2: Permeation and separation factor for a 1:1 mixture of CO_2 and CH_4 as a function of temperature. Binary permeances and separation factor **(a)**. Single-component permeances and ideal separation factor **(b)**. (Reproduced with permission from Van den Broeke[7])

3.2. Experimental Methods

3.2.1. MFI Membrane Synthesis

MFI membranes have been synthesized with a secondary growth method in this thesis. The procedure of Kumar *et al.*[107] was followed in preparing the lab made α-alumina supports. 2.1 g α-alumina powder is thoroughly mixed with 4% DI water in mortar and pestle. The mixture is put in a 25mm diameter press die It. is pressed for 30s at 5000 lbs, followed by 2 min at 15000 lbs. Disks are put in a 60 °C oven overnight to dry. The dried disks are put in the furnace for sintering. In this step, the disks are exposed to very high temperature (above 1000 °C), in order to cross-link the disks further and increase their mechanical stability. The furnace temperature program starts with ramping up the temperature to 600 °C by 1 °C/min rate. The 600 °C temperature is maintained for 3 hrs. Then the temperature is increased to 1150 °C with 1 °C/min rate. The temperature is maintained at 1150 °C for 35 hrs. Then the temperature is decreased to room temperature by 1 °C/min rate.

To get the fired disks to be good supports for MFI membranes, the surface of the α-alumina disks are polished with sand paper and water using a Buehler® polishing instrument until the surface is shiny. Supports are then dried for at least 4 hours in 60 °C. Supports are seed coated with dip coating method 3 times, using 100 nm-300 nm MFI particles. Seed particles are synthesized with molar composition of 5 SiO_2: 1 TPAOH: 161 H_2O: 20 EtOH. For two 45 ml autoclaves, 39.0 g DI H2O was mixed with 21.0 g TPAOH (1 M solution is water, Aldrich). Under vigorous stirring (~ 700 RPM), 20.0 g TEOS (98% Aldrich) is added to the solution dropwise. The solution is filtered in the

autoclaves and put in the synthesis oven for 24 hours at 100 °C while rotating. The particles are then washed and centrifuged three times and dried overnight. The MFI particles were calcined at 550 °C for 8 hours with 3 °C/min ramp rate.

The seed solution for dip coating is prepared at 2 g/L concentration of seeds in DI water. The supports were put in contact with the solution at the liquid/gas interface and remained for about 1 min. The capillary pressure helps in taking the solution during dip coating, and the suspended seeds get deposited on the support's surface. The supports are then taken out of the solution and put in an angle (~ 45 °) to dry. After drying, the seed coating procedure continues for another 2 times to make sure of uniform deposition of seeds on the surface of the support.

The MFI membrane synthesis used in this thesis has been reported in several papers from the Tsapatsis group.[18,19,22,39] The precursor solution composition was 4 TEOS: 0.9 TPABr: 0.9 KOH: 940 H_2O. First DI water, TPABr and KOH are mixed for about 5 minutes. Then TEOS is added to the solution dropwise. The solution is left stirring for 3-4 hours until it is clear. The solution is filtered and put in the autoclaves. Polished supports need to be put in the autoclave face down and at 30-60° angle to minimize direct deposition of MFI particles on top of the membrane. Figure 3.3 shows the support positioning in the autoclave before hydrothermal synthesis. Autoclaves were put in the oven for hydrothermal synthesis at 140°C for 24 or 48 hours. These conditions yield *[h0h]* (or *[101]*) oriented membranes with about 6 µm thickness for 24 hours

duration and about 10 µm thicknesses for 48 hours duration. I have reported the results for the 6 µm thickness membranes in this chapter.

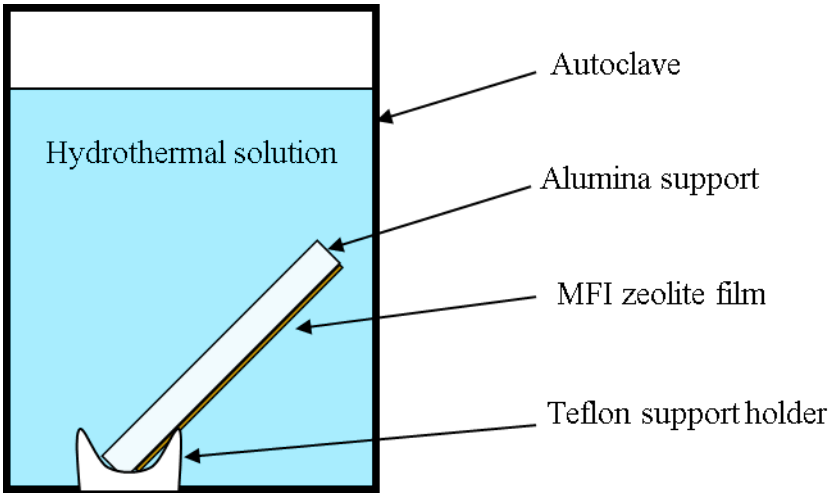

Figure 3.3: Schematic of MFI membrane support positioning during hydrothermal growth.

After taking the membranes out of autoclaves, they were washed with DI water to remove any organic residues and were put in the 60 °C oven to dry overnight. Membranes were then calcined at 500 °C for 8 hours with 1 °C/min for the ramp rate and the rate of cooling.

3.2.2. Organic-Modification Procedures

Organic modification reactions were done under neat conditions. In a 100 ml flat-bottom flask, the MFI membrane was degassed at 100 °C for 4 hours and then approximately 20 g of the desired organic material was added. The flask was then

immersed in silicone oil bath at 110 °C for 48 hours while stirring. For PA-FTIR study, membranes were modified with 1-butanol, 1-hexanol, 3-amino-1-propanol, 1-propaneamine, 1,3-diaminopropane, 2-[(2-aminoethyl)amino]ethanol, and benzenemethanol. The reaction conditions for 1-propaneamine were 25°C for 48 hours due to its low boiling point. For membrane permeation studies, membranes were modified 1-butanol, 3-amino-1-propanol, 2-[(2-aminoethyl)amino]ethanol, and benzenemethanol. After modification reaction at 110°C, back of the MFI membranes were dried gently by Kleenex and they were put on vacuum for 8 hours at room temperature. Similar to particle modification, this was followed by 24 hours of vacuum at 150 °C before performing other characterizations.

3.2.3. Characterization Methods

Scanning electron microscope (SEM) images of the MFI zeolite membranes were taken on a Zeiss Ultra 60 operating at 2-5 kV. Powder X-ray diffraction (XRD) patterns were obtained on a Philips X'pert Pro diffractometer equipped with X'celerator using Cu Kα radiation. Samples were analyzed over a range of 5-55° 2θ with a step size of 0.02°. Photo-acoustic IR (PA-FTIR) was employed in order to show existence of functional groups in the membranes. Single gas permeation of H_2, CO_2, N_2, CH_4, *i*-butane, *n*-butane, and SF_6 were measured for the bare and modified membranes at 30 psia feed pressure and vacuum at permeates side. The measurements were carried out on a lab-made permeation system which I fabricated and installed. The permeation system schematic is shown in Figure 3.4.

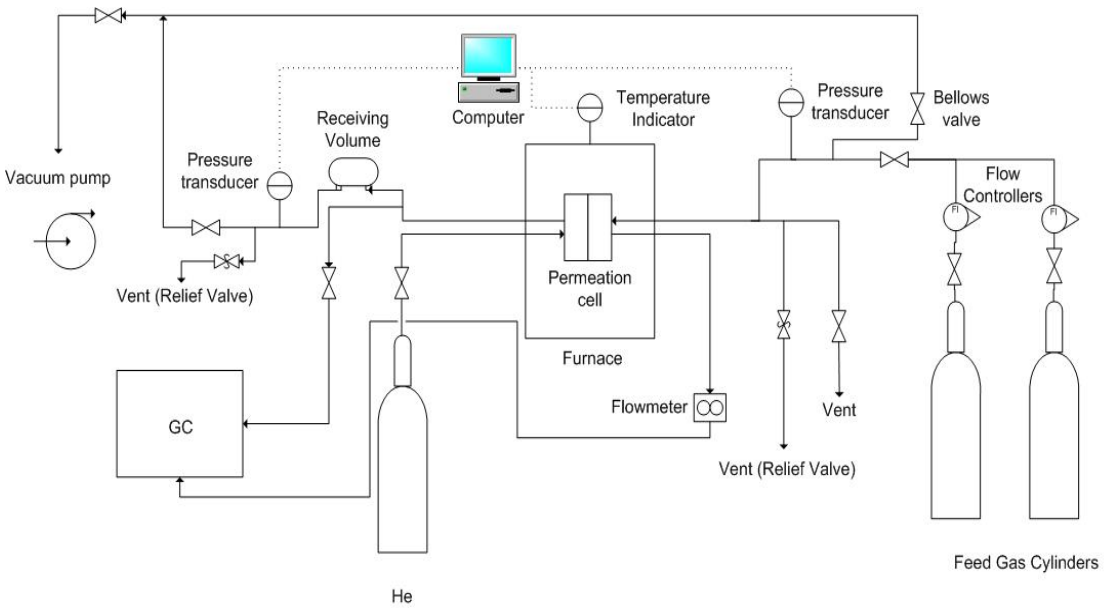

Figure 3.4: Schematic of the gas permeation system.

3.3. Results and Discussion

3.3.1. Orientation of the MFI Membranes

Figure 3.5 shows the typical XRD pattern of calcined membranes synthesized in this study. The dominant orientation is the *[hoh]* orientation in all of the synthesized membranes.

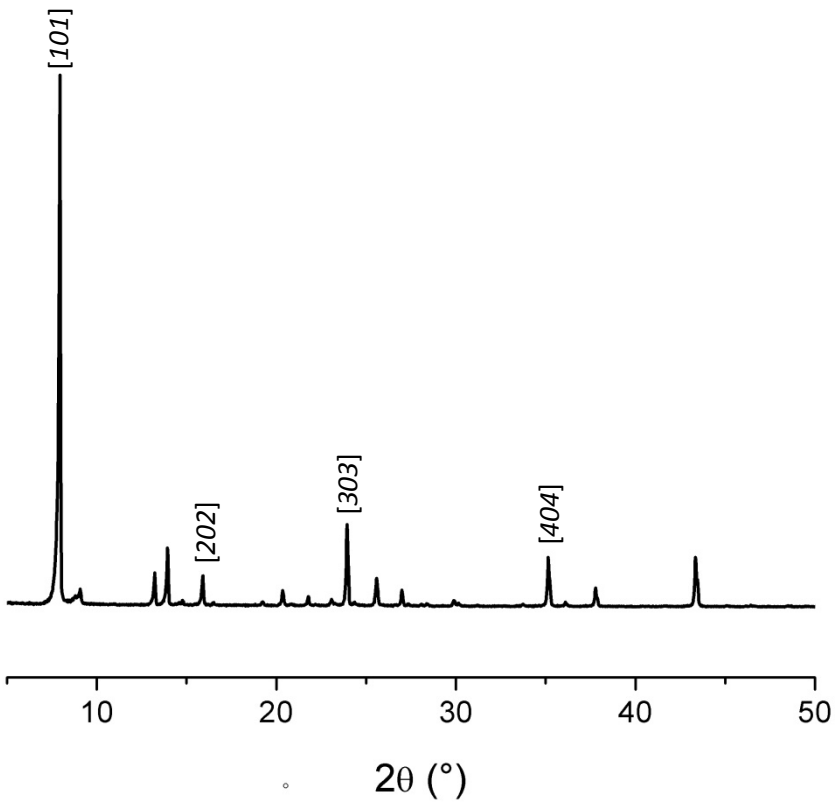

Figure 3.5: XRD pattern of a representative calcined MFI membrane.

The quality of the alumina support is one of the most important factors affecting the quality of the synthesized zeolite membrane. Before hydrothermal synthesis, the SEM images of the seed coated supports need to be observed to see if the seeds have covered the whole surface uniformly. Figure 3.6 shows SEM image of seed coated low quality (commercial) and lab made supports after seed coating. The low quality support has a rough surface that prevents having a uniform layer on top of the support.

(a)

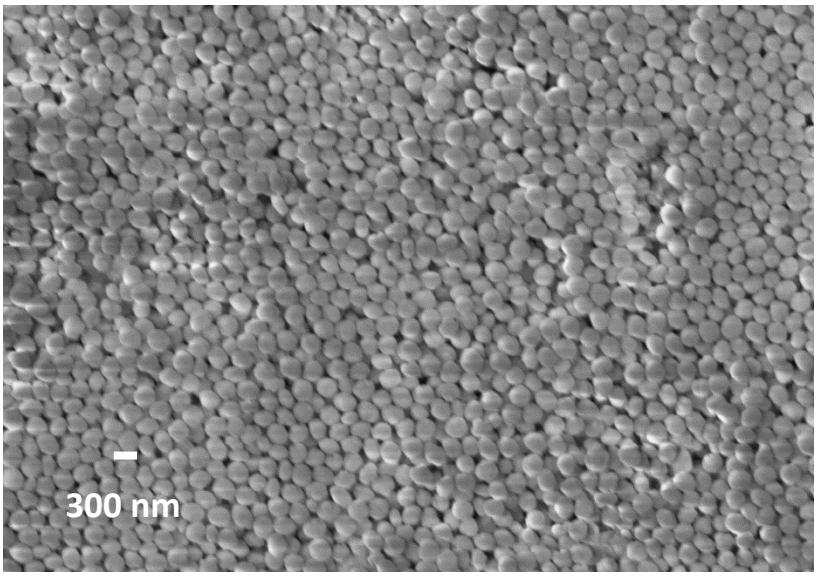

(b)

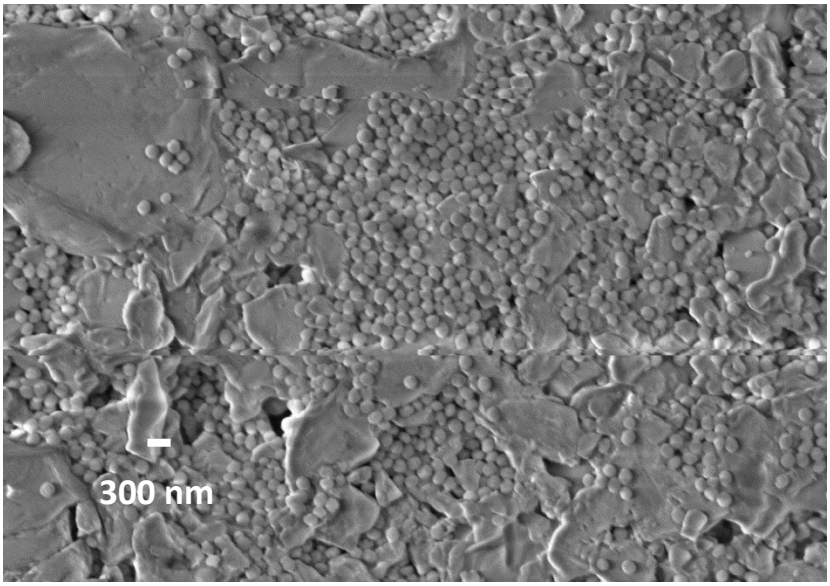

Figure 3.6: SEM of seed coated support on lab made support (a) and commercial support (b).

As described in the experimental section, MFI membranes were hydrothermally synthesized at 140°C for either 24 hours or 48 hours. Figure 3.7 shows SEM images of top view and cross section of membranes used in this study. The observed membrane

thickness for 48 hours duration is between 8-11 µm, while the thickness for the 24 hours duration is between 5-7 µm.

(a)

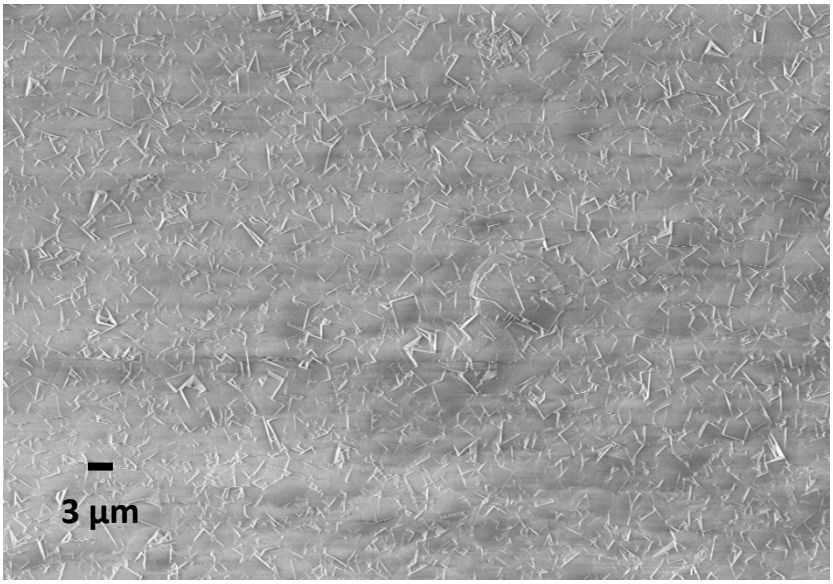

(b)

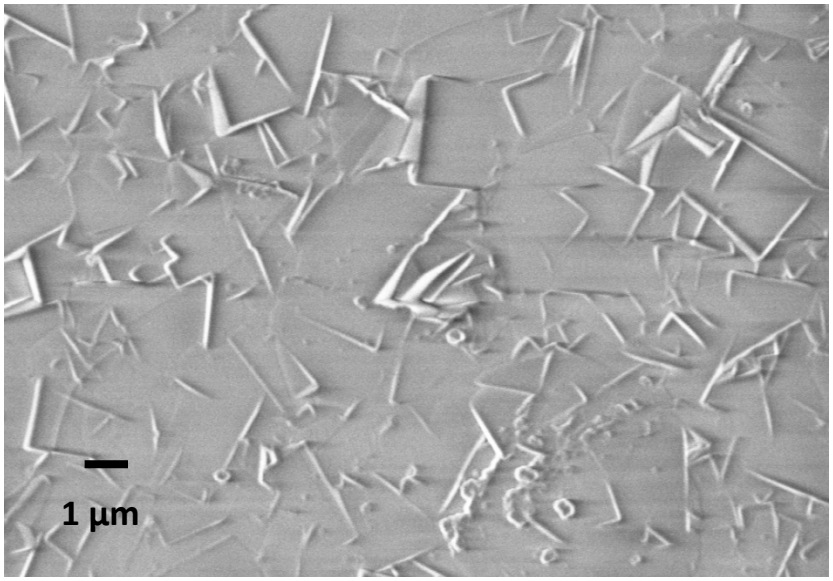

(c)

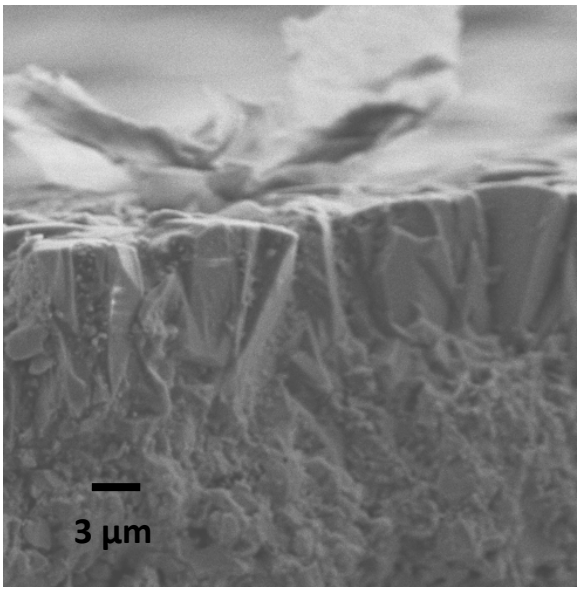

(d)

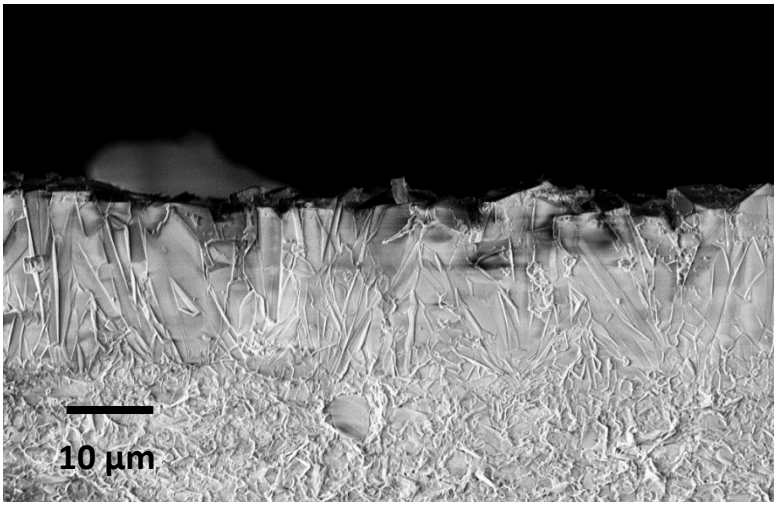

Figure 3.7: SEM images of synthesized MFI membranes: Top view (a), (b) and cross section view at 24 hours synthesis duration (c), and at 48 hours duration (d).

3.3.2. PA-FTIR Characterization

The PA-FTIR technique is used to detect and show the existence of functional groups in the modified membranes. A modulation frequency of 101 Hz was chosen for characterizing modified MFI membranes (or MFI films). This frequency probes a depth of approximately 50 μm in samples. This is appropriate since it covers the thickness of 10 μm membrane and some of the support. Due to high vacuum at 150 °C treatment of the membrane after modification, it is not expected to see organic contribution from the support. Figure 3.8 shows the PA-FTIR spectra of calcined MFI membrane (bare MFI) and functionalized MFI membrane with 1-butanol, 1-hexanol, 3-amino-1-propanol, 1-propaneamine, 1,3-diaminopropane, 2-[(2-aminoethyl)amino]ethanol, and benzenemethanol. The spectra for modified MFI were normalized in regard to bare MFI by scaling the spectra to match the highest peak of the spectrum.

All of the studied functional groups, if present, are expected to display C-H vibrational signatures. In Figure 3.8, the C-H stretching mode is indeed observed close to 2900 cm^{-1} in all of the modified MFI membranes. This clearly shows the existence of the functional groups in the MFI membranes.

(1)

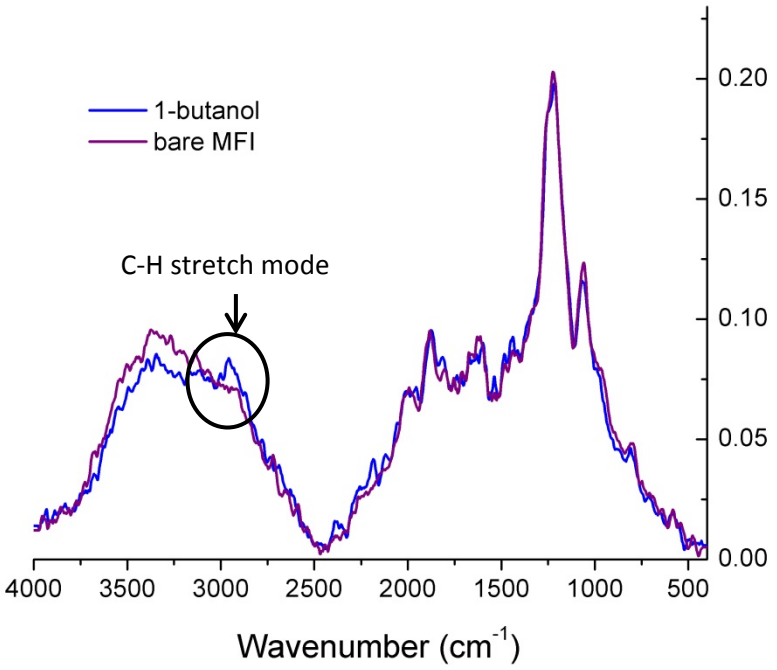
1-butanol
bare MFI
C-H stretch mode
0.20
0.15
0.10
0.05
0.00
4000
3500
3000
2500
2000
1500
1000
500
Wavenumber (cm-1)

(2)

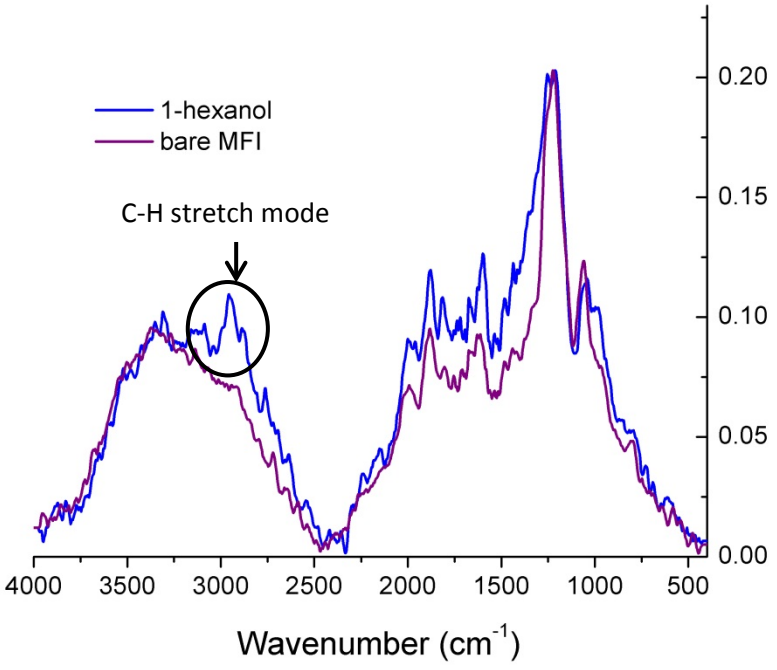
1-hexanol
bare MFI
C-H stretch mode
0.20
0.15
0.10
0.05
0.00
4000
3500
3000
2500
2000
1500
1000
500
Wavenumber (cm-1)

(3)

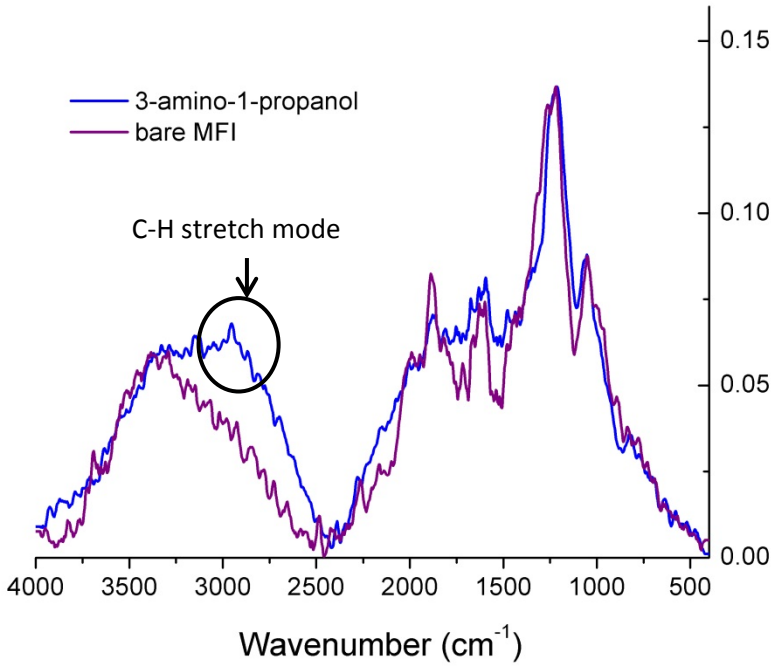
3-amino-1-propanol
bare MFI
C-H stretch mode
0.15
0.10
0.05
0.00
4000
3500
3000
2500
2000
1500
1000
500
Wavenumber (cm-1)

(4)

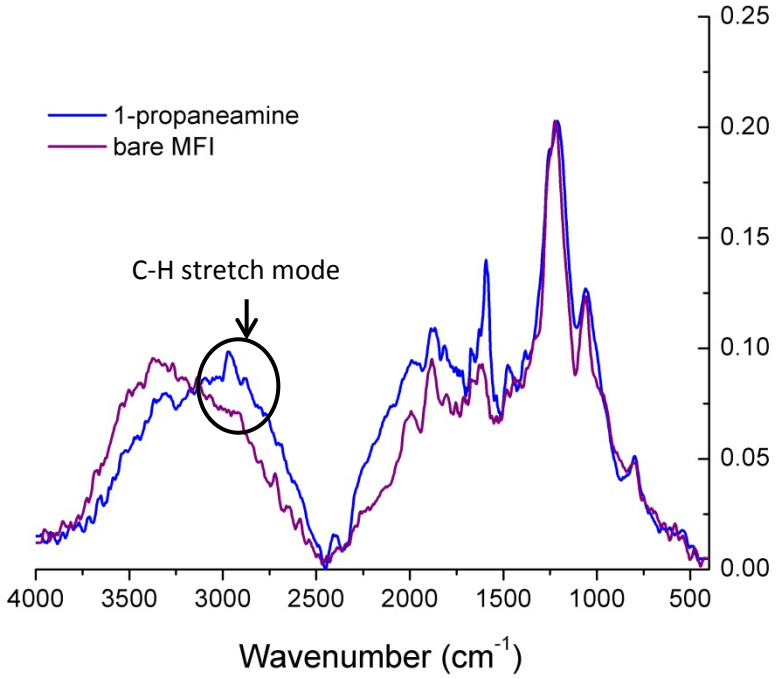
1-propaneamine
bare MFI
C-H stretch mode
0.25
0.20
0.15
0.10
0.05
0.00
4000
3500
3000
2500
2000
1500
1000
500
Wavenumber (cm-1)

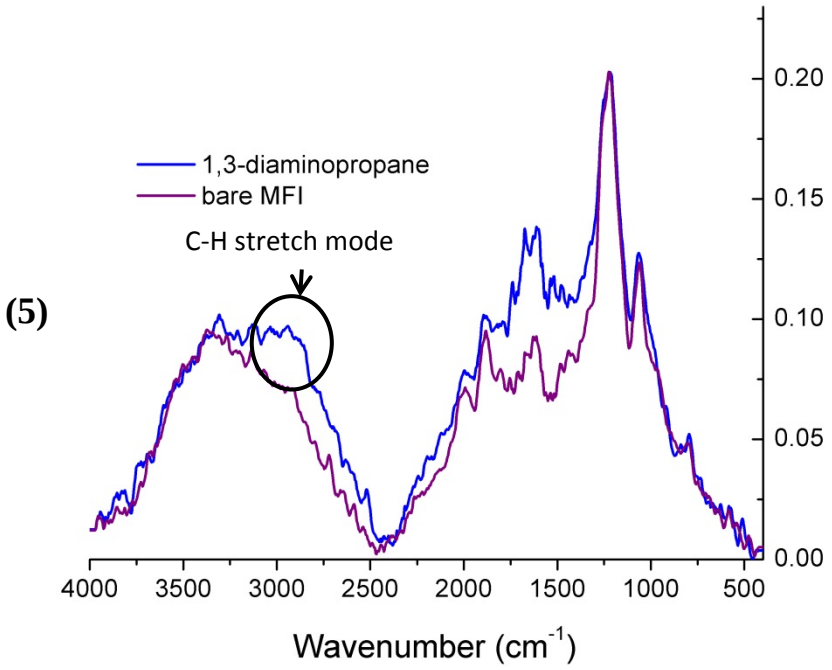
(5)
1,3-diaminopropane
bare MFI
C-H stretch mode
0.20
0.15
0.10
0.05
0.00
4000
3500
3000
2500
2000
1500
1000
500
Wavenumber (cm-1)

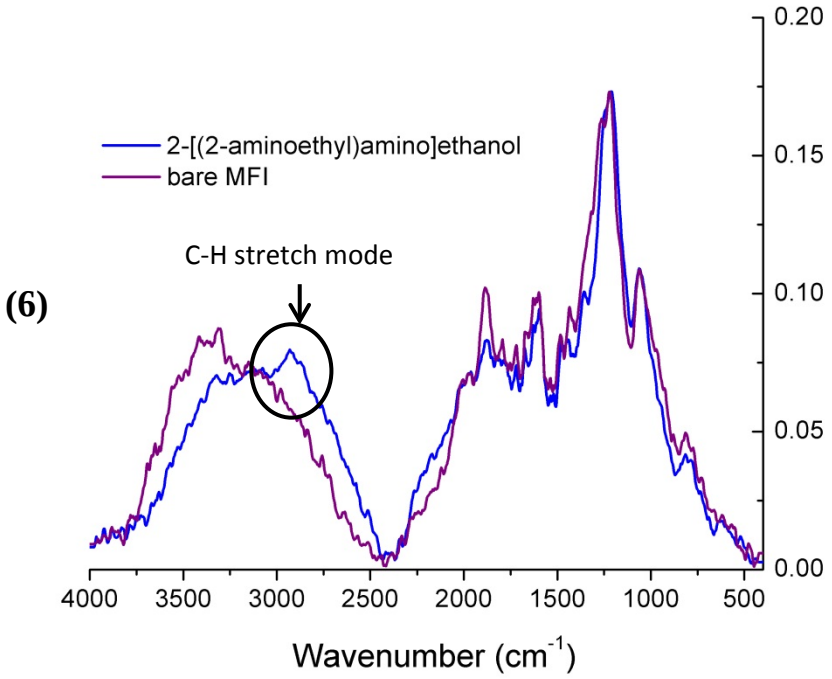
(6)
2-[(2-aminoethyl)amino]ethanol
bare MFI
C-H stretch mode
0.20
0.15
0.10
0.05
0.00
4000
3500
3000
2500
2000
1500
1000
500
Wavenumber (cm-1)

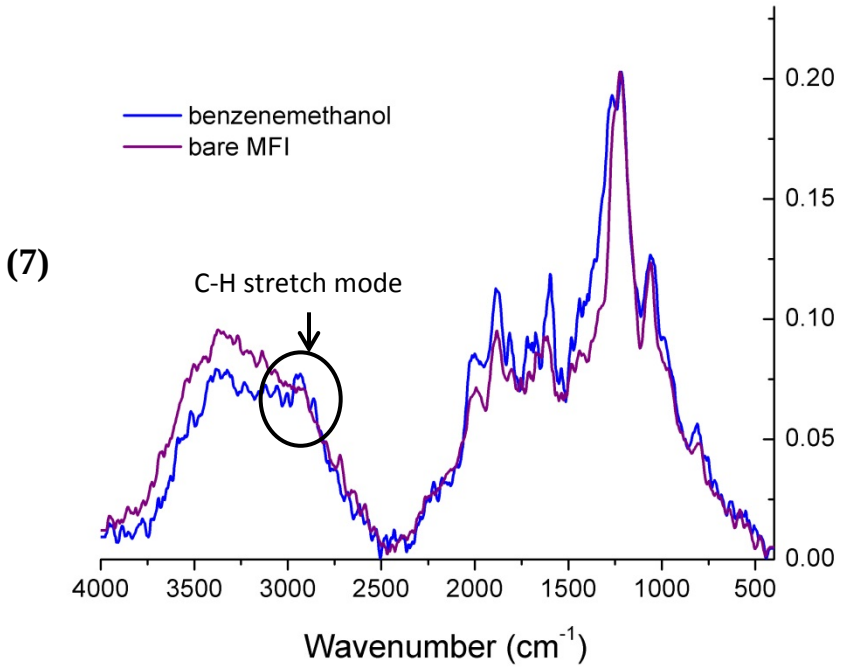

Figure 3.8: PA-FTIR spectra of calcined MFI membrane (bare MFI) and modified membrane with: 1-butanol (1), 1-hexanol (2), 3-amino-1-propanol (3), 1-propaneamine (4), 1,3-diaminopropane (5), 2-[(2-aminoethyl)amino]ethanol (6), and benzenemethanol (7).

3.3.3. Permeation Measurements

In order to study the effect of modification on MFI membrane permeability, I have measured single gas permeation properties of H_2, CO_2, N_2, CH_4 and SF_6 through the MFI membranes before and after modification Figure 3.9 shows the kinetic diameter of the gases being tested for permeation[108]. For permeation measurements, modification was performed with 1-butanol, 3-amino-1-propanol, 2-[(2-aminoethyl)amino]ethanol, and benzenemethanol. *n*-butane and *i*-butane permeation was carried out for one of the MFI membrane, before and after being modified with 1-butanol.

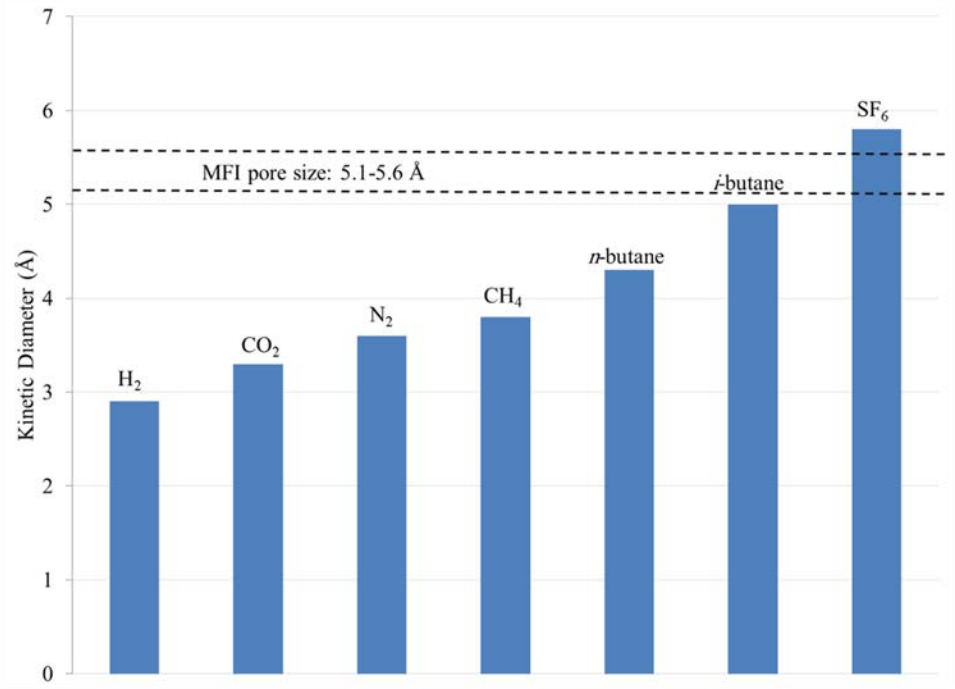

Figure 3.9: Kinetic diameters of test gases with respect to MFI pore size

Table 3.1 shows the permeances of different gases through bare and modified zeolite membranes. From permeation experiments, the total permeation through zeolite membrane and the support is measured. As shown in Equation 3.8, the permeances of the support ($P_{support}$) and zeolite membrane ($P_{zeolite\ membrane}$) are in series:

$$\frac{1}{P_{total}} = \frac{1}{P_{Support}} + \frac{1}{P_{zeolite\ membrane}} \tag{3.8}$$

Permeances of the support (α-alumina) were measured for H_2 (600), N_2 (409), CO_2 (429), CH_4 (598), SF_6 (400). The permeance unit is $10^{-8}\ \frac{mol}{Pa.m^2.s}$. Permeation through zeolite membrane is calculated from Equation 3.8. In the subsequent tables, the intrinsic permeances through the zeolite membrane are reported. After modification,

almost all of the gas permeances decrease by 1-2 orders of magnitude. This is a strong indication that the organic species are in fact strongly influencing the gas molecule transport through the MFI pores.

Table 3.1: Permeances of MFI zeolite membranes (~ 6 μm thickness) before and after modification (units are in $10^{-8}\ \frac{mol}{Pa.m^2.s}$)

Zeolite Membrane	H_2	N_2	CO_2	CH_4	SF_6
Before Modification (1-butanol)	81.4	38.5	36.6	46.3	4.3
After Modification (1-butanol)	12.7	2.9	13.1	11.8	0.3
Before Modification (benzenemethanol)	79.0	44.4	43.0	64.9	3.5
After Modification (benzenemethanol)	1.1	0.4	0.39	0.4	0.1
Before Modification (2-[(2-aminoethyl)amino]ethanol)	93.1	48.7	50.2	75.9	4.5
After Modification (2-[(2-aminoethyl)amino]ethanol)	24.1	6.6	4.5	8.3	2.3

Permeation measurements for each gas were performed on the membranes after exposing the membrane to at least 20 minutes of vacuum at room temperature on the feed and permeate side. This is done to make sure there are no pre-adsorbed molecules (or species) in the membrane before starting a new permeation measurement. Longer vacuum times (up to 1.5 hours) are applied for the molecules with higher heat of adsorption in MFI (e.g. SF_6 and butane isomers). In order to make sure the vacuum procedure is effective in removing pre-adsorbed species, N_2 permeation has been measured before

measuring each of other gas permeations. Comparing the measured permeation and the initial N_2 permeation, all of the permeations changed less than 40%. This shows that the employed vacuum procedure has been effective in removing most of the pre-adsorbed species, and significant changes in permeations are not seen as a result vacuum procedure.

Table 3.2: Single component permeation selectivity of MFI membranes (~ 6 μm) for four important gas pairs.

Zeolite Membrane	H_2/CO_2	N_2/SF_6	CO_2/CH_4	CO_2/N_2
Knudsen selectivity (for reference)	4.7	2.3	0.6	0.8
Before Modification (1-butanol)	2.2	9.0	0.8	0.9
After Modification (1-butanol)	1.0	10.0	1.1	4.5
Before Modification (benzenemethanol)	1.8	12.5	0.7	1.0
After Modification (benzenemethanol)	2.7	3.5	1.0	1.0
Before Modification (2-[(2-aminoethyl)amino]ethanol)	1.9	10.8	0.7	1.0
After Modification (2-[(2-aminoethyl)amino]ethanol)	5.3	2.8	0.5	0.7

Table 3.2 shows the single component selectivity for several gas pairs before and after modification. The N_2/SF_6 single component permeation selectivity has been used by several researchers for indicating the quality of MFI membrane[18,19,22,39]. The N_2/SF_6 single component permeation is between 9-12 for membranes before modification and is in agreement with earlier reports[39]. After modification, N_2/SF_6 selectivity decreases for all of the modified membranes to near Knudsen diffusion selectivity. This indicates that

most of the flux for N_2 and SF_6 is now going through non-zeolitic pores (or defects) in the membrane, since the pores of the zeolite are effectively blocked.

The CO_2/CH_4 permeation selectivity is close to the Knudsen value (0.6) for the membranes before modification. CO_2/CH_4 selectivity increases for MFI/benzenemethanol modified membrane (1.0), whereas it decreases for MFI/2-[(2-aminoethyl)amino]ethanol modified membrane (0.5). From the adsorption isotherms presented in chapter 2, the MFI/benzenemethanol crystals were shown to have a highest sorption capacity for CH_4 over all the other molecules due to the interaction between CH_4 and the benzene ring. The higher sorption of CH_4 in MFI/benzenemethanol and its strong binding to the material are likely to be the reasons for the higher CO_2/CH_4 permeation selectivity. From the adsorption isotherms, MFI/2-[(2-aminoethyl)amino]ethanol crystals were shown to have a highest sorption capacity for CO_2 over all other studied molecules. The higher sorption of CO_2 in MFI/2-[(2-aminoethyl)amino]ethanol and its strong binding to the material are likely to be the reasons for the lower CO_2/CH_4 permeation selectivity in the modified membrane.

The quality of ceramic supported MFI membranes has been systematically investigated with permeation measurements of *n*-butane and *i*-butane (isobutene) with kinetic diameters of 4.3 Å and 5 Å, respectively[22,109]. A high single-component or binary permeation flux ratio of these isomers is generally used as a measure of membrane quality. The separation of butane isomers is governed by the difference in their adsorption behavior and their diffusion motilities[110]. As these two molecules are isomers,

they cannot be separated in mesopores by Knudsen diffusion, which is dependent on the molecular weight. Therefore the butane selectivity is a good way to detect the presence of nonzeolitic transport paths in MFI membranes.

Table 3.3 shows *n*-butane and *i*-butane permeances and selectivity before and after modification of the 6-µm thick MFI membrane with 1-butanol. This membrane is the same membrane modified with 1-butanol that its other gas permeation measurements were reported in Table 3.2. Permeations of butane isomers through the support are $500\times10^{-8}\ \frac{mol}{Pa.m^2.s}$, and updated permeances through zeolite membranes are reported. Before modification, single component selectivity for butane isomers (3.8) is higher than Knudsen diffusion (1), which indicates selectivity for *n*-butane over *i*-butane. After modification, permeation for both of the butane isomers decreased by an order of magnitude, while *n*-butane over *i*-butane selectivity increased more than 300% (to 12.8). By modifying the membrane with 1-butanol, some of the pores were blocked or constricted, and this resulted in lower permeances. Making some of the MFI channels narrower by modification is the likely reason that the linear *n*-butane molecule shows a higher selectivity than the branched *i*-butane molecule after modification.

Table 3.3: Permeances of butane isomers in MFI zeolite membrane (~ 6 µm) before and after modification with 1-butanol and their single component selectivity (units are in $10^{-8}\ \frac{mol}{Pa.m^2.s}$)

Zeolite Membrane	*n*-butane	*i*-butane	*n*/*i* butane selectivity
Before Modification	12.5	3.2	3.8
After Modification	2.5	0.2	12.8

Assuming that most of the observed flux (in the modified 6-μm membranes) is from non-zeolitic pores, improvements in the membrane selectivity may be realized if: (1) the degree of modification of the MFI structure with functional groups can be controlled, and (2) better control of the defects (e.g., by synthesis of thicker membranes or by post-treatment of the membranes) is achieved. In this regard, I then investigated the effect of membrane thickness as a means of sealing off defects present in thinner membranes and allowing a better evaluation of the effects of organic-modification of the MFI membranes. MFI membranes with 10 μm thickness were synthesized and modified with 1-butanol and 3-amino-1-propanol respectively. Table 3.4 shows single-component permeation of various gases for before and after modification. Table 3.5 shows the single-component selectivity for gas pairs before and after modification for these membranes.

Table 3.4: Permeances of MFI zeolite membranes (~ 10 μm) before and after modification (units are in 10^{-8} $\frac{mol}{Pa.m^2.s}$)

Zeolite Membrane	H_2	N_2	CO_2	CH_4	SF_6
Before Modification (1-butanol)	11.2	25.2	43.3	52.2	1.1
After Modification (1-butanol)	0.3	0.2	0.3	0.2	0.04
Before Modification (3-amino-1-propanol)	12.9	40.4	68.3	97.5	4.1
After Modification (3-amino-1-propanol)	0.8	0.3	0.2	0.4	0.05

Table 3.5: Single-component permeation selectivity of MFI membranes (~10 μm) for four important gas pairs

Zeolite Membrane	H_2/CO_2	N_2/SF_6	CO_2/CH_4	CO_2/N_2
Knudsen selectivity	4.7	2.3	0.6	0.8
Before Modification (1-butanol)	0.3	22.2	0.8	1.7
After Modification (1-butanol)	1.0	4.0	1.3	2.0
Before Modification (3-amino-1-propanol)	0.2	9.8	0.7	1.7
After Modification (3-amino-1-propanol)	3.7	5.9	0.6	0.7

Similar to the 6 μm thick membranes, all of the gas permeances were reduced 1-2 orders of magnitude after modification. Before modification, 10 μm thick membranes have comparable or better N_2/SF_6 permeation selectivity compared to 6 μm thick membranes indicating good quality of the membranes.

The H_2/CO_2 selectivity is less than 1 for 10 μm membranes before modification, whereas it is over 1 for the 6 μm membranes. This shows that 10 μm membranes have fewer defects, as expected, compared to 6 μm membranes. Single or binary H_2/CO_2 selectivity has been used as a metric for quality of MFI membrane, with having values less than 1, showing better quality. Due to its smaller size, H_2 is expected to have much higher permeances than CO_2 in a defective membrane. However, CO_2 is adsorbed more favorably than H_2 in MFI framework leading to higher permeances than H_2, and H_2/CO_2 selectivity lower than one in a defect free MFI membrane.

3.4. Conclusions

In this chapter, I investigated whether transport of gas molecules can significantly change through organic-modified MFI membranes, compared to bare MFI membranes. Two types of MFI membranes were synthesized on α-alumina supports by secondary growth method with the *[h0h]* out-of-plane orientation, and thickness of about 6 μm and 10 μm. Organic modification procedures for membranes was based on the developed procedure for particles in Chapter 2. Similar to MFI particles, I chemisorbed several types of organic species on the silanol sites in MFI membrane. Photoacoustic IR (PA-FTIR) spectroscopy was used to verify the existence of functional groups in the MFI membrane. For PA-FTIR characterization, MFI membranes were functionalizaed with 1-butanol, 1-hexanol, 3-amino-1-propanol, 1-propaneamine, 1,3-diaminopropane, 2-[(2-aminoethyl)amino]ethanol, and benzenemethanol. For all of these membranes, the existence of functional group was verified by observing the C-H stretching mode close to 3000 cm^{-1}.

Single-component permeation measurements of H_2, CO_2, CH_4, N_2, and SF_6 were performed on all of the modified MFI membranes to see the overall change in properties of the membrane due to the presence of modifying organic groups. For permeation measurements, MFI membranes were modified with a subset of molecules probed in PA-FTIR studies such as 1-butanol, 3-amino-1-propanol, 2-[(2-aminoethyl)amino]ethanol, and benzenemethanol. The MFI membrane modified with 1-butanol was also tested with *n*-butane and *i*-butane single gas permeation before and after modification. In all of the modified membranes, almost all of the gas permeances were reduced 1-2 orders of magnitude after modification. This is attributed to partial pore blocking of the functional

groups. It was observed that N_2/SF_6 single component selectivity decreased for all of the membranes upon modification. This is explained by having a larger portion of the permeances going through membrane defects for modified MFI membranes. The CO_2/CH_4 selectivity was increased for MFI/benzenemethanol membrane and decreased for MFI/2-[(2-aminoethyl)amino]ethanol compared to bare MFI membrane. This is likely due to observing the highest CO_2 adsorption in MFI/2-[(2-aminoethyl)amino]ethanol particles and observing the highest CH_4 adsorption in MFI/ benzenemethanol among the studied modifications.

CHAPTER 4- FTIR STUDY OF CO_2 ADSORPTION ON MODIFIED MFI PARTICLES

4.1. Introduction

Zeolites have shown potential for separating CO_2 from gas mixtures and may be candidate sorbents for use in pressure-swing and temperature-swing adsorption (PSA and TSA) processes.[8] In this thesis, I have already shown the development and characterization of organic (e.g., amine)-modified MFI zeolite materials. A more detailed fundamental study of the CO_2 adsorption mechanism in such modified zeolites would be beneficial in understanding their behavior and developing them further for adsorption and membrane applications. This Chapter describes work in this direction.

Fourier transform infrared spectroscopy (FTIR) has been the most widely used technique to investigate CO_2 adsorption on zeolites.[8,9,111-119] CO_2 adsorption has also been used to monitor both Lewis acid centers and Lewis base centers on metal oxides and zeolite surfaces[111]. It is a linear centrosymmetric molecule having three fundamental vibrations, one stretching vibration ν_1, which is Raman active appearing as a doublet at 1285 and 1388 cm^{-1} and two other IR-active vibrations, doubly degenerate deformation ν_2 at 667 cm^{-1} and the antisymmetric stretching ν_3 at 2349 cm^{-1}. On unreactive surfaces, the infrared spectrum of physically adsorbed CO_2 shows mostly the ν_3 vibration near 2349 cm^{-1}. The IR spectrum of chemisorbed CO_2 species varies distinctly from the gas phase spectrum. And it is characterized with peaks in the 1300-1800 cm^{-1} region[111,120].

Wirawan et. al[119] reported that CO_2 adsorption in pure-silica MFI (silicalite-1) and M-ZSM-5 (M = H, Na and Ba) produces at least two different types of adsorbed species. The weakly adsorbed (physisorbed) species result in bands between 2350 and 2360 cm^{-1} and can be completely removed by degassing with Ar at 100°C. The 'irreversibly' adsorbed (chemisorbed) species show carbonate vibrational bands at wavenumber ranges of 1200–1800 cm^{-1}, and have different thermal stabilities and adsorbed quantities depending on the Si/Al ratio and the nature of the extraframework cations.

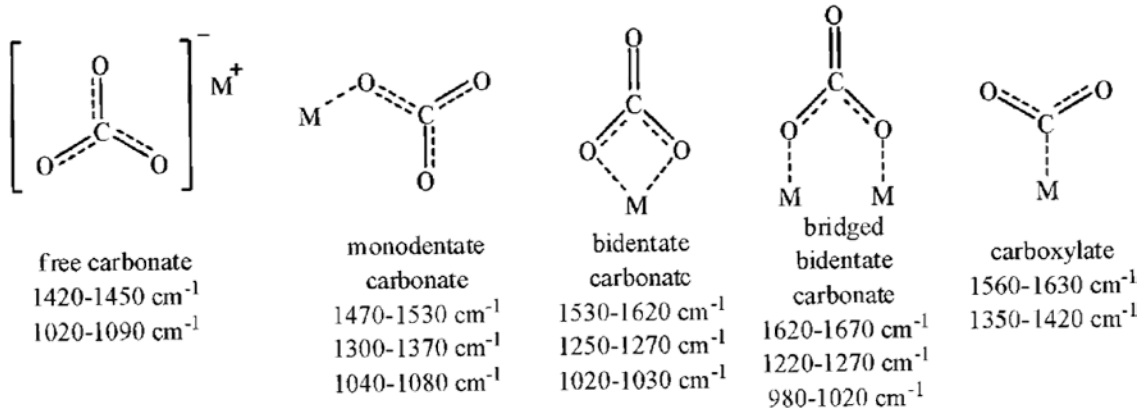

Figure 4.1: Modes of CO_2 adsorption (Reproduced with permission from Stevens et.al[8]).

Stevens *et al.*[8] studied adsorption of CO_2 in five zeolite materials (13X, WEG, AGP, 4A, and 5A) by *in-situ* infrared spectroscopy at 1 atm. CO_2 adsorption was investigated as a function of the pretreatment temperature (120 and 350°C) and adsorption temperature (30 and 120 °C). Adsorbed CO_2 species identified include physisorbed CO_2, bidentate carbonate, bridged bidentate carbonate, monodentate carbonate, and carboxylate. Figure 4.1 shows the structures of these adsorbed species and their expected vibrational band ranges. Interaction of the CO_2 with hydroxyl group (OH^-)

may lead to the formation of bicarbonate or formate.[8] Rege *et al*[116] assigned bands at 3605, 1640, 1480, and 1235 cm^{-1} during CO_2 adsorption on γ-alumina to bicarbonate species. Formate species are expected to display bands at 1597 and 1377 cm^{-1}.

Stevens *et al.*[8] also observed that both pretreatment temperature and CO_2 adsorption temperature affected the type and amount of the adsorbed CO_2 species in studied zeolites. Materials pretreated at 350°C, as opposed to 120°C, had more surface adsorption sites available as evidenced from more intense adsorption bands. Physisorbed CO_2 was the most abundant species observed. Bridged bidentate carbonate was found to be more stable than bidentate carbonate. In their tests involving both CO_2 and H_2O, it was shown that the two species competed for the same adsorption sites on the zeolite surface.

Galhotra et. al[115] studied CO_2 adsorption in zeolite Y in the presence and absence of co-adsorbed H_2O. Several different zeolite Y materials were investigated including commercial NaY, commercial NaY ion-exchanged with Ba^{2+}, and nanocrystalline NaY; herein referred to as NaY, BaY and nano-NaY. Following heating of these zeolites to 300 °C and cooling to room temperature, CO_2 was adsorbed at various pressures. FTIR spectra showed that a majority of CO_2 adsorbs in the pores of these three zeolites (NaY, BaY and nano-NaY) as a linear complex with the exchangeable cation; as indicated by the intense absorption band near 2350 cm^{-1} which is assigned to the ν_3 asymmetric stretch of adsorbed CO_2. Most interesting is the formation of carbonate and bicarbonate on the external surface of nano-NaY zeolites as indicated by the presence of several broad

absorption bands in the 1200–1800 cm^{-1} region, suggesting these are unique sites for CO_2 adsorption on the surface of the nanomaterial.

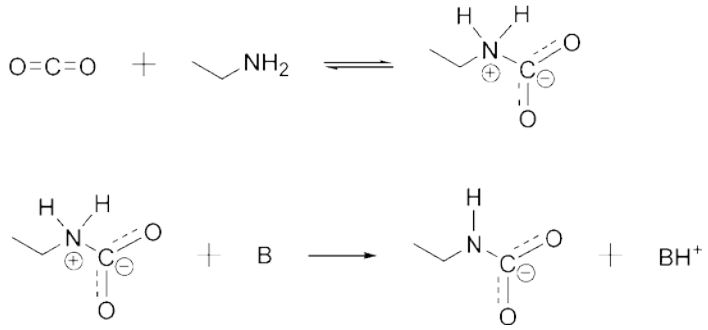

Figure 4.2: Carbamate formation from reaction of CO_2 with primary amines (Reproduced with permission from Choi et. al[9])

FTIR analysis of CO_2-amine interactions in solid sorbents have been reported by a number of authors.[9,112] A number of chemical structures have been identified using infrared spectroscopy, but some controversy exists with respect to the peak assignments. The interaction of CO_2 with amines can be governed by several different mechanisms.[9] Primary and secondary amines can react directly with CO_2 to produce carbamates through the formation of zwitterionic intermediates. Caplow[87] reported a zwitterionic mechanism for the formation of carbamate from the reaction of CO_2 with a primary amine. In Figure 4.2, the mechanism for carbamate formation is shown. The first step is the attack of the lone pair of the amine on the carbon of CO_2 to form the zwitterion. Then, a free base deprotonates the zwitterion to form the carbamate. In an aqueous amine environment, this base can be another amine, H_2O, or OH^-. This mechanism is applicable to secondary and sterically hindered amines as well. Sterically hindered amines are

defined as primary amines in which the amino group is attached to a tertiary carbon atom, or secondary amines wherein the amino group is attached to a secondary or a tertiary carbon atom.[118]

Overbury and co-workers[121] studied CO_2 sorption in a polyethylenimine (PEI) modified mesoporous molecular sieve (SBA-15). CO_2 sorption/desorption behavior studied by *in situ* transmission FTIR showed that CO_2 is sorbed on amine sites through the formation of alkylammonium carbamates and absorbed into the multiple layers of PEI located in mesopores of SBA-15. A new observation by *in situ* IR is that two broad IR bands emerged at 2450 and 2160 cm^{-1} with CO_2 flowing over PEI(50)/SBA-15, which could be attributed to chemically sorbed CO_2 species on PEI molecules inside the mesopores of SBA-15. The intensities of these two bands also increased with increasing CO_2 exposure time and with raising CO_2 sorption temperature. Comparative IR examination of the CO_2 sorption/desorption spectra on dry and prewetted PEI/SBA-15 sorbent showed that presorbed water does not significantly affect the CO_2-amine interaction patterns.

In this chapter, I investigate CO_2 adsorbed species at low pressures on bare MFI and MFI modified with 1-butanol, 3-amino-1-propanol, 1-propaneamine, 1,3-diaminopropane, 2-[(2-aminoethyl)amino]ethanol, and benzenemethanol. This investigation was carried out by the use of *in-situ* Fourier transform infrared (FTIR) spectroscopy in collaboration with John R. Copeland in the group of Prof. Carsten Sievers, with low pressures of CO_2 (up to 11 mbar).

4.2. Experimental Methods

4.2.1. Materials

Pure silica MFI crystals of 10μm were synthesized following Agger's procedure[79]. Organic modification of the crystals were conducted in the same manner as in Chapter 2.[68] MFI crystals were modified by 1-butanol, 3-amino-1-propanol, 1-propaneamine, 1,3-diaminopropane, 2-[(2-aminoethyl)amino]ethanol, and benzenemethanol.

4.2.2. CO_2 Adsorption Using *in-situ* Infrared Spectroscopy

Fourier transform infrared (FT-IR) spectroscopy was performed with a Thermo Scientific 8700 FT-IR instrument with a MCT/A detector. 64 scans were collected for each spectrum at a resolution of 4 cm^{-1}. For the *in-situ* FTIR spectroscopy of CO_2 adsorption/desorption, each sample was pressed into a self-supported wafer. The wafer was placed into a temperature controlled sample holder which was loaded into a high-vacuum transmission FT-IR cell. Vacuum (< 10^{-6} mbar) was applied to the wafer before it was heated to 110 °C for at least 4 h. After cooling to 25 °C, the FTIR spectrum was collected; this will be referred to as the "activated" sample spectrum. The background used for all samples was that of the empty transmission cell under high-vacuum and at 25 °C. FT-IR difference spectra of CO_2 adsorbed on the samples were obtained using CO_2 pressures from 0 to 11 mbar by subtracting the "activated" sample spectrum from the CO_2 exposed spectrum.

After the experiment, the wafer was removed from the cell, and a circle of exactly known diameter was cut from the wafer and weighed in order to obtain the area density (mg/cm^2) of the sample. FT-IR spectra collected from wafers of different area densities were normalized where noted, in order to be able to make direct comparison of absorbance values from different samples.

4.3. Results and Discussion

4.3.1. Effect of Sample Activation

Each sample is put under high vacuum at 110°C for at least 4 hours for "activation" to remove any physisorbed species (like water) before exposure to CO_2. Figure 4.3 shows the IR spectrum of bare MFI before and after sample activation. IR spectrum shows a slight loss of water as the broad band of hydroxyls decrease in intensity. Similar results are expected by activation of other samples.

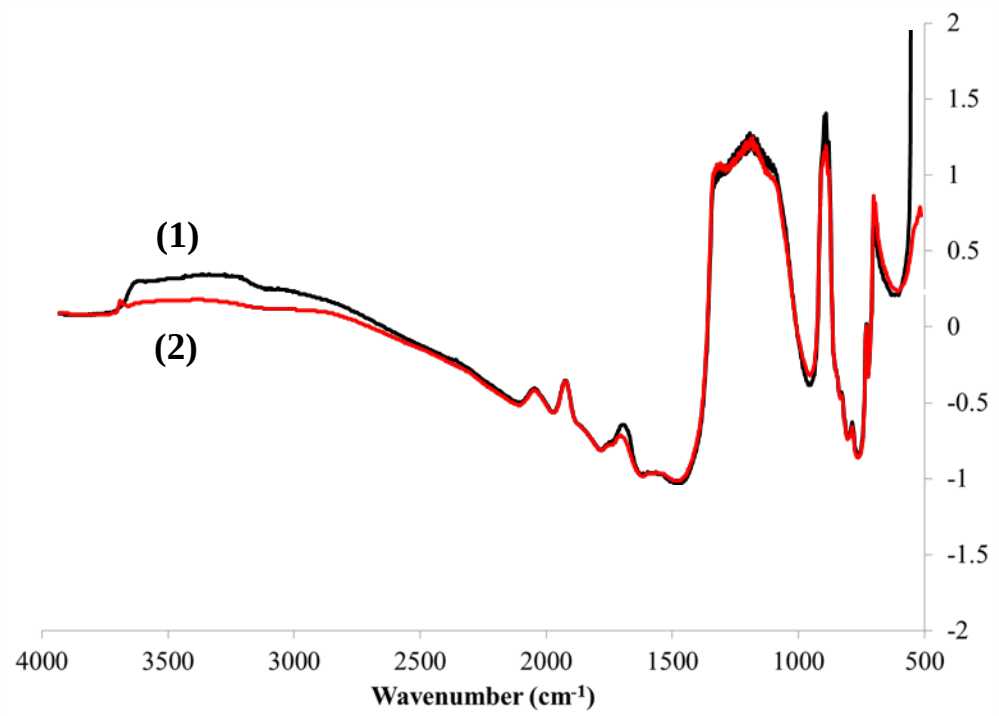

Figure 4.3: IR spectrum of bare MFI before (1) and after sample activation (2).

4.3.2. Difference Spectra of Bare and Modified MFI

Figure 4.4 shows the IR spectrum of MFI modified with 2-[(2-aminoethyl)amino]ethanol for various CO_2 pressures up to 11 mbar. Changes in spectra upon CO_2 exposure are difficult to resolve in Figure 4.4 due to the presence of many other strong bands. Therefore, the spectrum of the activated sample (Figure 4.3) is subtracted from the spectra of the CO_2 dosed sample. Such "difference spectra" bring out the details of CO_2 adsorption. Figure 4.5 shows the difference spectra for all of the modified materials.

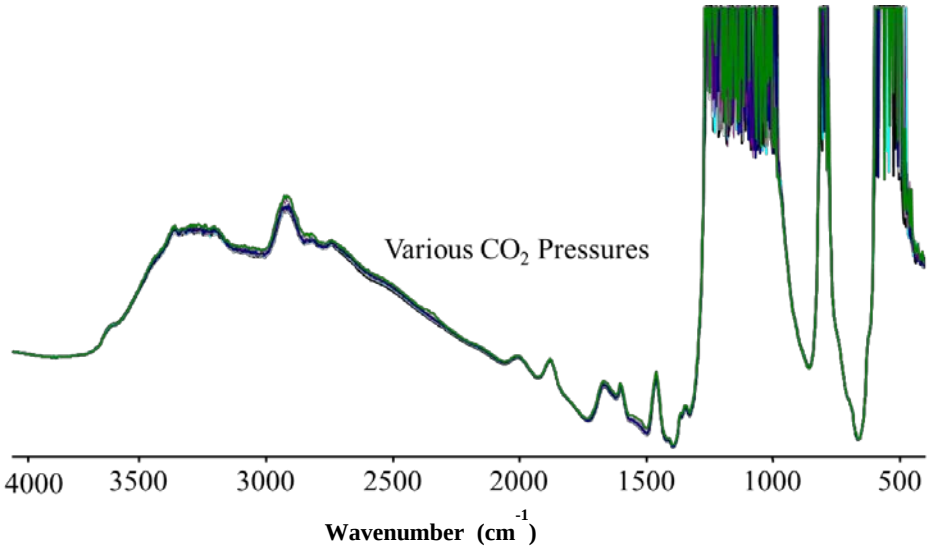

Figure 4.4: FTIR spectrum of MFI modified with 2-[(2-aminoethyl)amino]ethanol over the entire spectrum at various CO_2 pressures.

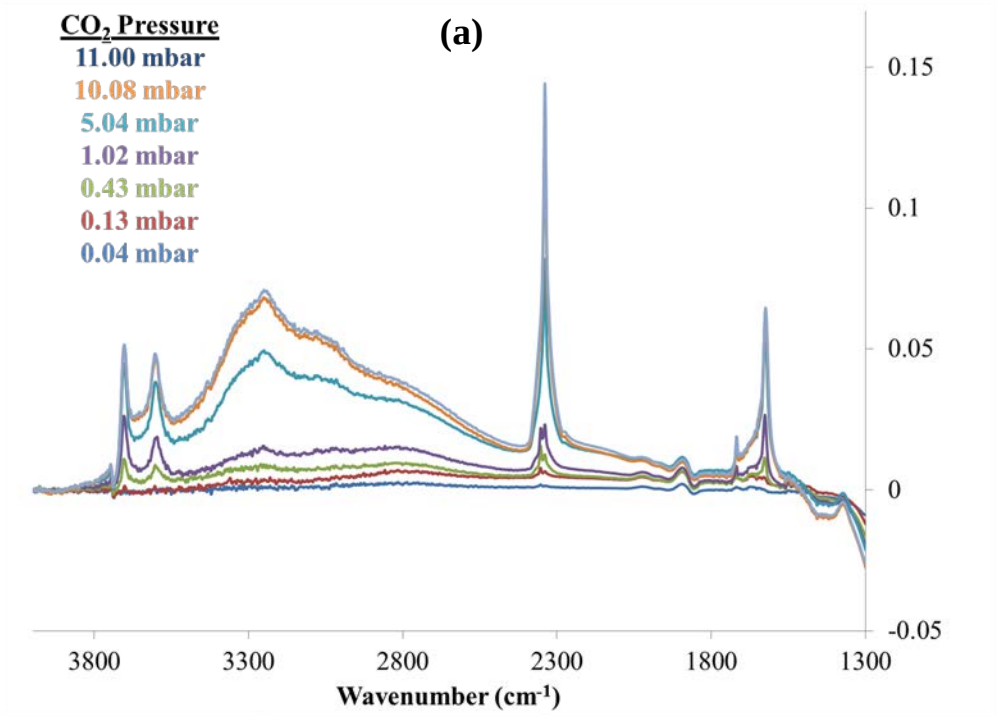

(b)

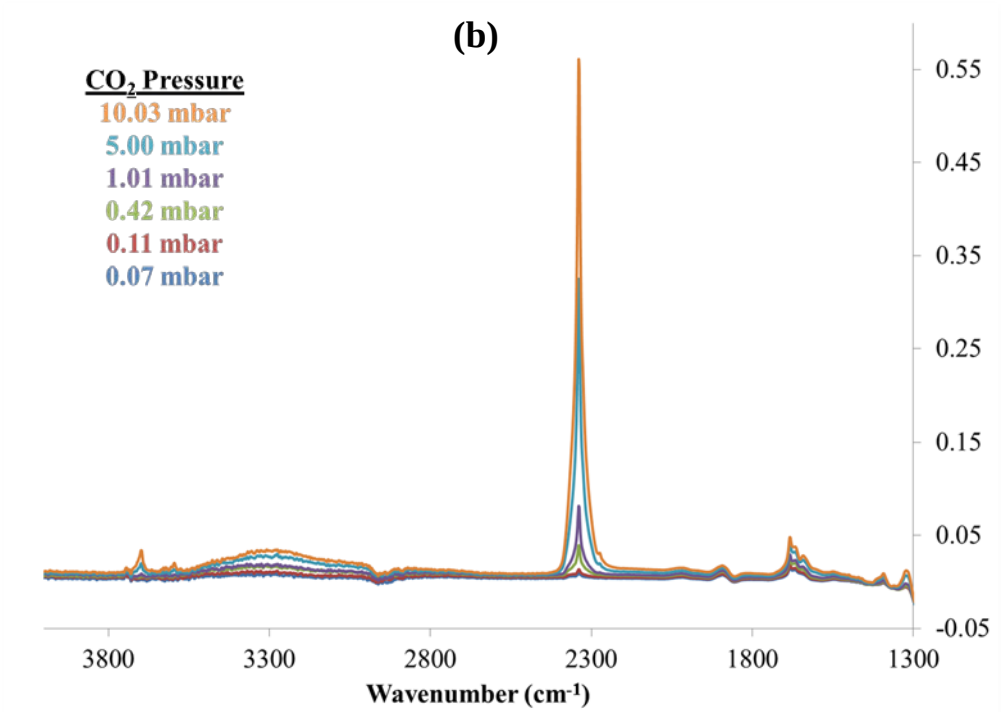
CO2 Pressure
10.03 mbar
5.00 mbar
1.01 mbar
0.42 mbar
0.11 mbar
0.07 mbar
0.55
0.45
0.35
0.25
0.15
0.05
-0.05
3800
3300
2800
2300
1800
1300
Wavenumber (cm-1)

(c)

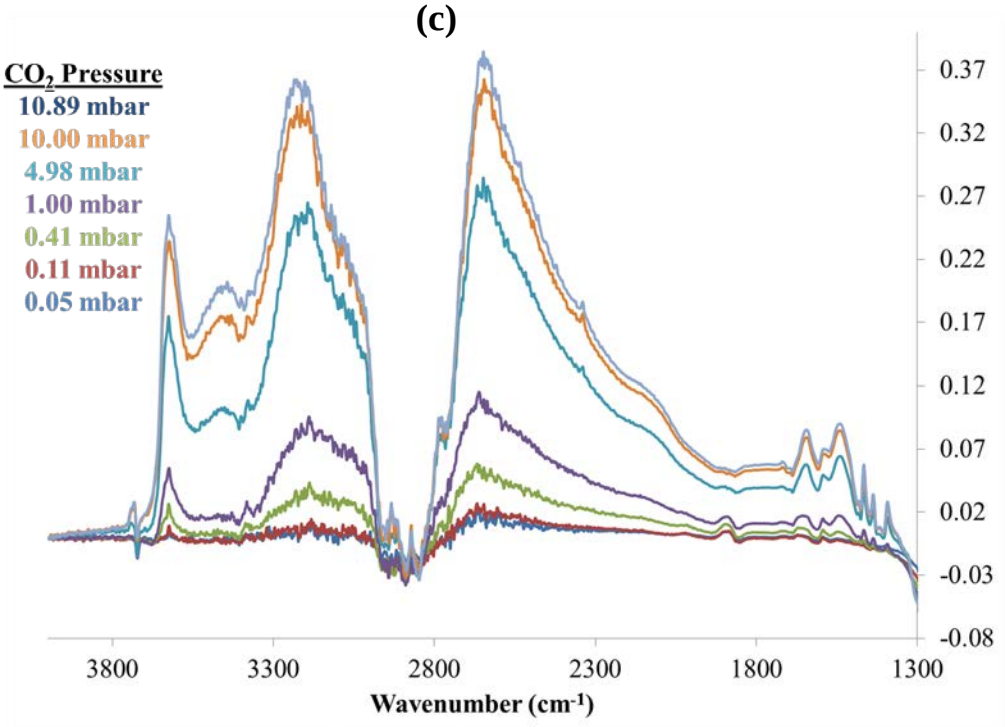
CO2 Pressure
10.89 mbar
10.00 mbar
4.98 mbar
1.00 mbar
0.41 mbar
0.11 mbar
0.05 mbar
0.37
0.32
0.27
0.22
0.17
0.12
0.07
0.02
-0.03
-0.08
3800
3300
2800
2300
1800
1300
Wavenumber (cm-1)

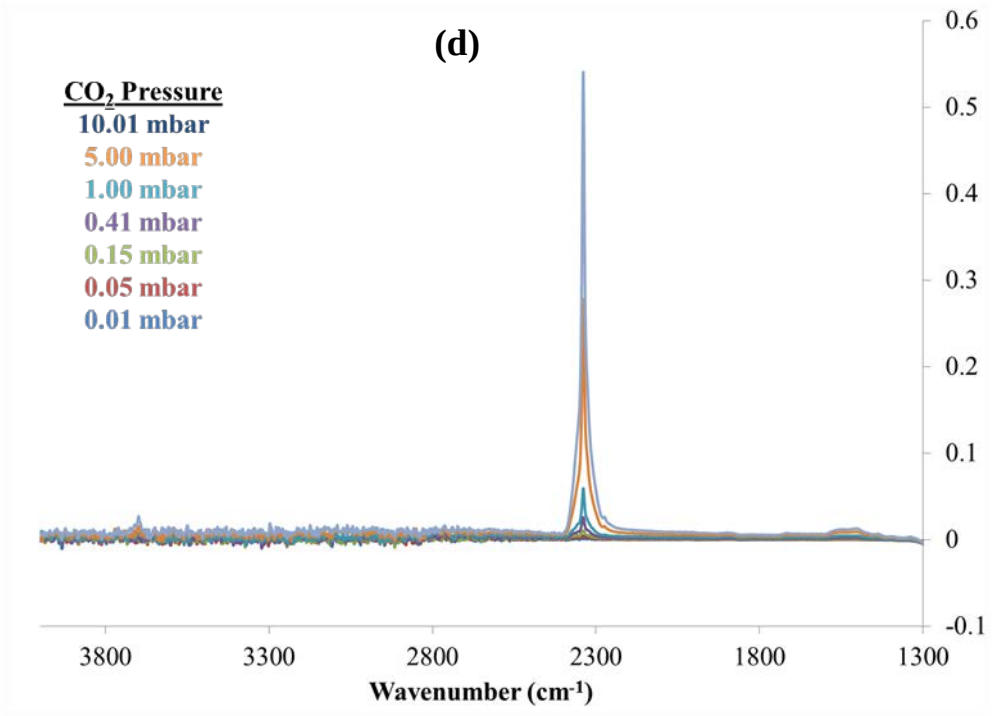
(d)
CO2 Pressure
10.01 mbar
5.00 mbar
1.00 mbar
0.41 mbar
0.15 mbar
0.05 mbar
0.01 mbar
0.6
0.5
0.4
0.3
0.2
0.1
0
-0.1
3800
3300
2800
2300
1800
1300
Wavenumber (cm-1)

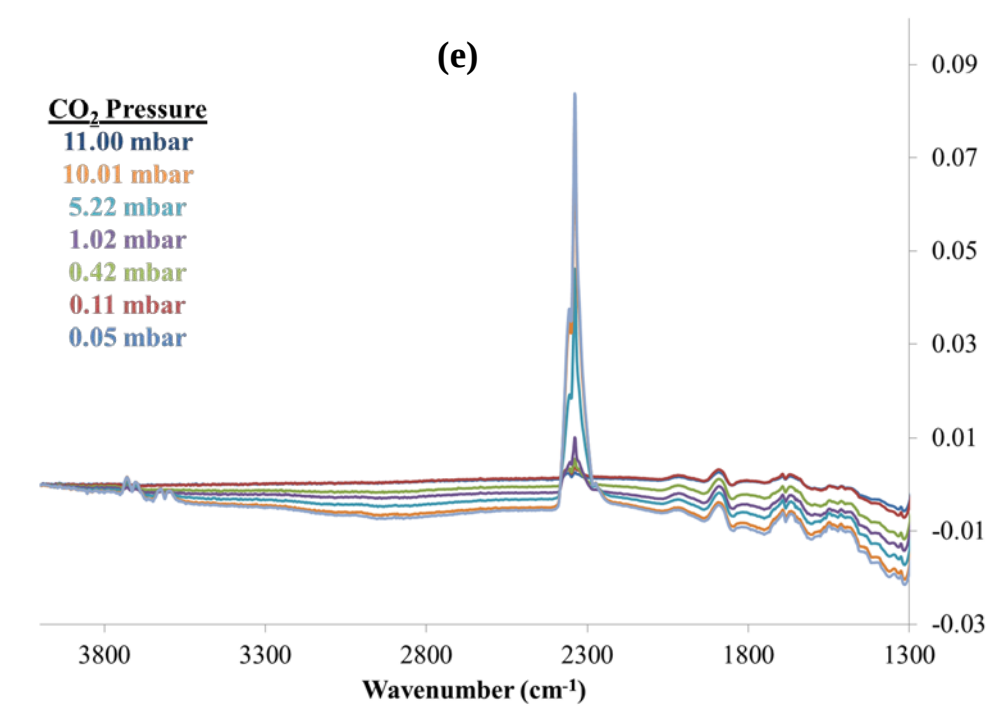
(e)
CO2 Pressure
11.00 mbar
10.01 mbar
5.22 mbar
1.02 mbar
0.42 mbar
0.11 mbar
0.05 mbar
0.09
0.07
0.05
0.03
0.01
-0.01
-0.03
3800
3300
2800
2300
1800
1300
Wavenumber (cm-1)

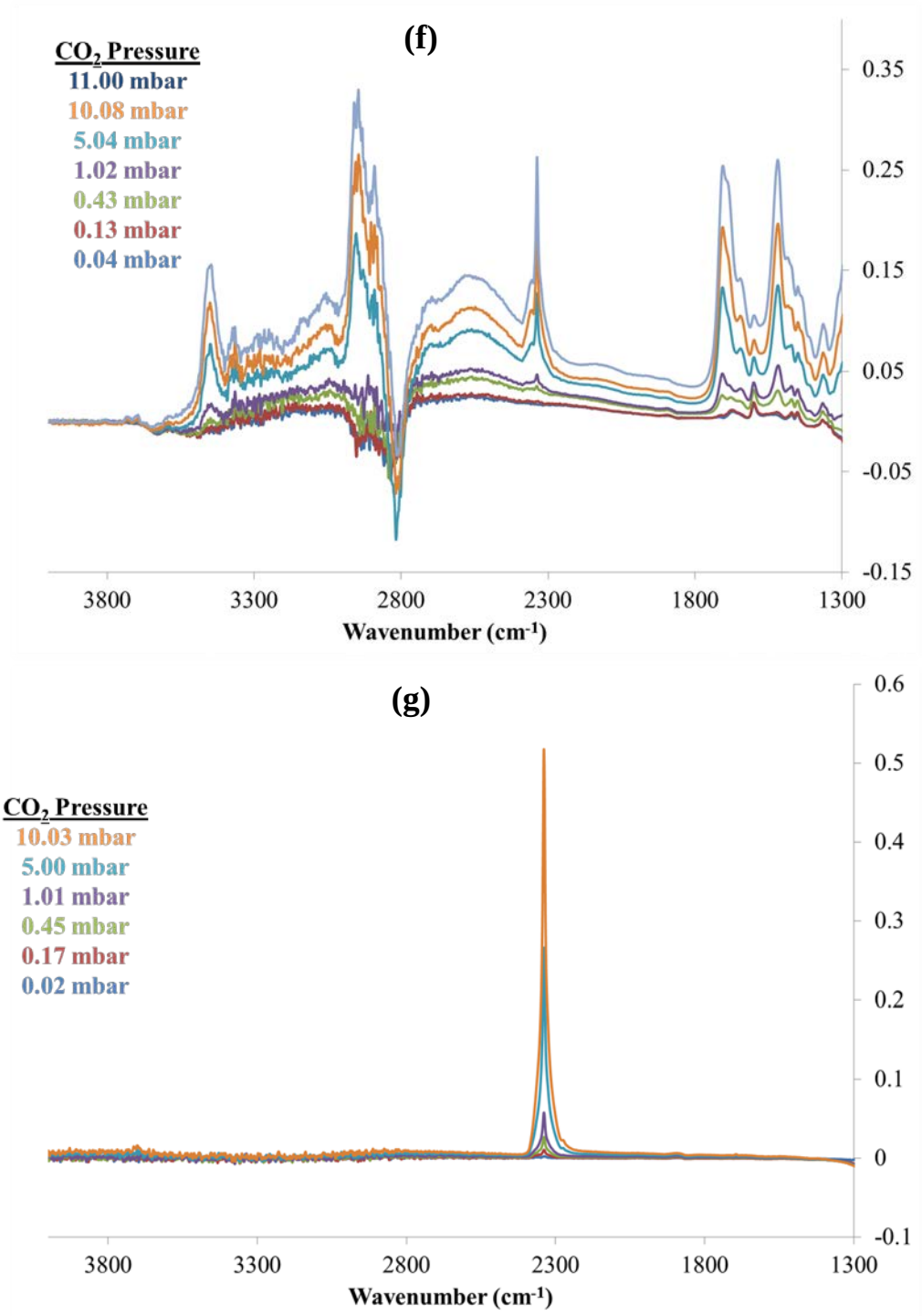

Figure 4.5: FTIR difference spectrum in the range of 1300-1800 cm^{-1} for pressure range of ~ 0.05 mbar to 11 mbar, for bare MFI (a) and MFI modified with 1-butanol (b), 3-amino-1-propanol (c), 1-propaneamine (d), 1,3-diaminopropane (e), 2-[(2-aminoethyl)amino]ethanol (f), and benzenemethanol (g).

In the FTIR spectra, the peak close to 2350 cm^{-1} corresponds to physisorbed, linear CO_2. For MFI modified with 1-butanol, 1-propaneamine, 1,3-diaminopropane and benzenemethanol, this is the only significant peak observed, and continues to increase in intensity upon increase in CO_2 pressure. Because there are no other peaks in difference spectra of these materials that would indicate other forms of CO_2 species binding to the surface, it is concluded that these materials only adsorb CO_2 by physical adsorption and have very limited chemical interactions with CO_2. This is intuitively expected for the case of 1-butanol, 1-propaneamine, and benzenemethanol, since the functional group (hydroxyl or amine) is occupied in binding to the zeolite framework defect site and is not available for chemisorbing CO_2. In the case of 1,3-diaminopropane, there is a free amine group available, but only physisorption of CO_2 is observed. Recent studies on CO_2 binding in amine-functionalized mesopourous material (SBA-15)[114] and an amine functionalized metal organic framework (MOF)[122] show that CO_2 is physically adsorbed on isolated amine groups. This case is discussed further in the present chapter.

On the other hand, in bare MFI and MFI modified with 3-amino-1-propanol or 2-[(2-aminoethyl)amino]ethanol, a number of different modes of vibration other than physisorbed CO_2 were observed that show existence of chemisorbed species. In order to identify these different species, the spectra in the 'carbon fingerprint' region needs to be examined.[114] In Figure 4.6, the FTIR spectra of bare MFI, MFI/3-amino-1-propanol and MFI/2-[(2-aminoethyl)amino]ethanol in this region (1300-1800 cm^{-1}) are presented.

(a)

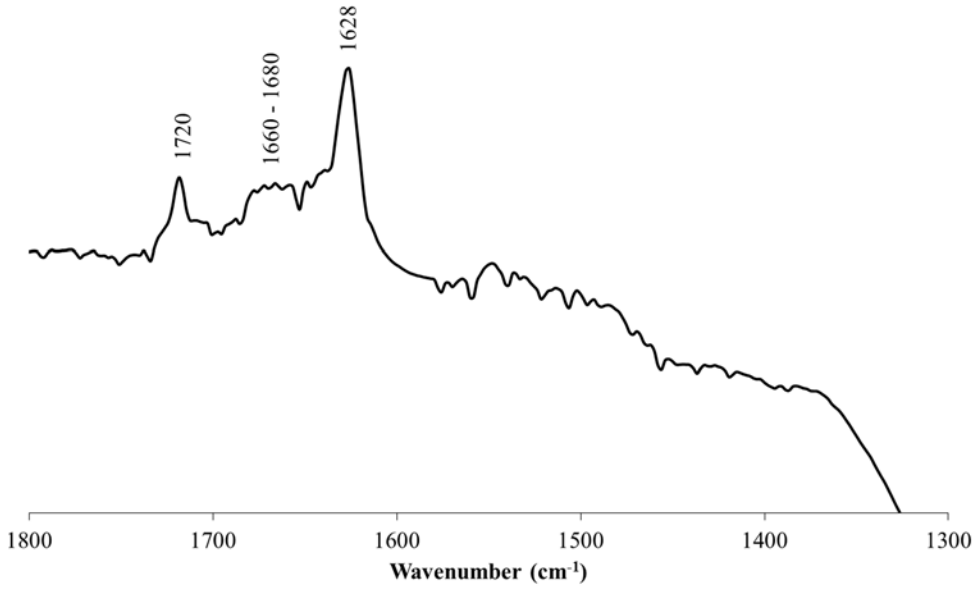
1720
1660 - 1680
1628
1800
1700
1600
1500
1400
1300
Wavenumber (cm-1)

(b)

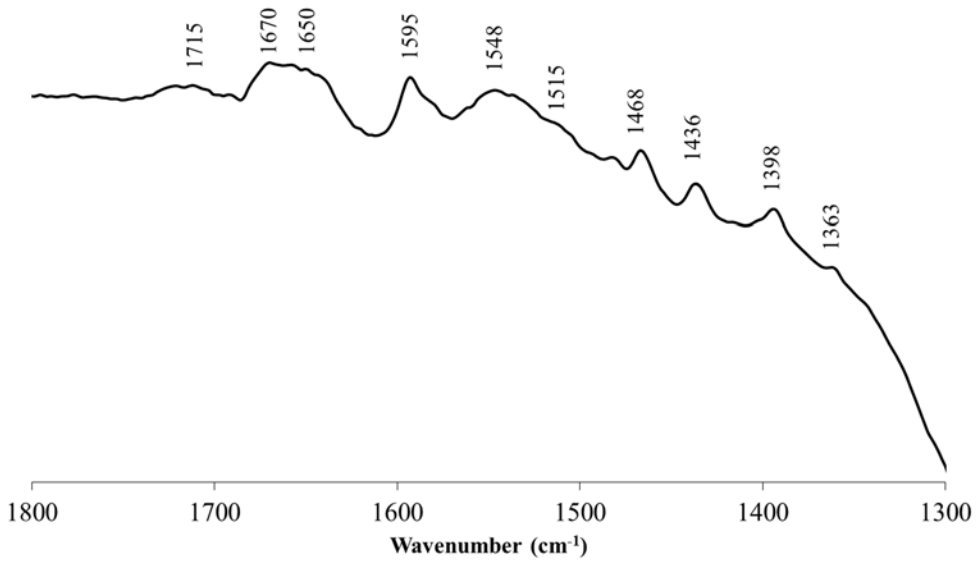
1715
1670
1650
1595
1548
1515
1468
1436
1398
1363
1800
1700
1600
1500
1400
1300
Wavenumber (cm-1)

(c)

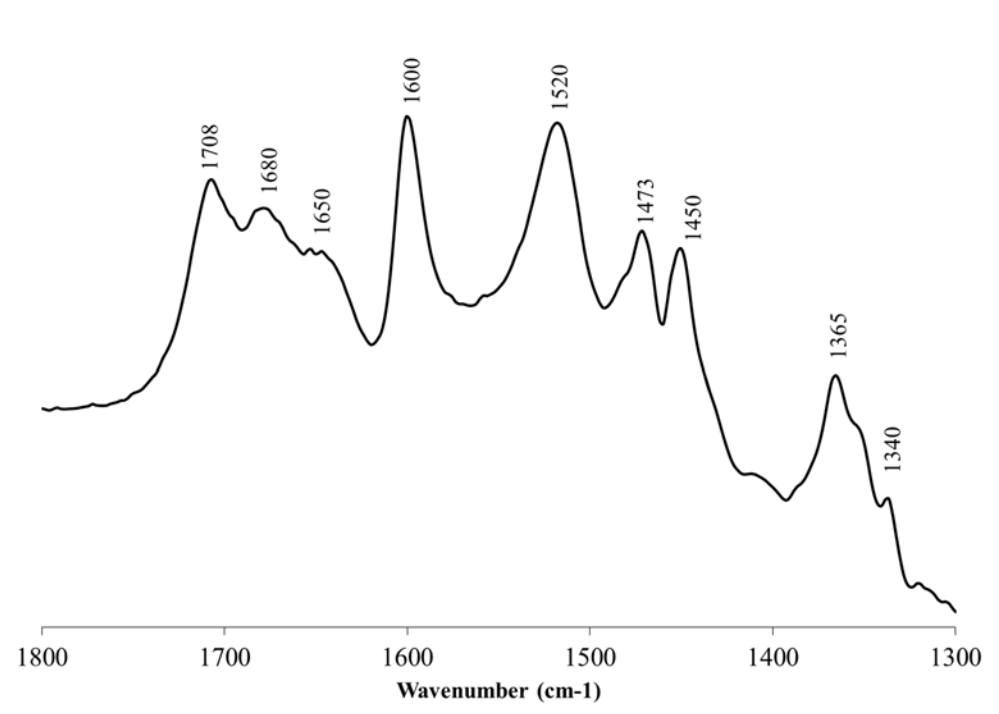

Figure 4.6: FTIR spectrum of bare MFI (a), MFI/3-amino-1-propanol (b), and MFI/2-[(2-aminoethyl)amino]ethanol (c), at 0.4 mbar CO_2 pressure over the range 1300-1800 cm^{-1}.

As mentioned in earlier chapters, it is known from FTIR and ^{29}Si NMR studies that there is one silanol defect site in each channel intersection of MFI zeolite structure[60,62]. Based on the TGA data reported in Chapter 2, almost all of the silanol defects are modified with the organic molecules.

In the bare MFI sample, the silanol defects are the only reactive sites that can chemisorb CO_2. Carbonate and carbonate-like species have been reported for CO_2 interaction with hydroxyl groups on metal oxides and silanol groups in zeolites.[8,111,115,119] Bare MFI shows peaks at 1628, 1660-1680, and 1720 cm^{-1}.

For the organic molecules that only have one functional group (1-butanol, benzenemethanol, and 1-propaneamine) only physisorbed CO_2 is seen in their IR spectrum. As mentioned earlier, the functional group in these molecules is bound to the silanol defects and there is no other functional group available to chemisorb CO_2. The IR spectrum of MFI modified with 1,3-diaminopropane is particularly interesting since it has two primary amine groups. The IR spectrum shows that CO_2 is only physisorbed in this material, although one might expect that the second amine group is free to chemisorb CO_2. In this material, isolated amine groups are present in the MFI zeolite pores and they are attached to the location of silanol defects at each channel intersection. The finding is that the isolated amine groups in organic-modified MFI do not interact strongly with CO_2 under anhydrous conditions. This is in agreement with a previous report from Danon et al.[114] that showed CO_2 physisorbs on isolated amine sites. Danon *et al.*[114] prepared isolated primary amine sites on SBA-15 by amine grafting. They used a bulky steric

group to limit nearest neighbor interactions and observed that CO_2 only physisorbs on the material. This case was also shown for an amine functionalized MOF by Vaidhyanathan *et al.*[122]. In this study, one of the main conclusions is that the CO_2 does not have strong interaction with the isolated amine group and the observed high loading is in part due to CO_2-CO_2 interactions in the pores.

In the case of MFI modified with 3-amino-1-propanol, either the hydroxyl or amine group could react with MFI silanol group. Since either of these functional groups can react with the silanol defect, the remaining functional group in the molecule would be available in the pores to interact with CO_2. Since, as show above, it is not expected to observe any chemisorption by isolated amine groups, all of the observed modes for chemisorbed species are rationally attributed to hydroxyl group interactions with CO_2. In MFI/3-amino-1-propanol, these peaks are observed at 1363, 1398, 1436, 1468, 1515, 1548, 1595, 1650, 1670, and 1715 cm^{-1}.

In the case of MFI modified with 2-[(2-aminoethyl)amino]ethanol, a hydroxyl, a primary amine, and a secondary amine group are present. Each of these groups can react with silanol defects. One expects to observe many of the same chemisorbed species as seen in MFI/3-amino-1-propanol. Based upon the distance (~ 3.5 Å) between the primary and secondary amine groups in the molecule, it is difficult to hypothesize any cooperative effects of the two groups in the confined zeolite structure; however, this possibility cannot completely be rule out based upon the available data. The MFI/2-[(2-

aminoethyl)amino]ethanol peaks are at 1340, 1365, 1450, 1473, 1520, 1600, 1650, 1680, and 1708 cm^{-1}.

Figure 4.7 shows a stacked plot of the difference IR spectra from bare MFI, MFI/3-amino-1-propanol, and MFI/2-[(2-aminoethyl)amino]ethanol at 0.4 mbar CO_2 pressure [1]. There are many similar peaks in MFI/3-amino-1-propanol, and MFI/2-[(2-aminoethyl)amino]ethanol including peaks close to 1710 cm^{-1}, 1600 cm^{-1} , 1470 cm^{-1} and peak between 1430-1450 cm^{-1}. It is known that the exact frequency of the modes of an adsorbed species is dependent on the material to which it is adsorbed. This coupled with the fact that many of the modes of different carbonate and carbamate species are expected in the same region, and likely overlap, would make it difficult to conclusively assign the observed peaks to different species. Therefore, assigning a specific carbonate or carbamate like species to the peaks with available data is challenging and may require more information to assist in identifying these species.

Overall, it is observed that bare MFI, MFI/3-amino-1-propanol, and MFI/2-[(2-aminoethyl)amino]ethanol chemisorb CO_2 at low pressures *via* silanol defect or hydroxyl group at the end of the modifying molecule. Based on literature, I expect to observe carbonate like species when CO_2 is interacting with hydroxyl group. There are many similar peaks between IR spectrum of MFI/3-amino-1-propanol, and MFI/2-[(2-aminoethyl)amino]ethanol suggesting the existence of similar CO_2 chemisorbed species. However, MFI/2-[(2-aminoethyl)amino]ethanol spectrum shows more unique vibrational mode compared to MFI/3-amino-1-propanol. This might be due to additional interactions

of secondary amine with CO_2, collaborative CO_2 adsorption of secondary and primary amine, or collaborative CO_2 adsorption between hydroxyl and secondary amine in MFI/2-[(2-aminoethyl)amino]ethanol.

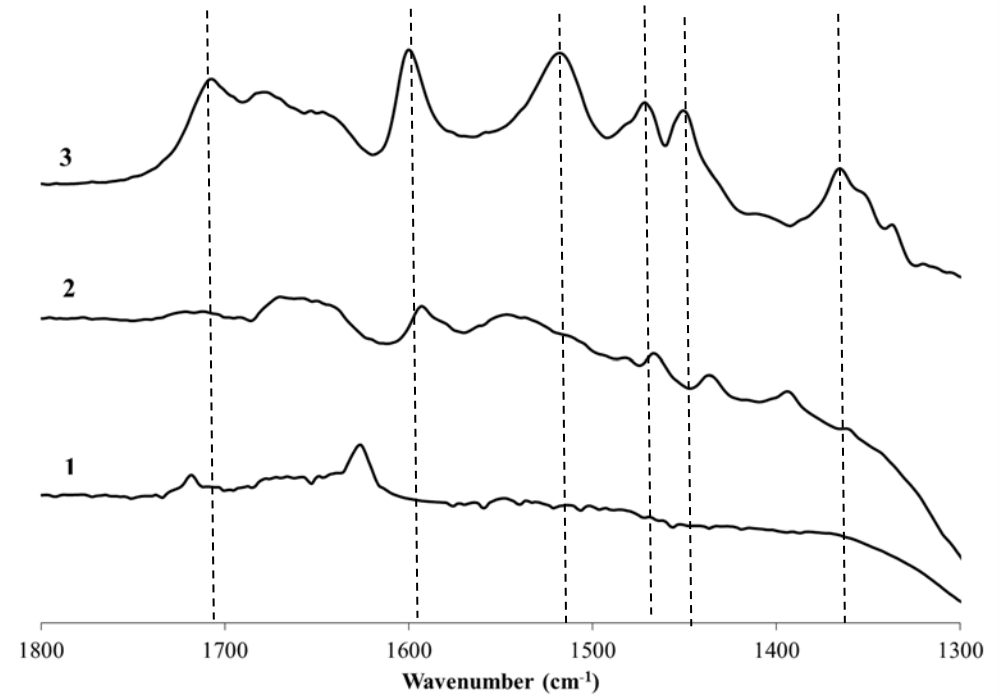

Figure 4.7: Stacked FTIR spectra of bare MFI (1), MFI modified with 3-amino-1-propanol (2), and MFI modified with 2-[(2-aminoethyl)amino]ethanol (3), at 0.4 mbar CO_2 pressure.

4.3.3. Effect of External Silanol Groups

In order to establish the reliability of the foregoing data and conclusions, it is important to rule out the contribution of external surface silanol groups in adsorbing CO_2. All of the previously discussed modified samples were synthesized using 10 μm MFI particles. The external surface area for these particles is less than 1% of the total surface, and the silanol densities per unit surface area are roughly comparable. Based on N_2 physisorption data from 10 μm MFI particles, internal surface area is about 430 m^2/g.

Based on the existence of 4 silanol defects per unit cell (~0.7 mmol/g)[49], I expect to have about 10 silanols/nm^2 of internal surface area. Based on literature values, an external surface silanol density of 4 Si-OH/nm^2 can be assumed[123]. The effect of using much smaller (900 nm) MFI particles was also examined. These particles would have more than an order magnitude larger number of external silanol sites due to having about 2 orders of magnitude more external surface. These particles were modified with 2-[(2-aminoethyl)amino]ethanol, since this molecule showed the strongest chemisorbed CO_2 signals compared to the other modified materials. The loading of the functional groups were found to be comparable to 10 μm particles.

Figure 4.8 shows the FTIR spectrum of 10 μm and 900 nm pure silica MFI particle modified with 2-[(2-aminoethyl)amino]ethanol at 0.4 mbar CO_2 pressure. For enabling quantitative comparison, the IR sample wafers were cut in a circle of known diameter after the experiment and were weighed. The wafer densities for both samples were obtained in this way and the spectra were normalized with respect to the wafer area densities. Based on the Beer-Lambert law[124], IR absorbance is proportional to molar absorptivity (ε), path length (l), and concentration of the substance (C). Area density of the sample (mg/m^2) is the combination of path length (m) and concentration (mg/m^3) and is used to normalize the spectra. If external silanol groups have a significant role in adsorbing chemisorbed CO_2 species, I would expect to see stronger signal from the 900 nm particles at the same CO_2 pressure. However, it was found that the IR intensity for 10 μm particles after normalization is somewhat higher than for the 900 nm particles. This means 10 μm particles adsorb more CO_2 species than 900 nm particles for the same

amount of loading. Therefore, it is clear that the external silanol groups do not play a significant role in adsorbing chemisorbed CO_2 species.

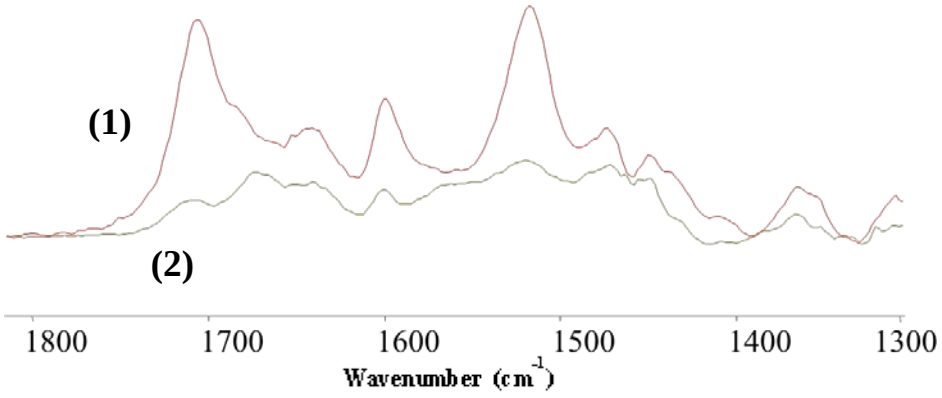

Figure 4.8: FTIR spectra of 10 µm (1) and 900 nm (2) pure-silica MFI particles modified with 2-[(2-aminoethyl)amino]ethanol, at 0.4 mbar CO_2 pressure.

4.4. Conclusions

In this chapter, I have investigated the CO_2 adsorption mechanism on bare MFI and MFI modified with 1-butanol, 3-amino-1-propanol, 1-propaneamine, 1,3-diaminopropane, 2-[(2-aminoethyl)amino]ethanol, and benzenemethanol. The study was performed using *in-situ* Fourier transform infrared (FTIR) spectroscopy. For organic molecules with one functional group (1-butanol, benzenemethanol, and 1-propaneamine), physical adsorption is, as intuitively expected, the only observed mode of attachment of

CO_2 to the zeolite material. For MFI modified with 1,3-diaminopropane, one still sees only physical adsorption. This is explained by the isolated nature of the amine groups in the material. On the other hand, chemisorbed CO_2 species are clearly observed on MFI modified with 3-amino-1-propanol and 2-[(2-aminoethyl)amino]ethanol. Moreover, these are carbonate-like species arise from the chemisorption of CO_2 to the alcohol groups of the functionalizing molecule. The possibility of significant contribution from external silanol groups in adsorbing CO_2 chemisorbed species was ruled out by a comparative examination of the FTIR spectra of 10 μm and 900 nm MFI particles modified with 2-[(2-aminoethyl)amino]ethanol. Overall, this study develops a basis for using the organic-modified zeolite materials in applications that may involve chemisorption of adsorbate molecules like CO_2.

CHAPTER 5- PARTICLE SIZE DEPENCENCE OF STRUCTURAL PHASE TRANSITION IN MFI ZEOLITE

5.1. Introduction

MFI is one of the most studied zeolites because its structure is suitable for separation or catalytic production of several industrially important organic molecules[4,22,39]. It has also served as a model for understanding zeolite structure and properties. Structural phase transitions of zeolites and nanoporous crystalline materials in general are still an area where fundamental understanding is lacking. Such phase transitions (e.g., in response to changes in temperature or pressure) can have a substantial effect on the pore structure and sorption/diffusion properties of the nanoporous material.

The ferroelastic and reversible monoclinic ($P2_1/n.1.1$) to orthorhombic (*Pnma*) solid state phase transition in MFI has been extensively studied in literature[125-129]. The phase transition is induced by application of temperature, and occurs at a critical temperature representing the onset of instability of one phase and the onset of stability of the other.

Van Koningsveld *et al.*[130] studied single-crystal MFI by X-Ray diffraction at different temperatures. They reported that the orthorhombic MFI (H-ZSM-5) single crystal changes into an aggregate of monoclinic twin domains when the temperature is lowered. The monoclinic angle α is about 90.5° in the twinned phase, and the crystal is an aggregate of domains in which the distortion is either +0.5° or -0.5° degrees. The

deviation of α from the orthorhombic value of 90° has been ascribed to a mutual shift of successive (010) pentasil layers along *c*, induced by a distortion or rotation of the four-membered and six-membered rings interconnecting the layers.[10,130]. De Vos Burchart *et. al*[10] performed molecular mechanics studies on the monoclinic-orthorhombic phase change. Both monoclinic and orthorhombic local energy minima were described successfully by the molecular mechanics forcefield, and it was suggested that the phase transition was induced through a low-frequency vibrational mode of approximately 20 cm^{-1} in wavenumber Figure 5.1 shows the directions of motion of zeolite MFI atoms when going from monoclinic to orthorhombic phase.

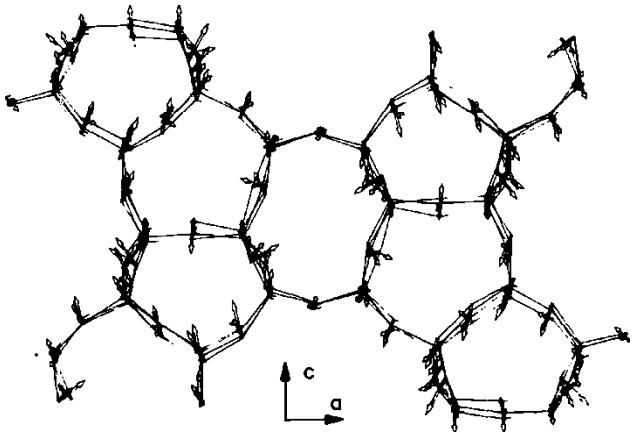

Figure 5.1: Motion of the atoms of the experimental monoclinic MFI structure due to the phase transition. Viewed along [010]. (Reproduced with permission from De Vos Burchart *et. al* [10]).

During the phase change from monoclinic to orthorhombic phase upon heating, the distortion in the monoclinic angle becomes progressively disordered and localized,

and the domains shrink in size until (at the phase transition temperature) the structure looks orthorhombic with α of 90°.

The effect of Si/Al ratio in the framework[131] and some adsorbed molecules (e.g. *p*-xylene) has been studied on the MFI phase transition temperature, however, the effect of particle size on the transition temperature has not previously been observed. In general, the dependence of the ferroelastic phase transition temperature in zeolites as function of the particle size has not been well studied, although size-dependent phase transition temperatures are known in ferroelectric materials such as ferromagnetic particles (e.g. $PbTiO_3$) and piezoelectric films[129,132,133]. There has been only one report suggesting such a relation might exist in zeolites, where Cheng *et. al*[49] suggested a possible correlation between MFI particle size and its structural phase transition temperature. Cheng *et al*. based the suggestion on the observation that the room temperature XRD spectra of pure-silica MFI showed a transition from monoclinic to orthorhombic symmetry as the particle size was varied. The orthorhombic phase was observed for 100 nm and 200 nm particles, and the monoclinic phase for 500 nm particles. This suggests that the ferroelastic phase transition temperature for 100 nm and 200 nm particles is lower than room temperature, whereas for 500 nm MFI particles it is above room temperature.

As mentioned, particle-size dependent phase transitions are known in ferroelectric materials[129,133]. Zhong *et al.*[129] reported size dependence of polarization and Curie temperature for ferroelectric materials (such as $PbTiO_3$ and $BaTiO_3$) and films (such as

$PbZr_xTi_{1-x}O_3$ film), and explained the data with different theories. The Curie temperature (also known as Curie point) is the transition temperature between the ferromagnetic/ferroelectric phase and the paramagnetic/paraelectric phase). Below the Curie temperature, neighboring magnetic spins (or electric dipoles) are aligned in parallel within ferromagnetic/ferroelectric materials. As the temperature is increased towards the Curie point, the alignment (magnetization/polarization) within each domain decreases. Above the Curie temperature, the material is paramagnetic and magnetic/dipole moments are in a completely disordered state. There are two main theoretical approaches in modeling phase transition in ferroelectric materials[129]. One is the Ising model[132], and the other is the Landau phenomenological theory[134]. The latter has been more fruitful and in is in better agreement with experiments. Zhong *et. al*[129] have applied Landau phenomenological theory to explaining the ferroelectric material phase changes.

The ferroelastic phase transition temperature in MFI has been studied using X-ray diffraction[125,126,131], ^{29}Si MAS NMR spectroscopy[125,131], and calorimetric techniques[127]. Hay *et al.*[125] studied the phase transition temperature (T_p) of pure silica MFI with both XRD and ^{29}Si MAS NMR. The crystal sizes were about 15 μm in the c-axis direction. The phase transition is observed and studied between 24 °C and 80 °C temperature range. Many subtle changes occur in the ^{29}Si MAS NMR spectra both above and below T_p. It has been suggested that such shifts are due to changes in Si-O-Si angles. On the basis of the quantitative relationship between the mean Si-O-Si angle and the Si NMR shifts, at 24°C the spectrum corresponds to bond angles ranging between 146° and 157°, and at 80°C to angles between 153° and 163°. These changes are accompanied by changes in

the relative intensities of the (501), (051), (151), and (303) diffraction peaks, which indicates that there are changes in the electron densities in these crystal planes taking place over the temperature range 24-80 °C.

Mentzen *et al*[127] determined the MFI phase transition temperature and enthalpy by calorimetric investigations. The phase transition enthalpy change is reported to be very sensitive to Al content in the framework. For $20 < Si/Al < 10000$, the enthalpy change (ΔH) corresponds to $1.8 < \Delta H < 18.3$ kJ/mol. ΔH increases with decreased Al content. The phase transition temperature for strictly anhydrous MFI materials was reported to be above 50°C. It was also reported that the phase transition is sensitive to the nature and the amount of sorbed or encaged guest molecules (e.g., water, aliphatic and aromatic hydrocarbons). Water adsorption by the sample led to the observation of lower phase transition temperatures.

Zecchina *et al.*[128] observed an orthorhombic structure (XRD peak at $2\theta = 24.4°$) for 220-260 nm pure silica MFI particles at room temperature. Sodium-containing MFI (after leaching with HCl) was observed to have monoclinic structure (splitting of the single XRD peak at $2\theta = 24.4°$ into two peaks) at room temperature. The particle sizes for Na-MFI were 2000-3500 nm, an order of magnitude higher than the studied silicalite-1 particles.

Structural phase transition of MFI from monoclinic to orthorhombic can be investigated by studying XRD spectra of MFI at different temperatures. to the region

around 24.4° 2θ shows the transition more clearly. Figure 5.2 shows MFI phase transition of 8 µm particles in monoclinic, phase transition and orthorhombic states at different temperatures. In orthorhombic structure, a single peak is observed in the plotted region. If MFI orthorhombic structure is gradually cooled down, the single peak ('singlet') seen at 24.4° broads and eventually turns into two distinct peaks ('doublet') in the monoclinic phase. In XRD measurements, the transition from singlet to doublet (or vice versa) is seen in a continuous manner over a large range of temperatures. Therefore, the phase transition temperature is determined, when a single Gaussian curve cannot be fitted, or when the valley between two monoclinic peaks near 24.4° flattens.

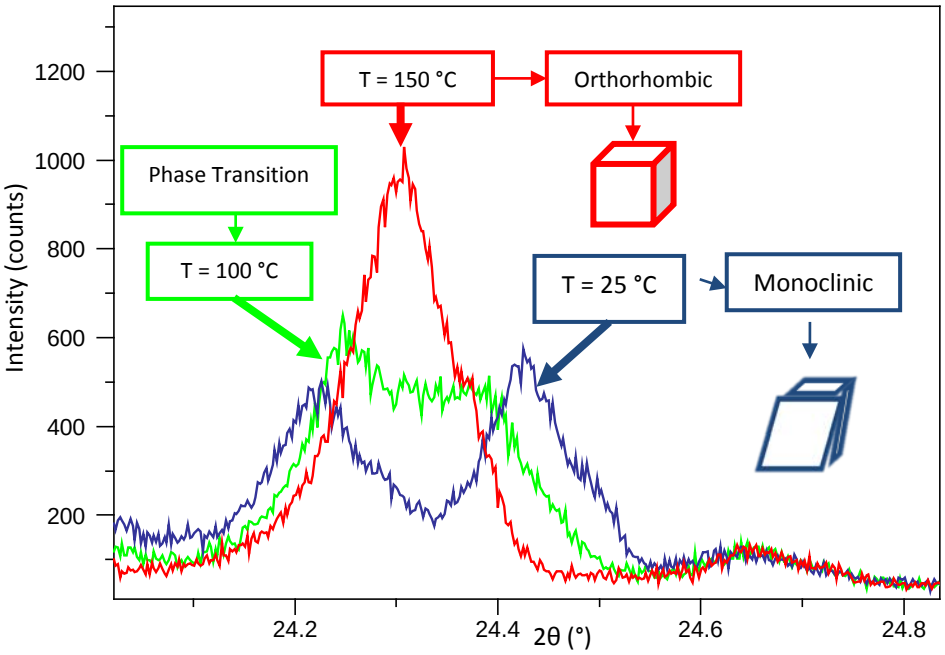

Figure 5.2: Phase transition in 8 µm pure silica MFI

In this chapter, I investigate the hypothesis that the phase transition temperature of MFI may vary with particle sizes of pure silica MFI, obtained from different synthesis routes. This study was performed by *in situ* variable temperature XRD measurements under vacuum conditions.

5.2. Experimental Methods

5.2.1. Materials

Different sizes of pure silica MFI crystals were synthesized by modifying the procedures of Agger[79] and Chezeau[135], and by methods developed in our laboratory. Six different particle sizes of pure-silica MFI were prepared. The particle sizes, measured along the longest dimension using SEM images, were 900 nm, 2 μm, 7 μm, 8 μm, 13 μm, 35 μm and 50 μm. The synthesis procedures for 900 nm, 2 μm, and 7 μm particles were developed in our lab. The Agger procedure was used and slightly modified to get 8 μm and 13 μm particles. The Chezeau procedure for defect free crystals with fluoride ion present was followed to obtain 35 μm and 50 μm particles. The following are the synthesis methods for preparing these particles:

900 nm particles. 5.38g of tetrapropylammonium hydroxide (TPAOH, 40% w/w aq. soln., Alfa Aesar) was mixed with 92.03g of DI water for 5 minutes. Then, 6.25g of tetraethylorthosilicate (TEOS, 98%, Aldrich) is added dropwise to the solution while stirring. The molar ratio is 1 TEOS/ 0.36 TPAOH / 180 H_2O. The solution is vigorously stirred for 2 hours at room temperature and then it is transferred to reaction autoclaves (45 ml) for hydrothermal synthesis at 150 °C for 48 hours. The solution is stirred during

hydrothermal synthesis. After taking the autoclaves out of the oven, the particles are washed with DI water three times, dried at 50 °C overnight, and calcined at 550 °C for 8 hours.

2 µm particles. 3.83g of tetrapropylammonium hydroxide (TPAOH, 40% w/w aq. soln., Alfa Aesar) was mixed with 99.30g of DI water for 5 minutes. Then, 6.67g of tetraethylorthosilicate (TEOS, 98%, Aldrich) is added dropwise to the solution while stirring. The molar ratio is 1 TEOS/ 0.24 TPAOH / 180 H_2O. The solution is vigorously stirred for 2 hours at room temperature and then it is transferred to reaction autoclaves (45 ml) for hydrothermal synthesis at 150 °C for 48 hours. The solution is stirred during hydrothermal synthesis. After taking the autoclaves out of the oven, the particles are washed with DI water three times, dried at 50 °C overnight, and calcined at 550 °C for 8 hours.

7 µm particles. 1.91g of tetrapropylammonium hydroxide (TPAOH, 40% w/w aq. soln., Alfa Aesar) was mixed with 99.30g of DI water for 5 minutes. Then, 3.33g of tetraethylorthosilicate (TEOS, 98%, Aldrich) was added dropwise to the solution while stirring. The molar ratio was 1 TEOS/ 0.24 TPAOH / 360 H_2O. The solution was vigorously stirred for 3.5 hours at room temperature and then it was transferred to reaction autoclaves (45 ml) for hydrothermal synthesis at 150 °C for 72 hours. The solution was stirred during hydrothermal synthesis. After taking the autoclaves out of the oven, the particles were washed with DI water three times, dried at 50 °C overnight, and calcined at 550 °C for 8 hours.

8 µm particles. 0.4g sodium hydroxide (NaOH) and 2.71g tetrapropylammonium bromide (TPABr, 98% Aldrich) were mixed with 177g DI water and stirred for 10 minutes. Then, 20.5g of tetraethylorthosilicate (TEOS, Aldrich 98%) was added dropwise to the solution. The molar ratio was 1 TEOS/ 0.1 TPABr / 0.1 NaOH / 98 H_2O. The solution was vigorously stirred for 48 hours at room temperature and then it was aged for 7 days at 50 °C. The resulting solution was transferred to autoclaves for hydrothermal synthesis at 130 °C for 48 hours. The particles were washed with DI water three times, dried at 50 °C overnight, and calcined at 550 °C for 8 hours

13 µm particles. 0.4g sodium hydroxide (NaOH) and 2.71g tetrapropylammonium bromide (TPABr, 98% Aldrich) were mixed with 177g DI water and stirred for 20 minutes. Then, 20.5g of tetraethylorthosilicate (TEOS, Aldrich 98%) was added dropwise to the solution. The molar ratio was 1 TEOS/ 0.1 TPABr / 0.1 NaOH / 98 H_2O. The solution was vigorously stirred for 48 hours at room temperature and then it was aged for 7 days at 50 °C. The resulting solution was transferred to autoclaves for hydrothermal synthesis at 130 °C for 52 hours. The particles were washed with DI water three times, dried at 50 °C overnight, and calcined at 550 °C for 8 hours

35 µm particles. 0.81g of tetrapropylammonium bromide (TPABr, 98% Aldrich), and 0.053g of ammonium fluoride (NH_4F, 96% Alfa Aesor) were mixed with 13.44g of DI water and stirred for 10 minutes until dissolved. Then, 2.24 g CabosilM5 was added to the solution. The solution was blended with a spatula for 10 minutes until it formed a

homogeneous gel. The gel was put in a 20 ml autoclave and in the oven at 180 °C for 14 days with no rotation. After reaction, the gel was washed three times with DI water, dried at 50 °C overnight, and calcined at 550 °C for 8 hours

50 μm particles. This synthesis procedure is the same as the procedure for 35 μm particles, with the only difference of being 16 days at the 180 °C oven instead of 14 days for 35 μm particles.

5.2.2. Characterization

Powder X-ray diffraction (XRD) patterns were obtained on a Philips X'pert Pro diffractometer using Cu Kα radiation equipped with X'celerator detector. An Anton Paar TTK 450 attachment to Phillips diffractometer was used in in order to control sample conditions. Experiments were conducted under high vacuum (~ 10^{-2} mbar) to minimize the effect of adsorbates in the MFI structure. The zeolite sample was packed in the TTK 450 sample holder and the temperature of sample was controlled with a TTU 110 unit. The sample holder was cooled with a cold finger using liquid nitrogen and cooling water and heated with an embedded electric heater. Samples were analyzed over a range of 21-31° 2θ. Due to reports in literature on the dependence of phase transition temperature on adsorbed species in the structure, I have performed all of the experiments under high vacuum to eliminate this variable.

All of the samples were maintained for at least 1 hour under high vacuum (~ 10^{-2} mbar) before the measurements begin. The first XRD measurement was conducted at 20°C for all the samples. Observing a singlet peak near 24.4° 2θ in the XRD spectrum means the structure is orthorhombic. Observing a doublet near 24.4° in XRD spectrum means the structure is monoclinic and the temperature needs to be increased to reach the transition. The temperature was changed according to the XRD spectrum observed at 20°C to determine the phase transition temperature. The temperature was changed in 10°C increments with a rate of 2°C/min. After every 10 °C increment, the sample temperature is maintained for 30 min to allow it to thermally equilibrate. The effect of equilibration time has been studied by comparing XRD spectra close to the transition temperatures, taken after equilibration times of 15 min, 30 min and 1 hour. All of the XRD spectra looked identical; however, I chose a 30 min equilibration time to make sure the sample is at thermal equilibrium before measurement. Temperature fluctuations are usually ± 3°C under high vacuum.

5.3. Results

Different sizes of pure silica MFI particles were synthesized. Variable temperature XRD measurements were performed on all of the samples, in order to determine their phase transition temperature.

5.3.1. Phase Transition for 900 nm Particles

Figure 5.3 shows the XRD spectra of 900 nm particles at different temperatures along with the SEM image of the particles. The lowest temperature (-150°C) shows the monoclinic structure for the particles, and the highest temperatures show the orthorhombic structure. The phase transition temperature occurs at -50°C where the valley between two peaks of the monoclinic structure 2θ=24.4° is flattened.

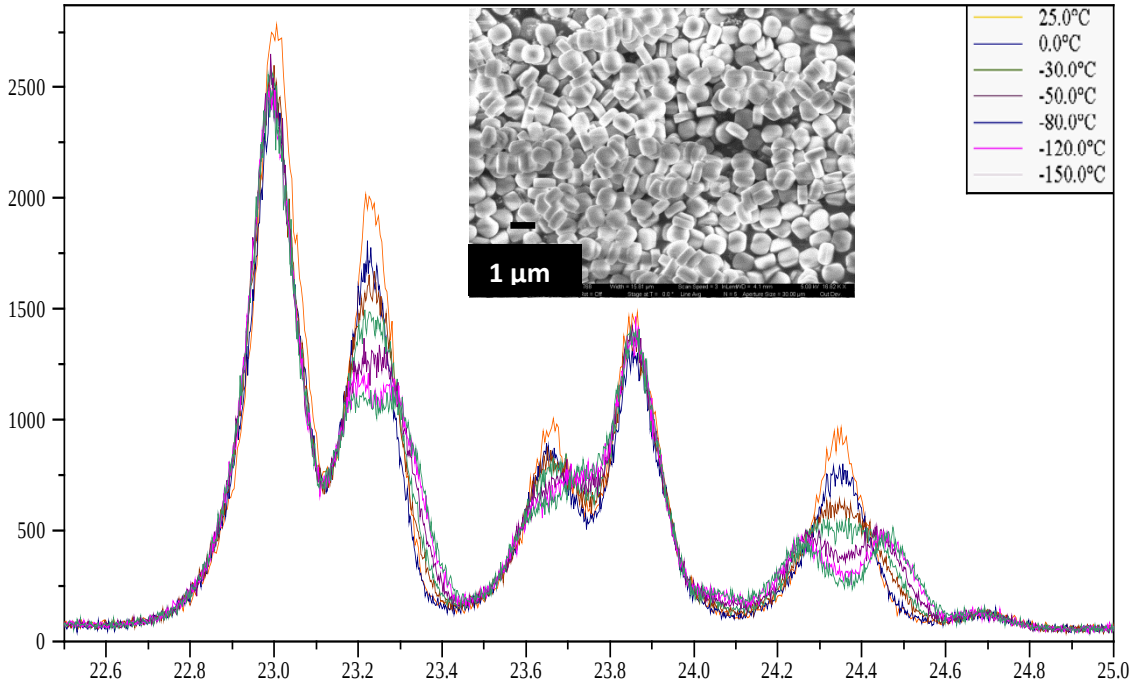

Figure 5.3: XRD spectrum of 900 nm particles near the phase transition temperature and its SEM image.

5.3.2. Phase Transition for 2 µm Particles

Figure 5.4 shows the XRD spectra of 2 µm particles at different temperatures along with the SEM image of the particles. The lowest temperature (-80°C) shows the monoclinic structure, and the highest temperature shows the orthorhombic structure. The phase transition temperature occurs at -30°C.

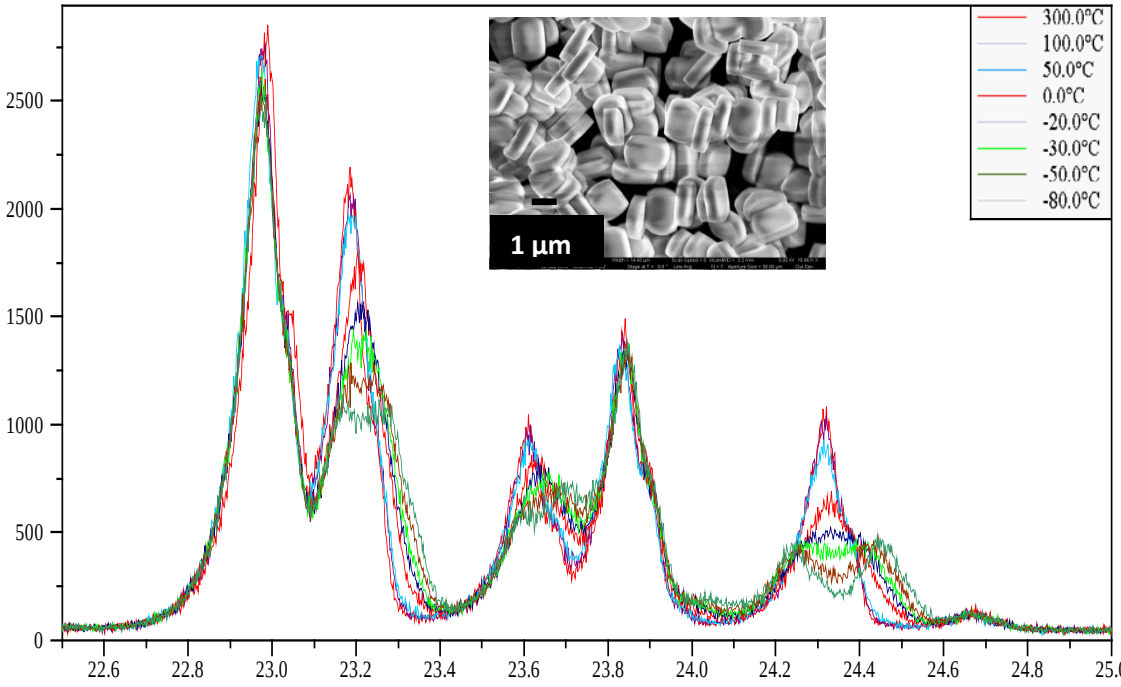

Figure 5.4: XRD spectrum of 2 µm particles near the phase transition temperature and its SEM image.

5.3.3. Phase Transition for 7 µm Particles

Figure 5.5 shows the XRD spectra of 7 µm particles at different temperatures along with the SEM image of the particles. The lowest temperature (-80°C) shows the monoclinic structure for the particles, and the highest temperatures show the orthorhombic structure. The phase transition temperature occurs at -20°C.

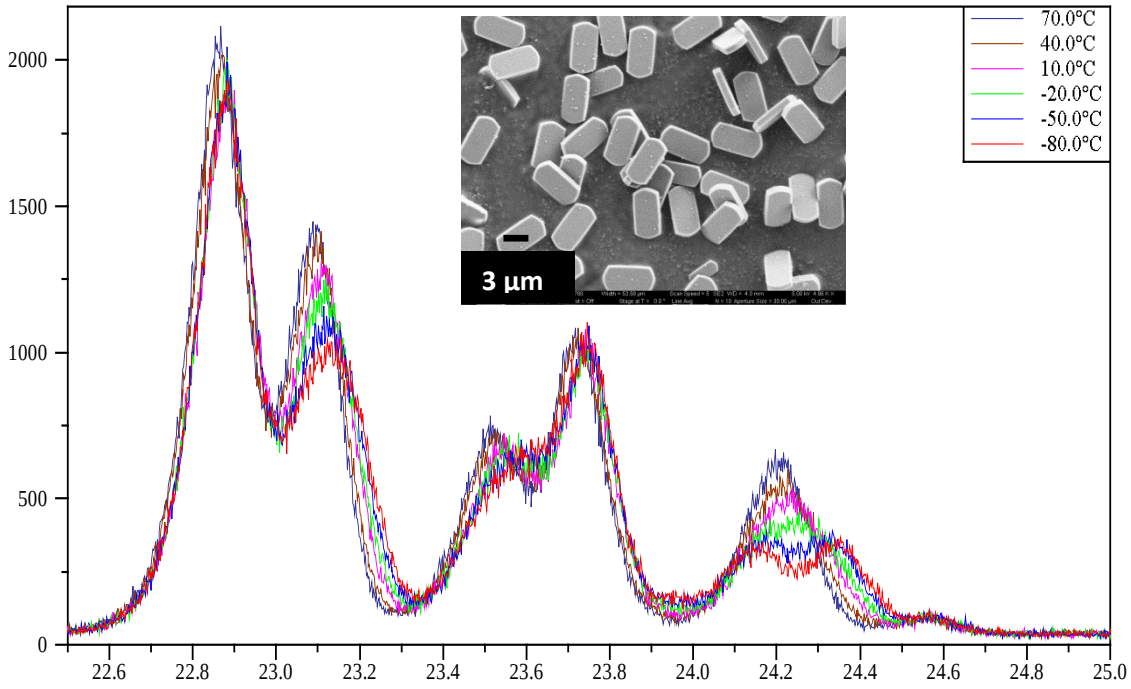

Figure 5.5: XRD spectrum of 7 µm particles near the phase transition temperature and its SEM image.

5.3.4. Phase Transition for 8 µm Particles

Figure 5.6 shows the XRD spectra of 8 µm particles at different temperatures along with the SEM image of the particles. As seen in the SEM image, much higher degree of twinning is observed in the 8 µm particles. The lowest temperature (30°C) shows the monoclinic structure for the particles, and the highest temperatures show the orthorhombic structure. The phase transition temperature occurs at 100°C.

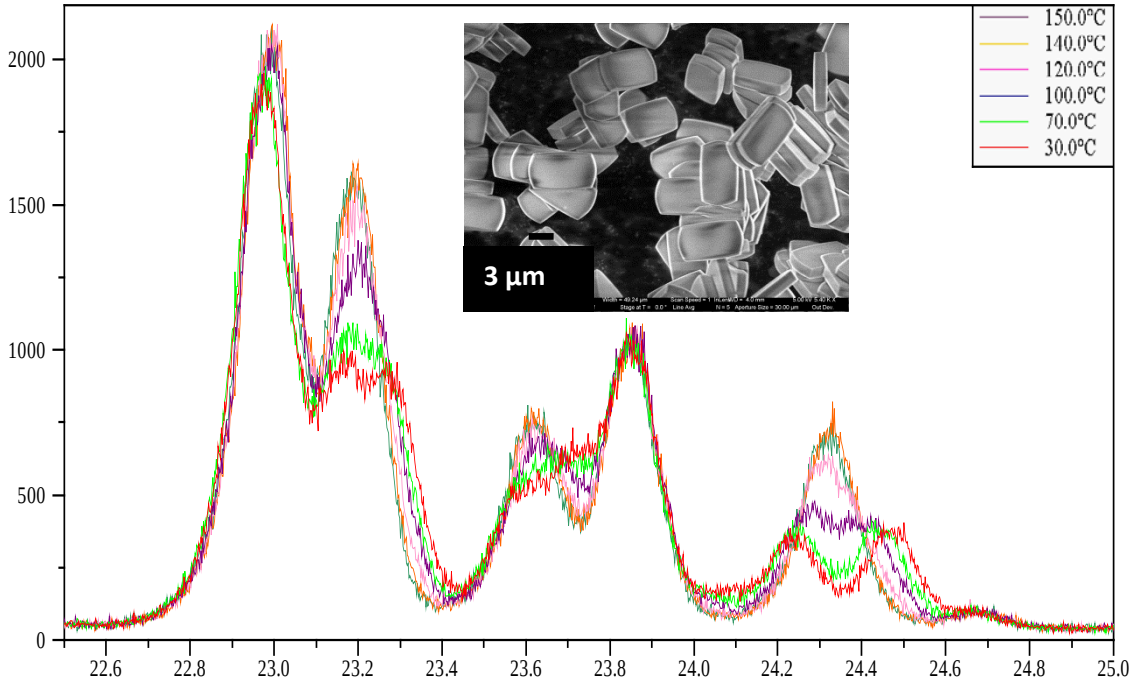

Figure 5.6: XRD spectrum of 8 µm particles near the phase transition temperature and its SEM image.

5.3.5. Phase Transition for 13 µm Particles

Figure 5.7 shows the XRD spectra of 13 µm particles at different temperatures along with the SEM image of the particles. Some twinning is observed in this SEM image which is similar to 8 µm particles. Considering that 8 µm and 13 µm particles were synthesized by the similar procedure, similar crystal property behavior and phase transition temperature is expected. The lowest temperature (30°C) shows the monoclinic structure for the particles, and the highest temperature shows the orthorhombic structure. The phase transition temperature occurs approximately at 140°C.

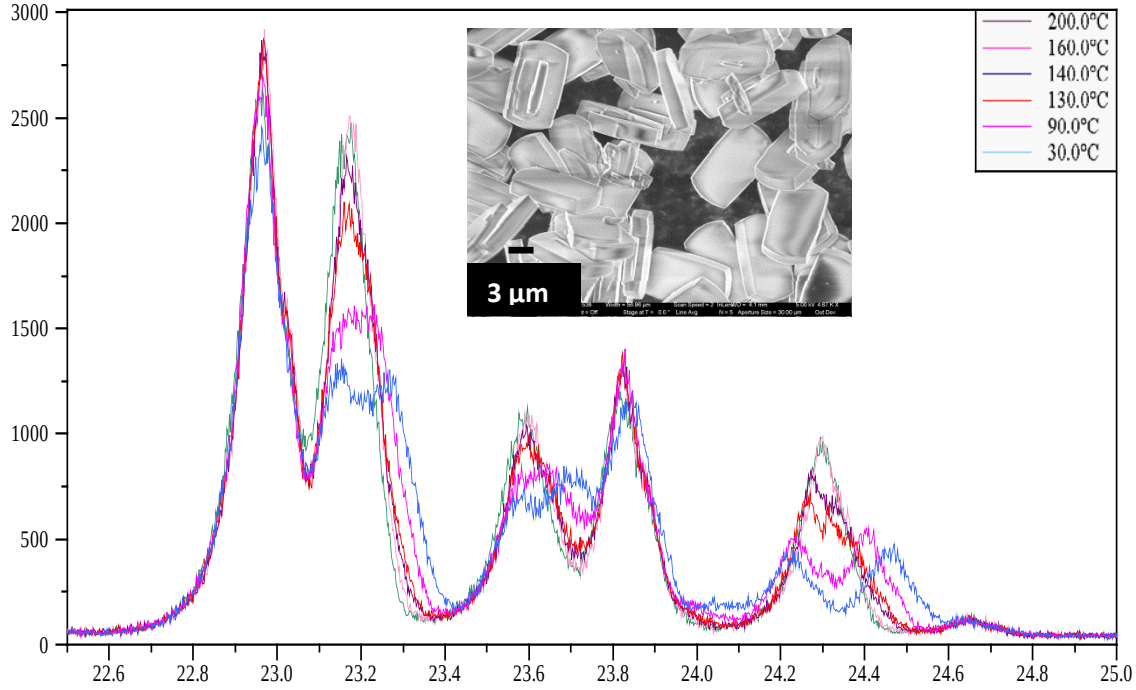

Figure 5.7: XRD spectrum of 13 µm particles near the phase transition temperature and its SEM image.

5.3.6. Phase Transition for 35 µm Particles

Figure 5.8 shows the XRD spectra of 35 µm particles at different temperatures along with the SEM image of the particles. The lowest temperature (25°C) shows the monoclinic structure, and the highest temperature shows the orthorhombic structure. The phase transition temperature occurs at 150°C.

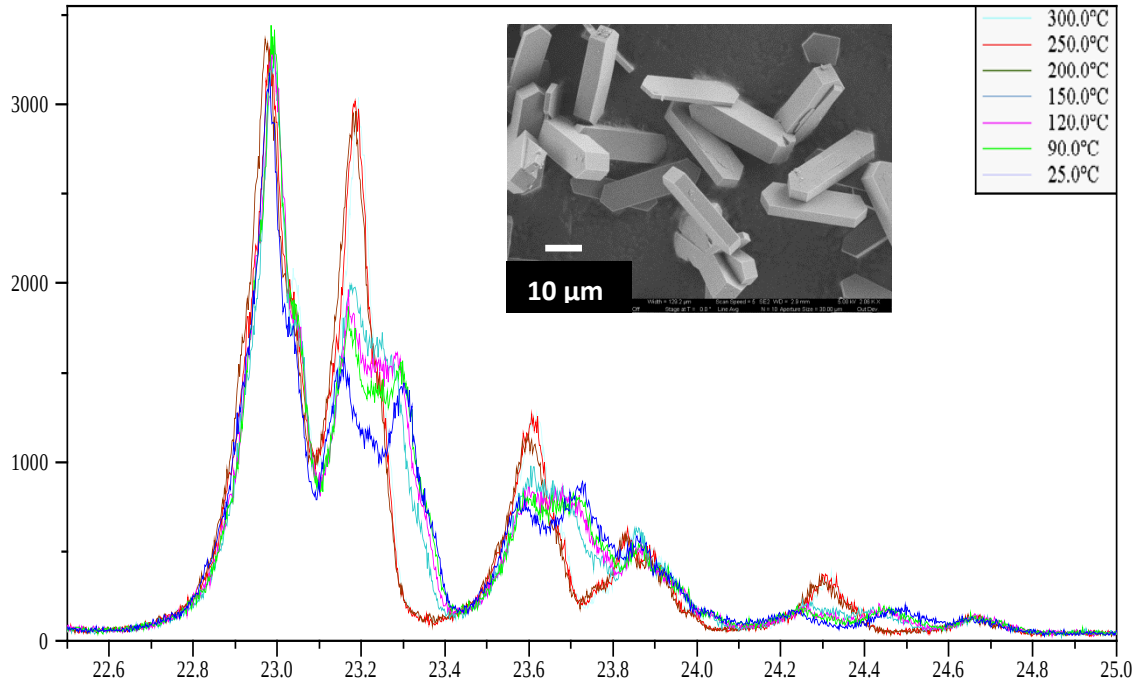

Figure 5.8: XRD spectrum of 35 µm particles near the phase transition temperature and its SEM image

In measuring XRD spectra of 35 µm particles, the sample was heated up to 300°C as XRD patterns were taken at 10°C increments. The sample was maintained at 300°C to ensure that any residual stress within the structure is eliminated. The XRD spectra showed no 'hysteresis' upon cooling the sample to room temperature. This experiment

shows that the internal stress in MFI particles upon heating did not play a determining role in the phase transition.

5.3.7. Phase Transition for 50 µm Particles

Figure 5.9 shows the XRD spectra of 50 µm particles at different temperatures along with the SEM image of the particles. The lowest temperature (80°C) shows the monoclinic structure for the particles, and the highest temperature shows the orthorhombic structure. The phase transition temperature occurs at 170°C.

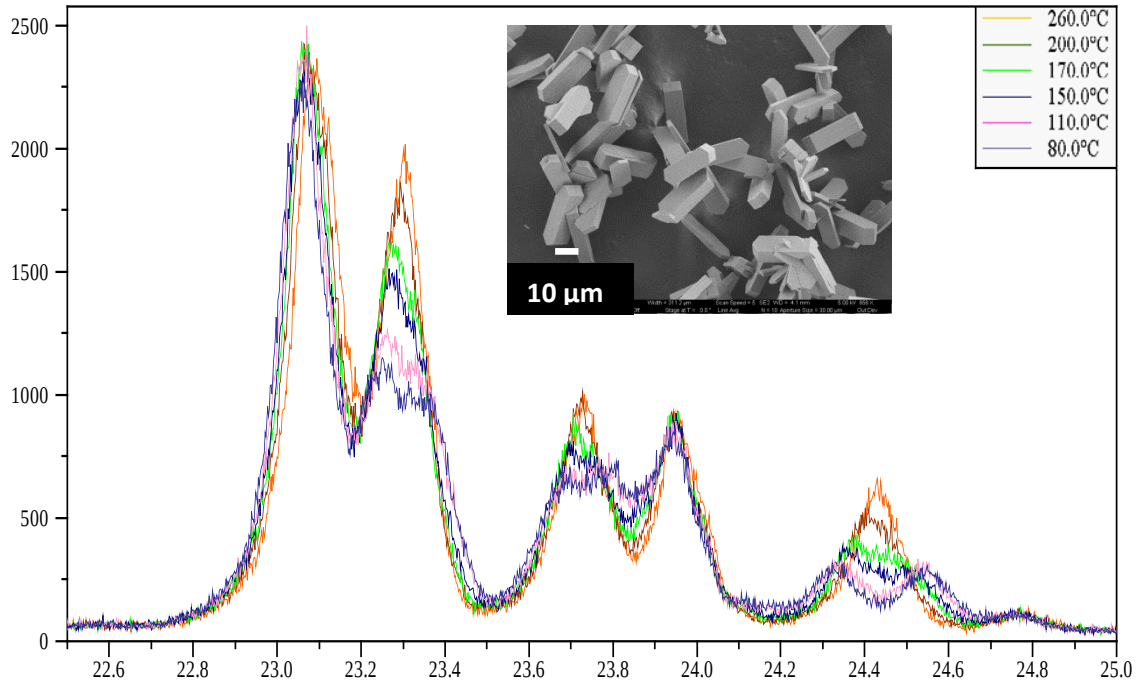

Figure 5.9: XRD spectrum of 50 µm particles near the phase transition temperature and its SEM image.

In Table 5.1, the observed phase transition temperatures for different particle sizes have been summarized.

Table 5.1: Observed phase transition temperature for different sizes of pure silica MFI

Particle Size (μm)	Phase Transition Temperature (°C)
50	170
35	150
13	140
8	100
7	-20
2	-30
0.9	-50

Figure 5.10 shows the observed phase transition temperature for particle sizes synthesizes with different procedures. In this study, particle size is defined as the *c*-axis dimension of the particle. This is the longest dimension of MFI particles. I clearly find that as the particle size increases, the phase transition temperature increases as well. The smallest three particle sizes (900 nm, 2 μm, 7 μm) show sub-zero transition temperatures. They were synthesized from the same synthesis methods. For these particles, I used TPAOH as both mineralizing agent and structure directing agent (SDA). The sudden change in the phase transition temperatures from 7 μm to 8 μm is not understood. Differences in synthesis procedures and starting compounds can lead to different defect structure and grain sizes within each particle. However, for 8 μm and 13 μm particle

synthesis, the roles of the basic solution (OH- as mineralization agent) and the SDA have been separated by using TPABr and NaOH, instead of TPAOH. In the fluoride route synthesis, F- is acting as mineralization agent and TPABr as the SDA.

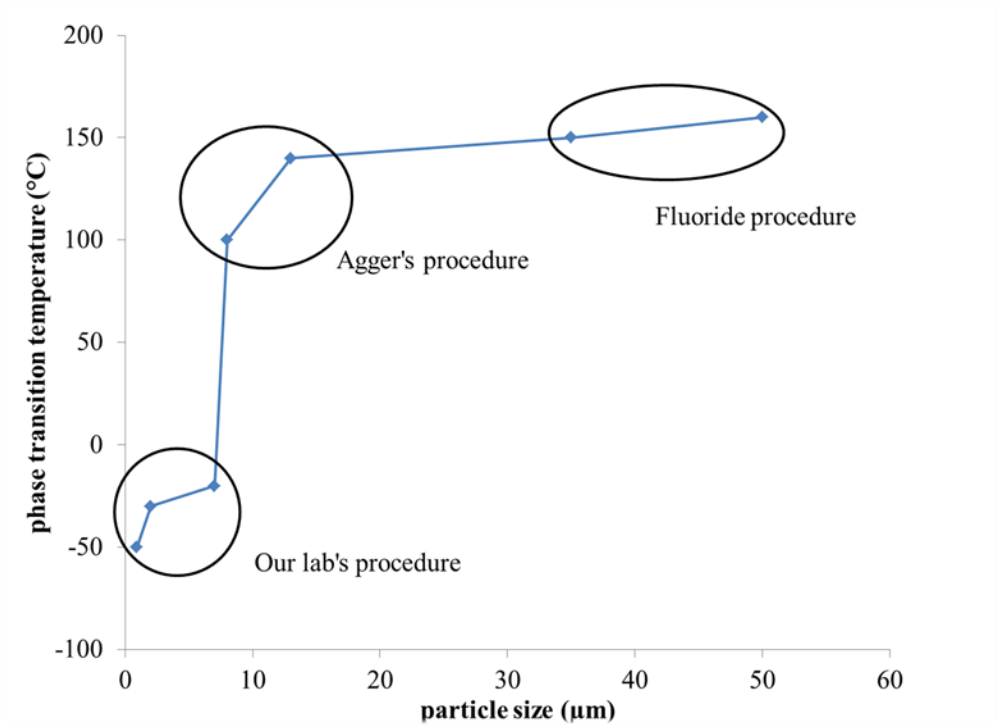

Figure 5.10: Observed phase transition temperature for different sizes of pure silica MFI, with synthesis procedures for different samples indicated.

5.4 Conclusions

In this chapter, in order to advance understanding of the nature of phase transition in MFI, the reversible structural phase change from monoclinic ($P2_1/n$.l.1) to orthorhombic (*Pnma*) phase in MFI framework was studied as a function of particle size. The MFI phase change is induced by application of temperature, and occurs at a critical temperature representing the onset of instability of one phase and the onset of stability of

the other. The hypothesis regarding dependence of phase transition temperature on particle size of pure silica MFI was investigated. Experiments were performed using *in situ* variable temperature XRD instrument under vacuum conditions. For the seven studied particle sizes, it was observed that as the particle size increased, the phase transition temperature was higher as well. However, phase transition temperature shows a sudden increase when changing the particle size from 7 µm to 8 µm which is not fully understood. Different synthesis routes were used to prepare the range of studied particles sizes and each synthesis route could lead to different crystal properties such as defect site density, and crystal grain size. Change in these crystal properties are suspected of being responsible for the observed behavior.

CHAPTER 6- CONCLUSIONS AND FUTURE RESEARCH DIRECTIONS

6.1.Conclusions

In this thesis, I studied and further developed a relatively new means for altering the adsorption and transport properties of zeolite MFI adsorbents and membranes by incorporating different organic functional groups into the zeolite pore structure. Firstly, I synthesized ~10 μm pure-silica MFI particles, which were large enough to minimize external silanol group effects. Modified MFI materials were obtained by direct reaction of these particles with seven organic molecules containing alcohol and/or amine functional groups. I have investigated and reported the gas adsorption properties of these zeolite MFI/organic hybrid materials. I have shown that the interactions of zeolite MFI with CO_2, CH_4, and N_2 can be influenced by internal-surface modification with organic molecules, thereby providing a "handle" to tune the adsorption and transport properties of zeolitic materials beyond their framework structure and composition. This was achieved by chemisorbing several types of organic species on the silanol defect sites in zeolite MFI. TGA/DSC and $^{13}C/^{29}Si$ NMR characterizations indicated that the functional groups were chemically bound to the zeolite framework, and the loading is strongly related to the concentration of internal silanol defects. Gas adsorption isotherms of the modified zeolite materials show a range of properties different from that of the bare MFI zeolite, with the MFI/3-amino-1-propanol, MFI/2-[(2-aminoethyl)amino]ethanol, and MFI/ benzenemethanol materials showing the largest differences from bare MFI. These properties are qualitatively explained by the known affinity of amino- and hydroxyl groups for CO_2, and of the phenyl group for CH_4.

The chemisorbed organic species were also hypothesized to have significant effects on the diffusion behavior of molecules in the zeolite channels. The combined influence of adsorption and diffusion changes due to modification can be studied by measuring permeation of different gases on modified MFI membranes. To study these effects, I synthesized MFI membranes with *[h0h]* out-of-plane orientation on α-alumina supports and modified them by the same procedures as used for MFI particles. The MFI membranes were modified with 1-butanol, 3-amino-1-propanol, 2-[(2-aminoethyl)amino]ethanol, and benzenemethanol. The existence of functional groups in the pores of the zeolite was confirmed by PA-FTIR measurements. Permeation measurements of H_2, N_2, CO_2, CH_4, and SF_6 were performed at room temperature on membranes before and after modification. Permeation of *n*-butane, and *i*-butane were measured on a MFI membrane, before and after it was modified with 1-butanol. Gas permeances decreased by 1-2 orders of magnitude for all of the gases in modified membranes, compared to bare MFI membranes. This is a strong indication that the organic species are in fact blocking the gas molecule transport through the MFI pores. The CO_2/CH_4 permeation selectivity was close to the Knudsen selectivity (0.67) for the membranes before modification. CO_2/CH_4 selectivity increased for MFI/benzenemethanol modified membrane (1.00), whereas it decreased for the MFI/2-[(2-aminoethyl)amino]ethanol modified membrane (0.54). MFI/benzenemethanol crystals were shown to have a highest sorption capacity for CH_4, whereas, MFI/2-[(2-aminoethyl)amino]ethanol crystals were shown to have a highest sorption capacity for CO_2 over all other studied molecules Higher sorption of CH_4 in MFI/benzenemethanol and higher sorption of CO_2 in MFI/2-[(2-aminoethyl)amino]ethanol and their strong

binding to the material are likely the reasons for observing lower and higher CO_2/CH_4 permeation selectivity respectively, compared to bare MFI membrane. A further detailed fundamental study of the CO_2 adsorption mechanism in modified zeolites is necessary to gain a better understating of the adsorption and permeation behavior of such materials.

I used *in-situ* FTIR measurements to study CO_2 adsorption mechanism on modified MFI particles. This study was performed in collaboration with John R. Copeland in the group of Prof. Carsten Sievers. It was done on bare MFI particles, and MFI modified with 1-butanol, 3-amino-1-propanol, 1-propaneamine, 1,3-diaminopropane, 2-[(2-aminoethyl)amino]ethanol, and benzenemethanol. For organic molecules with one functional group (1-butanol, benzenemethanol, and 1-propaneamine), physical adsorption is, as intuitively expected, the only observed mode of attachment of CO_2 to the zeolite material. For MFI modified with 1,3-diaminopropane, still only physical adsorption is seen. This is explained by the isolated nature of the amine groups in the material. On the other hand, chemisorbed CO_2 species are clearly observed on bare MFI, MFI modified with 3-amino-1-propanol and 2-[(2-aminoethyl)amino]ethanol. Moreover, these are carbonate-like species arise from the chemisorption of CO_2 to the silanol group in bare MFI and the alcohol groups of the modifying molecule. The possibility of significant contribution from external silanol groups in adsorbing CO_2 chemisorbed species was ruled out by a comparative examination of the FTIR spectra of 10 μm and 900 nm MFI particles modified with 2-[(2-aminoethyl)amino]ethanol. The basis for using the organic-modified zeolite materials was developed in applications that may involve chemisorption of adsorbate molecules like CO_2. Other than the influence of

organic groups in changing adsorption or diffusion properties of a zeolite, phase transitions in zeolite framework can also influence these properties substantially.

To gain a better understanding of the nature of structural phase transitions in MFI, I studied the reversible phase transition of MFI framework from monoclinic ($P2_1/n$.l.1) to orthorhombic (*Pnma*) phase. The MFI phase change is induced by application of temperature, and occurs at a critical temperature representing the onset of instability of one phase and the onset of stability of the other. I investigated the hypothesis that the phase transition temperature of MFI may vary with particle sizes of pure silica MFI, obtained from different synthesis routes. Experiments were performed using *in situ* variable temperature XRD instrument under vacuum conditions. As the particle size increased, the observed phase transition temperature was higher as well. However, the sudden increase in phase transition temperature when changing the particle size from 7 μm to 8 μm is not fully understood. Considering different synthesis routes used to prepare these particles, differences in crystal grain sizes and defect densities is suspected to be responsible for the observed behavior.

Overall, this research led to advances in finding new ways to alter adsorption and transport properties of zeolite MFI adsorbents or membrane by incorporation of different organic species in the internal pore structure. Insight into the interactions of adsorbed CO_2 molecules with the organic groups was also obtained. The results on membranes highlighted the need for further control of the organic modification process so as to control the degree of blockage of the zeolite pores by functional groups. The insights

attained from this research can be utilized in developing organic-modification “handles” for tuning zeolite properties, and in moving towards a predictive basis for the selection of organic molecules to rationally design modified materials for different applications.

I conclude this thesis by presenting some future directions suggested by the present research work. These studies, upon successful completion, would substantially further the ongoing efforts in developing modified zeolite sorbents and membranes enabling their use in various technological applications.

6.2.Future Research Directions

6.2.1. Control over Organic Loading

In this thesis, I have shown organic modification of zeolite MFI with different molecules including amine containing molecules. For the selection of future organic molecules, it is suggested to use long linear molecules with multiple functional groups. In Chapter 3, I observed that the permeation from MFI membranes was decreased 1-2 orders of magnitude. This pore blocking is likely due to the high loading of the functional group, and it is also possible that some of the physisorbed organic molecules may still be located in the membrane due to diffusion limitations. Therefore, it is desirable to develop more detailed methods that allow control over the number of organic molecules attached to the zeolite pores. At the same time, predictions of single-component and multicomponent diffusion and adsorption (by molecular simulation techniques) could elucidate the dependence of these properties on the loading and type of functional groups. The synthesis and modification of *[h00]* or *[0k0]*-oriented MFI membranes[5,42,136,137]

(instead of the present *[h0h]*-oriented membranes) is also an avenue for future study, since the direct perpendicular orientation of the zeolite channels promotes the ease of access to the modifying organic molecules and also increases the flux of permeants through the resulting membranes.

6.2.2. Organic-Modification of Other Zeolites

The modification method described in this thesis can be extended to functionalize other types of zeolite structure. Such zeolites may already contain silanol defects in the structure, or such defects can be introduced by several techniques (such as synthesis of the aluminosilicate zeolite framework followed by dealumination to create silanol defects)[138,139]. Modification of small-pore (e.g. DDR, LTA) as well as large-pore (e.g., FAU, BEA) zeolites could be done with different types of molecules and cause different and yet-unknown effects on adsorption and transport.

REFERENCES

1. Payra, P., Dutta, P. K.,*Zeolites: A Primer* In *Handbook of Zeolite Science and Technology*; Marcel Dekker, Inc: **2003**.

2. Yamamoto, K., Tatsumi, T. *Chem. Mater*. **2008**, 20, 972.

3. Cejka, J., Bekkum, H. V., Corma, A., Schuth, F. *Introduction to Zeolite Science and Practice*; 3rd ed.; Elsevier: Oxford, UK, **2007** 755-759.

4. Nair, S., Tsapatsis, M.,*Synthesis and Properties of Zeolitic Membranes* In *Handbook of Zeolite Science and Technology*; Auerbach, S. M., Carrado, K. A., Dutta, P. K. , Ed.; Marcel Dekker, Inc.: New York, **2003**.

5. Lai, Z., Bonilla, G., Diaz, I., Nery, J. G., Sujaoti, K., Amat, M. A., Kokkoli, E., Terasaki, O., Thompson, R. W., Tsapatsis, M., Vlachos, D. G. *Science* **2003**, 300, 456.

6. Oh, W. N., S. *Applied Physics Letters* **2005**, 87, 151912.

7. Van den Broeke, L. J. P., Bakker, W. J. W., Kapteijn, F., Moulijn, J. A. *AIChE J.* **1999**, 45, 976.

8. Stevens, R. W., Siriwardane, R. V., Logan, J. *Energy & Fuels* **2008**, 22, 3070.

9. Choi, S., Drese, J. H., Jones, C. W. *ChemSusChem* **2009**, 2, 796.

10. de Vos Burchart, E., van Bekkum, H., van de Graaf, B. *Zeolites* **1993**, 13, 212.

11. Davis, M. E. *Nature* **2002**, 417, 813.

12. Snyder, M. A., Tsapatsis, M. *Angew. Chem. In t. Ed.* **2007**, 46, 7560.

13. Koros, W. J. *AIChE J.* **2004**, 50, 2326.

14. Freemantle, M. *Chemical & Engineering News* **2005**, 83, 49.

15. Auerbach, S. M., Carrado, K. A., Dutta, P. K. *Synthesis and Properties of Zeolitic Membranes*; Marcel Dekker, Inc.: New York, **2003** 1184.

16. International Zeolite Association, *In* Database of Zeolite Structures, **2012**, http://izasc.ethz.ch/fmi/xsl/IZA-SC/ft.xsl.

17. Bernardo, P., Drioli, E., Golemme, G. *Ind. Eng. Chem. Res.* **2009**, 48, 4638.

18. Xomeritakis, G., Lai, Z., Tsapatsis, M. *Ind. Eng. Chem. Res.* **2001**, 40, 544.

19. Nair, S., Lai, Z., Nikolakis, V., Xomeritakis, G., Bonilla, G., Tsapatsis, M. *Microporous and Mesoporous Materials* **2001**, 48, 219.

20. Kusakabe, K., Kuroda, T. M. A., Morooka, S. *Ind. Eng. Chem. Res.* **1997**, 36, 649.

21. Giannakopoulos, I. G., Nikolakis, V. *J. Membr. Sci.* **2007**, 305, 332.

22. Xomeritakis, G., Nair, S.,Tsapatsis, M. *Microporous and Mesoporous Materials* **2000**, 28, 61.

23. Bradley, S. A., Broach, R. W., Mezza, T. M., Prabhakar, S., Sinkler, W.,*Overview in Zeolite Adsorptive Separation* In *Zeolites in Industrial Separation and Catalysis*; Kulprathipanja, S., Ed.; John Wiley & Sons **2010**.

24. Flanigen, E. M. *Pure and Applied Chemistry* **1980**, 52, 2191.

25. Milton, R. M. *Molecular Sieves*; Soc. Chem. md.: London, **1968** 199.

26. Caro J., N. M. *Microporous and Mesoporous Materials* **2008**, 115, 215.

27. Caro, J., Noack, M., Kolsch, P., Schafer, R. *Microporous Mesoporous Mater.* **2000**, 38, 3.

28. Yang, M., Crittenden, B. D., Perera, S. P., Moueddeb, H., Dalmon, J. A. *J. Membr. Sci.* **1999**, 156, 1.

29. Calzaferri, G., Pauchard, M, Maas H. , Huber, S., Khatyr, A., Schaafsma, T. *J. Mater. Chem.* **2002**, 12, 1.

30. Lai, R., Gavalas, G. R. *Ind. Eng. Chem. Res.* **1998**, 37, 4275.

31. Yan, Y., Davis, M. E., Gavalas, G. R. *Ind. Eng. Chem. Res.* **1995**, 34, 1652.

32. Cundy, C. S., Cox, P. A. *Microporous and Mesoporous Materials* **2005**, 82, 1.

33. Jansen, J. C., Nugroho, W., van Bekkum, H. In *In Proceedings from the Ninth International Zeolite Conference;*; von Ballmoos, R., Higgins, J. B., Treacy, M. M. J., Ed.; Buttenvorth-Heinemann: Boston, **1993**.

34. Koegler, J. H., Zandbergen, H. W., Harteveld, J. L. N., Nieuwenhuizen, M. S., Jansen, J. C., van Bekkum, H. *Stud Surf. Sci. Catal.* **1994**, 84.

35. Funke, H. H., Kovalchick, M.G., Falconer, J.L., Noble, R.D., *Industrial and Engineering Chemistry Research* **1996**, 35, 1575.

36. Hedlund, J., Noack, M., Kölsch, P., Creaser, D., Caro, J., Sterte, J. *Journal of Membrane Science* **1999**, 159, 263.

37. Schoeman, B. J., Erdem-Şenatalar, A., Hedlund, J., Sterte, J. *Zeolites* **1997**, 19, 21.

38. Li, K. *Ceramic Membranes for Separation and Reaction*; John Wiley & Sons: West Sussex, England, **2007**.

39. Xomeritakis, G., Gouzinis, A., Nair, S., Okubo, T., He, M., Overney, R. M., Tsapatsis, M. *Chemical Engineering Science* **1999**, 3521.

40. Lovallo, M., Tsapatsis, M. *AIChE Journal* **1996**, 42, 3020.

41. Lovallo, M. C. G., A.; Tsapatsis, M. *AIChE Journal* **1998**, 44, 1903.

42. Choi , J., Ghosh , S. , King , L. , Tsapatsis , M. . *Adsorption* **2006**, 12, 339

43. Boudreau, L. C., Tsapatsis, M. *Chem. Mater.* **1997**, 9, 1705.

44. Mintova, M., Valtchev, V., Engstrom, V., Schoeman, B. J., Sterte, J. *Microporous Materials* **1997**, 11, 149.

45. Ha, K., Lee, Y. J., Lee, H. J., Yoon, K. B. *Adv. Mater.* **2000**, 12, 1114.

46. Liu, Y., Li, Y., Yang, W. *Langmuir* **2011**, 2327.

47. Dong, J., Lin, Y. S., Hu, M., Peascoe, R. A., Payzant, E. A. *Microporous Mesoporous Mater.* **2000**, 34, 241.

48. O'Brien-Abraham , J., Kanezashi , M. , Lin , Y.S. *Microporous and Mesoporous Materials* **2007**, 105, 140.

49. Cheng, C. H., Bae, T. H., McCool, B. A., Chance, R. R., Nair, S., Jones, C. W. *J. Phys. Chem. C* **2008**, 112, 3543.

50. Fong, Y. Y., Abdullah, A. Z., Ahmad, A. L., Bhatia, S. *Chemical Engineering Journal* **2008**, 139, 172.

51. Beck, J. S., Vartuli, J. C., Roth, W. J., Leonowicz, M. E., Kresge, C. T., Schmitt, K. D., Chu, C. T. W., Olson, D. H., Sheppard, E. W., et. al. *J. Am. Chem. Soc.* **1992**, 114, 10834.

52. Jones, C. W., Tsuji , K., Davis, M. E. *Nature* **1998**, 52.

53. Jones, C. W., Tsuji, K., Davis, M. E. *Microporous and Mesoporous Materials* **1999**, 33, 223.

54. Jones, C. W., Tsapatsis, M., Okubo, T., Davis, M. E. *Microporous Mesoporous Mater.* **2001**, 42, 21.

55. Tsuji, K. *Zeoraito* **2000**, 17, 162.

56. Petrovic, I., Navrotsky, A., Davis, M. E., Zones, S. I. *Chem. Mater.* **1993**, 5, 1805.

57. Su, F. S., Lu, C. Y., Kuo, S. C., Zeng, W. T. *Energy Fuels* **2010**, 24, 1441.

58. Fegan, S. G., Lowe, B. M. *J. Chem. Soc. Chem. Commun.* **1984**, 437.

59. Boxhoorn, B., Kortbeek, A.G.T.G., Hays, G. R., Alma, N. C. M. *Zeolites* **1984**, 4, 15.

60. Dessau, R. M., Schmitt, K. D., Kerr, G. T., Woolery, G. L., Alemany, L. B. *J. Catal.* **1987**, 104, 484.

61. Woolery, G. L., Alemany, L. B., Dessau, R. M., Chester, A. W. *Zeolites* **1986**, 6, 14.

62. Datka, J., Tuznik, E. *Zeolites* **1985**, 5, 230.

63. Lobo, R. L., Zones, S. I., Davis, M. E. J. *Incl. Phenom. Mol. Recogn. Chem.* **1995**, 21, 47.

64. Koller, H., Wolker, A., Villaescusa, L. A., Diaz-Cabanas, M. J., Valencia, S., Camblor, M. A. *J. Am. Chem. Soc.* **1999**, 121, 3368.

65. Flanigen, E. M., Patton, R. L. In *U.S. Patent 4073865* **1978**.

66. Kraushaar, B., De Haan, J. W., Van Hooff, J. H. C. *J. Catal.* **1987**, 109, 470.

67. Zumbulyadis, N., O'Reilly J. M. *Macromolecules* **1991**, 24, 5294.

68. Kassaee, M. H., Sholl, D. S., Nair, S. *Journal of Physical Chemistry C* **2011**, 115, 19640.

69. Tang, Z., Dong, J., Nenoff, T. M. *Langmuir* **2009**, 25, 4848.

70. McCool, B. A., DeSisto, W. J. *Adv. Func. Mater.* **2005**, 15, 1635.

71. Wee, S.-L., Tye, C.-T., Bhatia, S. *Separation and Purification Technology* **2008**, 63, 500.

72. Guo, J., Han, A.-J., Yu, H., Dong, J.-P., He, H., Long, Y.-C. *Microporous and Mesoporous Materials* **2006**, 94, 166.

73. Han, A.-J., He, H.-Y.,Guo, J.,Yu, H., Huang, Y.-F., Long, Y.-C. *Microporous and Mesoporous Materials* **2005**, 79, 177.

74. Luo, L., Labinger, J.A., Davis, M.E. *Journal of Catalysis* **2001**, 200, 222.

75. Murray, D. K., Howard, T., Goguen, P.W., Krawietz, T.R., Haw, J.F. *J. Am. Chem. Soc.* **1994**, 116, 6354.

76. Cabello, J. A. C., J.M., Garcie, A., Luna, D., Marinas, J. M. *J. Org. Chem.* **1984**, 49, 5195.

77. Carter, T. G., Yantasee, W., Sangvanich, T., Fryxell, G. E., Johnson, D. W., Addleman, R. S. *Chem. Commun.* **2008**, 5583.

78. Angloher, S., Bein, T. *J. Mater. Chem.* **2006**, 16, 3629.

79. Agger, J. R., Hanif, N., Cundy, C. S., Wade, A. P., Dennison, S., Rawlinson, P. A., Anderson, M. W. *J. Am. Chem. Soc.* **2003**, 125, 830.

80. Barquist, K., Larsen, S. C. *Microporous and Mesoporous Materials* **2008**, 116, 365.

81. Larsen, S. C. *J. Phys. Chem. C* **2007**, 111, 18464.

82. Mitamura, Y., Komori, Y., Hayashi, S., Sugahara, Y., Kuroda, K. *Chem. Mater.* **2001**, 13, 3747.

83. Sarneski, J. E., Surprenant, H. L., Molen, F. K., Reilley, C. N. *Analytical chemistry* **1975**, 47, 2116.

84. Online Database for Spectral Database for Organic Compounds (SDBS), **2012.**

85. Inui, M., Ikeda, T., Suzuki, T., Sugita, K., Mizukami, F. *Bull. Chem. Soc. Jpn.* **2009**, 82, 1160.

86. Vaidya, P. D., Kenig, E. Y. *Chem. Eng. Technol.* **2007**, 11, 1467.

87. Caplow, M. *J. Am. Chem. Soc.* **1968**, 90.

88. Morita, S., Fujii, A., Mikami, N., Tsuzuki, S. *J. Phys. Chem. A* **2006**, 110, 10583.

89. Ringer, A. L., Figgs, M. S., Sinnokrot, M. O., Sherrill, C. D. *J. Phys. Chem. A* **2006**, 110, 10822.

90. Caro, J., Noack, M., Kolsch P. *Adsorption* **2005**, 11, 215.

91. Zheng, Z., Hall, A. S., Guliants, V. V. *J. Mater. Sci.* **2008**, 43, 2499.

92. Kanezashi, M., O'Brien, J., Lin, Y. S. *AIChE J.* **2008**, 54, 1478.

93. Hong, M., Falconer, J. L., Noble, R. D. *Ind. Eng. Chem. Res.* **2005**, 44, 4305.

94. Masuda, T., Fukumoto, N., Kitamura, M. *Microporous Mesoporous Mater.* **2001**, 48, 239.

95. Lu, D., Kondo, J. N., Domen, K., Begum, H. A., Niwa, M. *J. Phys. Chem. B* **2004**, 108, 2295.

96. Yeong, Y. F., Abdullah, A. Z., Ahmad, A. L., Bhatia, S. *Journal of Membrane Science* **2010**, 360, 109.

97. Ko, C. H., Bae, J.-S., Yeum, J. H., Kang, N., Park, Y.-D., Kim, Y.-S., Lee, J.-W., Nair, S., Oh, W. *Journal of Ceramic Processing Research* **2009**, 10, 9.

98. Oh, W., Nair, S. *J. Phys. Chem. B* **2004**, 108, 8766.

99. Bakker, W. J. W., Van den Broeke, L. J. P., Kapteijn, F., Moulijn, J. A. *AIChE J.* **1997**, 43, 2203.

100. Burggraaf, A. J. *J. Membr. Sci.* **1999**, 155, 45.

101. Shindo, Y., Hakuta, T.,Yoshitome, H., Inoue, H. *J. Chem. Eng. Japan* **1985**, 16, 120.

102. Krishna, R., van den Broeke, L. J. P. *Chem. Eng. J.* **1995**, 57, 155.

103. Krishna, R., Baur, R. *Sep. Purif. Technol.* **2003**, 33, 213.

104. Chen, Y. D., Yang, R. T. *AIChE J.* **1991**, 37, 1579.

105. Karger, J., Ruthven, D. M. *Diffusion in Zeolites*; Wiley: New York, **1992**.

106. Van den Broeke, L. J. P., Kapteijn, F., Moulijn, J. A. *Chem. Eng. Sci.* **1999**, 54, 259.

107. Kumara, P., Ida, J., Kim, S., Guliants, V.V., Lin, J.S.Y. *Journal of Membrane Science* **2006**, 279, 539.

108. Breck, D. W. *Zeolite Molecular Sieves: Structure, Chemistry, and Use*; Wiley: New York, **1974**.

109. Coronas, J., Noble, R. D., Falconer, J. L. *Ind. Eng. Che. Res.* **1998**, 37, 166.

110. van de Graaf, J. M., van der Bijl, E., Stol, A., Kapteijn, F., Moulijn, J.A. *Industrial and Engineering Chemistry Research* **1998**, 37, 4071.

111. Bal, R., Tope, B. B., Das, T. K., Hegde, S. G., Sivasanker, S. *Journal of Catalysis* **2001**, 204, 358.

112. Bollini, P., Didas, S. A., Jones, C. W. *Journal of Material Chemistry* **2011**, 21, 15100.

113. Bradley, S. A., Broach, R. W., Mezza, T. M., Prabhakar, S., Sinkler, W.,*Zeolite Characterization* In *Zeolites in Industrial Separation and Catalysis*; Kulprathipanja, S., Ed.; John Wiley & Sons **2010**.

114. Danon, A., Stair, P. C., Weitz, E. *Journal of Physical Chemistry C* **2011**, 115, 11540.

115. Galhotra, P., Navea, J. G., Larsen, S. C., Grassian, V. H. *Energy and Environmental Science* **2009**, 2, 401.

116. Rege, S. U., Yang, R. T. *Chem. Eng. Sci.* **2001**, 56, 3781.

117. Rhodes, C. J. *Annu. Rep. Prog. Chem., Sect. C* **2010**, 106, 36.

118. Sartori, G., Savage, D. W. *Ind. Eng. Chem. Res.* **1983**, 22, 239.

119. Wirawan, S. K., Creaser, D. *Microporous and Mesoporous Materials* **2006**, 91, 196.

120. Solymosi, F., Knozinger, H. *J. Catal.* **1990**, 122, 166.

121. Wang, X., Schwartz, V., Clark, J. C., Ma, X., Overbury, S. H., Xu, X., Song, C. *J. Phys. Chem. C* **2009**, 113, 7260.

122. Vaidhyanathan, R., Iremonger, S. S., Shimizu, G. K. H., Boyd, P. G., Alavi, S., Woo, T. K. *Science* **2010**, 330, 650.

123. Diaz, U., Vidal-Moya, J. A., Corma, A. *Microporous Mesoporous Mater* **2006**, 93, 180.

124. Ingle, J. D. J., Crouch, S. R. *Spectrochemical Analysis*; Prentice Hall: New Jersey **1988**.

125. Hay, D. G., Jaeger, H., West, G. W. *J. Phys. Chem.* **1985**, 89, 1070.

126. van Koningsveld, H. V., Jansen, J. C, Bekkum, H. V. *Zeolites* **1987**, 7, 564.

127. Mentzen, B. F., Letoffe, J.-M., Claudy, P. *Thermochimica Acta* **1996**, 288, 1.

128. Zecchina, A., Bordiga, S., Spoto, G., Marchese, L., Petrini, G., Leofanti, G., Padovan, M. *J. Phys. Chem.* **1992**, 96, 4985.

129. Zhong, W. L., Wang, Y. G., Zhang, P. L., Qu, B. D. *Phys. Rev. B* **1994**, 50, 698.

130. van koningsveld, H., Jansen, J. C., van Bekkum, H. *Zeolites* **1987**, 7.

131. Hay, D. G., Jaeger, H. *J. Chem. Soc., Chem. Commun.* **1984**, 1433.

132. Aguilera-Granja, F., Moran-Lopez, J. L. *Solid State Commun.* **1990**, 74, 4743.

133. Ishikawa, K., Yoshikawa, K., Okada, N. *Phys. Rev. B* **1988**, 37, 5852.

134. Mills, D. L. *Phys. Rev. B* **1971**, 3, 3887.

135. Chezeau, J. M., Delmotte, L., Guth, J. L., Soulard, M. *Zeolites* **1989**, 9, 78.

136. Lai, Z., Tsapatsis, M. , Nicolich, J. P. *Advanced Functional Materials* **2004**, 14, 716.

137. Liu, Y., Li, Y.,Yang, W. *J. Am. Chem. Soc.* **2010**, 132, 1768.

138. Fejes, P., Kiricsi, I., Hannus, I Kiss, A, Schobel, G *Reaction Kinetics and Catalysis Letters* **1980**, 14, 481.

139. Najar, H., Zina, M. S., Ghorbel, A. *Reaction Kinetics Mechanisms and Catalysis* **2010**, 100, 385.